Flow Field Within the Vertical Slot of a Fish Passage: the Effect of Turbulence, Velocity and Slot Length and the Design of a Lamprey Passage System at the John Day Dam

A Thesis

Presented in Partial Fulfillment of the Requirements for the

Degree of Master of Science

with a

Major in Civil Engineering

in the

College of Graduate Studies

University of Idaho

by

James Channing Syms

Major Professor: Daniele Tonina, Ph.D.

Co-Major Professor: Christopher Caudill, Ph.D.

Committee Member: Ralph Budwig, Ph.D.

Department Chair: Patricia Colberg, Ph.D.

April 2016

AUTHORIZATION TO SUBMIT THESIS

The thesis of James Channing Syms, submitted for the degree of Master of Science with a major in Civil Engineering and titled, "Flow Field Within the Vertical Slot of a Fish Passage: the Effect of Turbulence, Velocity and Slot Length and the Design of a Lamprey Passage System at the John Day Dam," has been reviewed in final form. Permission, as indicated by the signatures and dates given below, is now granted to submit final copies to the College of Graduate Studies for approval.

Major Professor: _____ Date: _____
Daniele Tonina, Ph.D.

Co-Major Professor: _____ Date: _____
Chris Caudill, Ph.D.

Committee Member: _____ Date: _____
Ralph Budwig, Ph.D.

Department Chair: _____ Date: _____
Patricia Colberg, Ph.D.

ACKNOWLEDGEMENTS

I would like to thank the US Army Corps of Engineers Portland District for funding of this research. I'd like to thank my Co-Major Professors, Daniele Tonina and Chris Caudill, for all of their assistance through the project and their patience in the huge amount of data processing. Mark Kirk has been invaluable in his biological insight and data collection for this project. Ida Royer, Andy Traylor, and Brian Bissell from USACE at Bonneville Dam provided on-site support. Sean Tackley, USACE, provided administrative and technical support. I thank Bob Basham and Ralph Budwig from the University of Idaho's Center for Ecohydraulics Research (CER) for building the three-axis robot that made the ADV measurements.

DEDICATION

This work is dedicated to my wife, Teresa Syms. Without her help with two new children during this time it would not have been possible. Also my children Max and Bianca, you make light within life. I also dedicate this work to my Dad who passed from cancer during my research. I miss you every day.

ABSTRACT

To understand the flow conditions encountered by migratory fish within a vertical slot section of fishways, measurements were made in an experimental flume where velocity, turbulence, and slot length were manipulated. The results show that turbulence intensity increases with slot length and mean flow velocity regardless of turbulence treatment. The high velocity zone moves from downstream to upstream by adding a turbulence-inducing wall upstream of the slot. High turbulence zones preferentially formed toward the entrance of the slot for the control treatment whereas high turbulence zones were distributed through the entire slot in the turbulence treatment. These changes likely affect upstream migrating fish. Observations of Pacific lamprey passing the experimental serpentine weir show that they chose paths with low turbulence under the high velocity treatments. The design and installation of a Lamprey Passage System at the North Fishway on the John Day Dam are also described.

TABLE OF CONTENTS

TABLE OF FIGURES

Chapter 1: Flow field within the vertical slot of a fish passage: The effect of turbulence, velocity and slot length

Many fish passageways were designed to facilitate upstream migration at anthropogenic barriers for targeted species, such as salmonids, typically by reducing velocity with hydraulic structures forming high turbulence. However, the generated flow field may remain a barrier for many other species, such as the Pacific lamprey (*Entosphenus tridentatus*, Gardener) found in the Columbia River. Vertical slot sections are typically used in the designs of upper fishways allowing flow regulation within the ladder as forebay elevations fluctuate. Bonneville Dam uses a somewhat unusual vertical slot design that has relatively long slots of variable length and large changes in directions between slots. The sections at both of the two upper fishway exit areas are thus known as 'serpentine weir sections'. We designed and built an experimental flume idealizing the vertical slot in an effort to understand how velocity, slot length and turbulence conditions of water entering the slot affected hydraulics. Velocity and turbulence were measured with an acoustic doppler velocimeter on a grid pattern at three different depths 0, 0.3, and 0.65 m from the bottom of the flume. The flow field was measured for 18 different scenarios from a combination of three slot lengths (0.33.0.66 and 1m), three mean flow velocities (1.2, 1.8 and 2.4 m s^{-1}), and two turbulence treatments, without (control treatment, with average turbulence kinematic energy, *TKE*, 795 cm^2 s^{-2}) and with (turbulence treatment, with average *TKE* 1967 cm^2 s^{-2}) a turbulence-inducing wall. Our results show that turbulence intensity increases with slot length and mean flow velocity regardless of turbulence treatment. The high velocity zone

moves from downstream to upstream by adding the turbulence-inducing wall. Similarly, high turbulence zones preferentially formed toward the entrance of the slot for the control treatment whereas they were distributed through the entire slot length, for the turbulence treatment. These changes alter hydraulics and sensory cues encountered by passing fishes. A fish that must travel through turbulent conditions for the entire length of the slot may not have a resting location like those found when the turbulence is low until the upstream end of the slot. Observations from a companion study (Kirk, Caudill, Tonina, & Syms., 2015) of Pacific lamprey passing the experimental serpentine weir show that they did not avoid high turbulence areas at low velocity treatments, but they chose paths with low turbulence in the high velocity treatments.

Introduction

Fishways allow passage of barriers including hydroelectric dams, irrigation diversions, and culverts along rivers and streams (Clay, 1961, 1995; Katopodis, 1992; NMFS, 2008). These barriers have decreased habitat by more than 40% in some watersheds. Fishways are generally designed to meet depth and velocity requirements for a set of target species considered important or protected by regulation in a given stream, leaving all the other species to cope with those hydraulic conditions (Clay, 1961, 1995; Katopodis, 1992; NMFS, 2008; Rodríguez, Agudo, Mosquera, & González, 2006). Salmonids have frequently been the target design group in the Pacific Northwest.

Hydrodynamic variables other than velocity and depth may affect passage of fish through fishways. In general, studies have found that turbulence always increases the bioenergetics cost of fishway passage (J F Orsborn & Powers, 1985; John F. Orsborn, 1987). Turbulence may prevent passage of fish and a fishway may have a high bioenergetics cost to

anadromous fish and may reduce the fish energy budget required for their entire migration (T. Castro-Santos, 2005; Theodore Castro-Santos, Cotel, & Webb, 2009). Both velocity and turbulence are used by fish as movement cues using mechanoreceptors (Barton, 2007) and thus hydraulics likely affect behavior as well as energetics. Vertical slot fishways that are aligned parallel to the flow have a higher passage rate than serpentine weirs or drop pool structures (Kim, 2001). These vertical slots aligned to the flow have lower turbulence than those that include serpentine type sections to decrease velocity and increase depth. Recently the importance of turbulence in fishways has become recognized in fishway studies with the realization that quantification of turbulence can be challenging (Kemp, 2012). The intensity, periodicity, orientation, and scale, IPOS, framework proposes four metrics for quantifying and qualifying turbulence (Lacey, Neary, Liao, Enders, & Tritico, 2012). For instance, the scale of turbulence vortices as they compare to the size of the fish may be as important as intensity in passage. In Blacknose Dace (Goettel, Atkinson, & Bennett, 2015) turbulence intensity did not affect fish movement, but fish followed paths of similar turbulence linking low or high turbulence areas through passage. The authors suggest that better indices inclusive of turbulence metrics should be investigated along with the effect of turbulence on passage success of a wider range of fish species beyond those regulated or with an economical value, e.g. salmon.

Historically fishways were designed for salmonids and other non economically important species were not considered (Theodore Castro-Santos et al., 2009). The fishways require high discharges to attract salmonids into fishways (Mallen-Cooper & Brand, 2007). Using fishway criteria based on salmonid swimming capabilities may not allow passage of all species because fish locomotion varies with species. Anguilliform swimmers such as

lamprey and eels reach exhaustion much sooner than subcarangiform swimmers such as salmonids. The anguilliform swimmers also generally have much lower swimming speeds (Katopodis & Gervais, 2012). Studies on the River Mondego in Portugal documented that vertical slot fishways of the Açude-Ponte dam can provide passage for the European eel (*Anguilla anguilla L.*) and other nonanadramous species (Mateus et al., 2015). The fish passage structure over the Açude-Ponte dam provided a passage of 165% more eels over the year prior to the installation of the fishway. The velocities of the vertical slots were maintained below 2.0 $m \cdot s^{-1}$ within the fishway and this was thought to be the primary reason for passage. The 2.0 $m \cdot s^{-1}$ is lower than the 2.4 $m \cdot s^{-1}$ found in most salmonid fishways (Mallen-Cooper & Brand, 2007). Higher velocities in salmonid fishways require more energy to pass and higher burst swim speeds than velocities found in many rivers.

Here we investigate the hydrodynamic conditions within a vertical slot passage structure under two configurations. One configuration, which we defined as control treatments, had flow in-line with the vertical slot. The other configuration, which we referred as the turbulence treatment had a turbulence-inducing wall upstream of the vertical slot that disrupted the flows linearity, similar to conditions in many vertical slot fishways, including the Bonneville Dam serpentine weir system. Our goal was to quantify the changes in hydraulic conditions, including measures of turbulence, as measures of "difficulty" for fish in passing the structure under each configuration. We also integrated these measures into a work model, which accounted for both turbulence and mean velocity. Our hydraulic data was compared to the findings in the companion study analyzing swim path and attachment time for Pacific lamprey within the flume (Kirk et al., 2015). Our experiments were located at the Adult Fish Facility (AFF) laboratory at the Bonneville Dam, on the

Columbia River, United States of America. Previous studies have shown only half (49%) of the Pacific lamprey that enter the fishway pass the dam and move upstream (Matthew L. Keefer, Caudill, Clabough, et al., 2013). The serpentine weir, a turbulence inducing vertical slot weir, has one of the lowest passage rates of any section of the dam for Pacific lamprey, but high passage rates in salmonids. Pacific lamprey are anguilliform swimmers that have the additional characteristic of an oral disc that allows the fish to attach during passage of high velocities, to climb wetted surfaces, and to attach and rest when they reach physiological exhaustion (Keefer, et al., 2010). The oral disc allows the lamprey to rest in regions of high hydrodynamic conditions.

Methods

Experiments were conducted in the experimental fishway at the Adult Fish Facility of the Bonneville Dam on the Columbia River (Washington State, USA) within an 11.6 m long, 1.2 m wide and 2.4 m high flume (Keefer et al., 2010, 2011). Experimental section within the flume was a 9 m long with a 10% slope, and had a downstream chamber, where fish could be acclimated prior to the experiments, with a removable gate, and an upstream chamber at the top of the flume with fyke nets that fish could enter but not exit. The flume was supplied with river water with a maximum discharge of 835 $L \cdot s^{-1}$. Additional details of the flume are available in Keefer et al. (2010, 2011).

The experimental section simulated a vertical slot design and allowed for manipulation of three treatment variables: (1) three velocity levels (2.4, 1.8, and 1.2 $m \cdot s^{-1}$), (2) three slot lengths (1, 0.66, 0.33 m), and two turbulence levels (a control treatment with average turbulent kinetic energy, *TKE*, of 795 $cm^2 \cdot s^{-2}$ and a turbulence treatment with

average *TKE* 1967 $cm^2 \cdot s^{-2}$), for a total of 18 treatment combinations. Velocity was manipulated by changing discharge and hydraulic head at the downstream end of the flume.

A 3-m long false floor was fixed to the bottom and placed in the middle of the flume, and three pairs of 2.44-m high weirs were placed within this experimental section. Each weir was 33-cm long and 38-cm wide and formed a 46-cm wide vertical slot that fish had to pass. The first set of weirs was permanently fixed in the false floor and represented the short slot length treatment (0.33 m) (Figure 1). The other two sets were removable in order to create the medium (0.66 m) (Figure 1) and long (1 m) (Figure 1) length treatments. Turbulence for the turbulence treatment cases was induced by adding a 2.44 m high wall projecting half-flume width from the left flume side and placed 1.5 m upstream from the weirs (Figure 1). The wall produced large, circular eddies upstream of the experiment weirs similar to those observed at the serpentine weir at Bonneville Dam fishway. Two aluminum HD-PIT antennas were custom designed to slide into the frame of the first and last set of weirs to monitor individual Pacific lamprey movements.

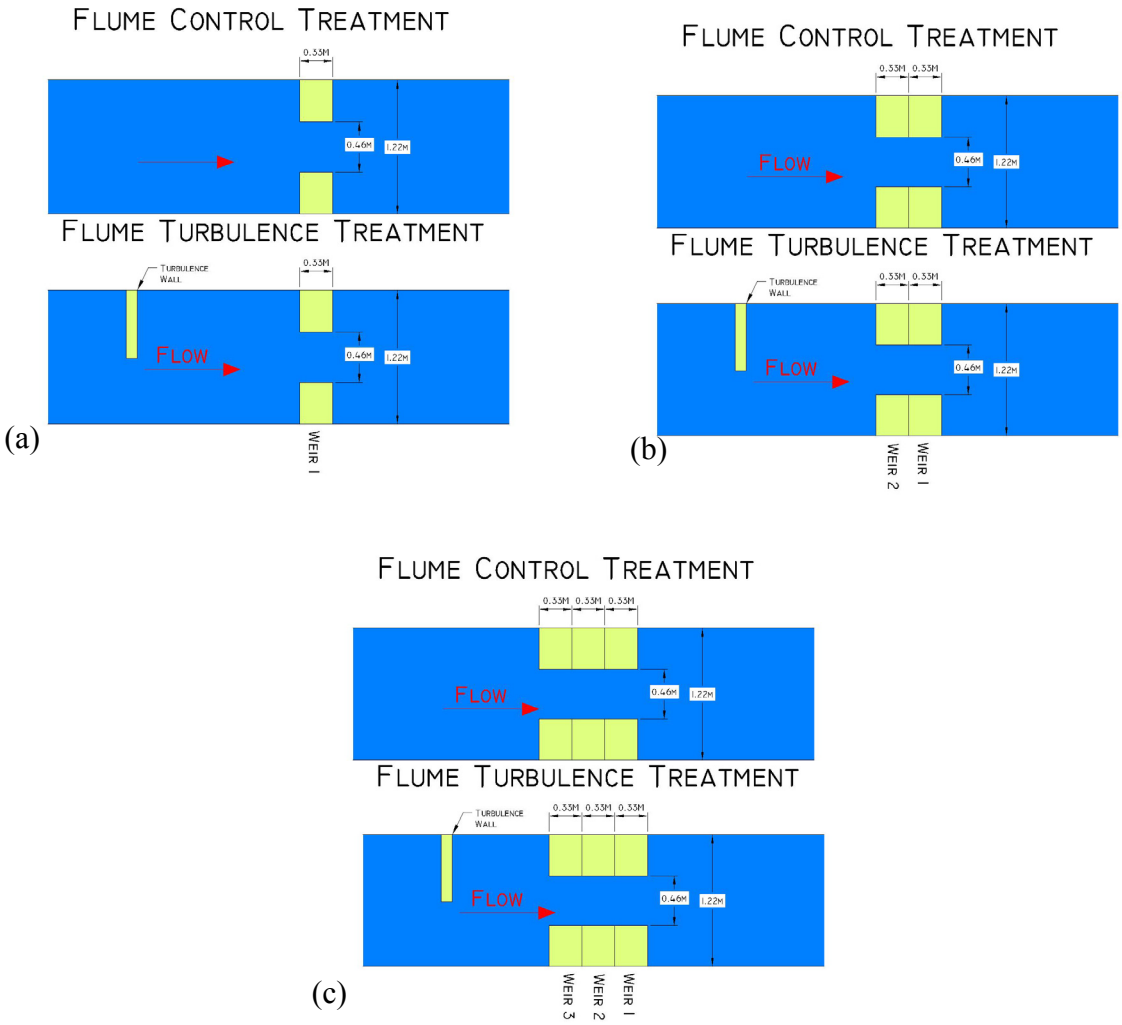

Figure 1: Experiment configuration for (a) short slot length, (b) medium slot length, (c) long slot length for the turbulence control scenario upper row and turbulent treatment scenario lower row.

Fish monitoring

Detailed monitoring of fish behavior was conducted as part of a companion study (Kirk 2015) and data on lamprey attachment times and swim paths were analyzed here in relation to hydraulics. Details and additional behavioral results are given in Kirk (2015). Briefly, we targeted at least three replicates per treatment combination to test the fish's ability to pass the slot. The movements of Pacific lamprey were recorded within the vertical slot passage structure using four underwater digital cameras (SPECO CVC-320WP IR LED

Bullet Camera) and three infrared lamps. Experiments occurred at night because Pacific lamprey are primarily nocturnal migratory fish (Matthew L. Keefer, Caudill, Peery, & Moser, 2013). One camera was positioned on the floor directly upstream and one was directly downstream of the vertical slot. These viewpoints provided a lamprey-level view that oriented across the channel into the slot weir. The other two cameras were also located directly upstream and downstream of the vertical slot, but were positioned 0.75 m above the flume floor and provided a top-down view across the channel. Placement of the camera's allowed for full coverage of lamprey activity within the vertical slot, as well as ~ 0.5 m upstream and downstream.

Video and HD-PIT data were used to quantify six elements of Pacific lamprey performance and behavior; two at the trial-level and approach time, attachment time, and total passage time at the individual level. Success was defined as the number of unique lamprey that passed the experimental weirs divided by the number of unique lamprey that approached the weirs in each trial. Individuals that never approached the experimental weirs were censored from further analyses. Attachment time was defined as the total time individual fish spent attached to a surface in the experimental weirs and was associated with the time spent passing the weirs. The swim paths to pass the slot were defined from observation of lamprey behavior for all 18 scenarios.

Hydraulic measurements

A SonTek 16 MHz Micro Acoustic Doppler Velocimeter (ADV) with 50 Hz sampling rate was used to measure velocity and turbulence magnitude and direction within the test flume (Figure 2). The ADV measures the flow field at a distance 5 cm from transducers with a 0.4 cm diameter and 0.45 cm high cylinder. It was mounted to the *z*-axis

of 3-axis robot, which was controlled with MACH3 CNC software and automated to collect the measurements. Each measurement consisted of 4,000 to 4,500 samples, which were sufficient to stabilize the moments of the turbulence fluctuations and with 1% average velocity accuracy. Thirty-three measurements were taken at three different elevations at 0, 0.3 and 0.65 m from the bottom of the flume, for a total of 99 measurements per scenario (Figure 3).

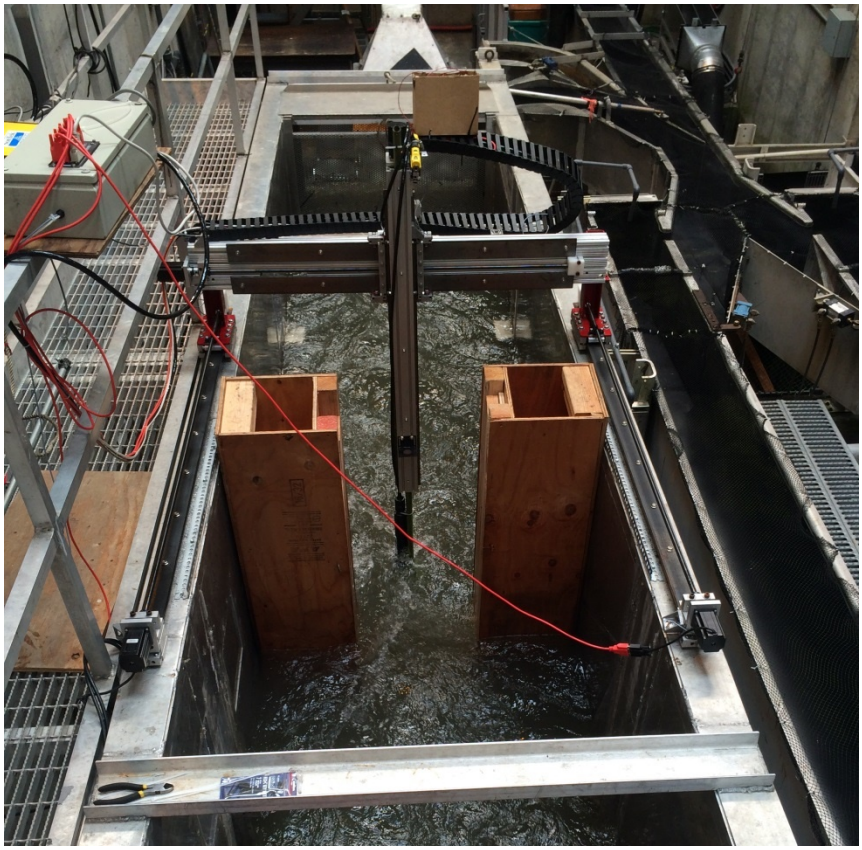

Figure 2: ADV with short slot length control treatment

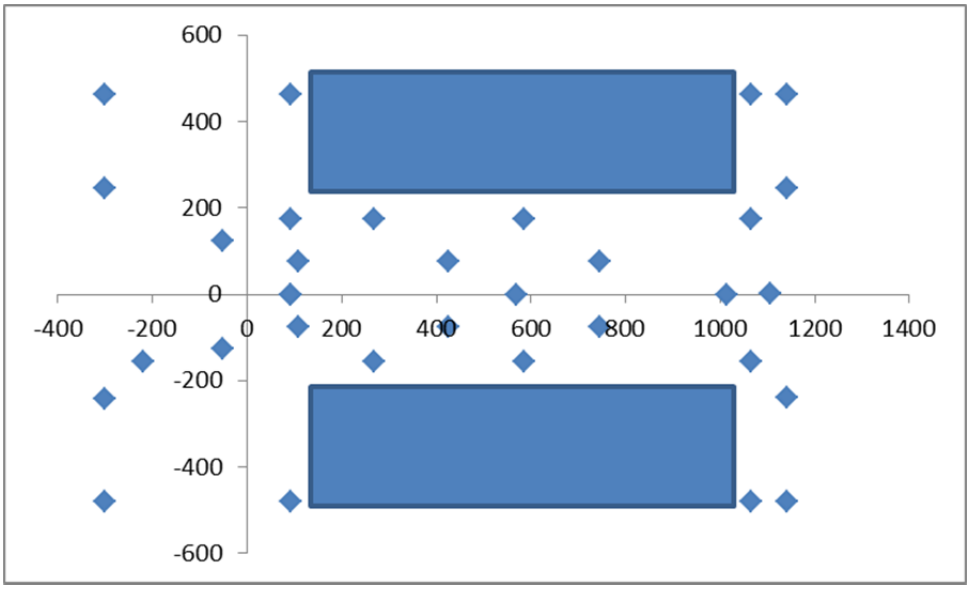

Figure 3: Measurement locations at each elevation

Data processing

The data was processed using the WinADV software and despiked with a phase-threshold relationship following the work of Goring & Nikora (2002) as modified in Wahl , (2000). Instantaneous velocities were analyzed in their three component vectors, *u, v, w* along *x*, *y*, *z* axis respectively, with *z* the vertical axis and with the Reynolds decomposition, $u=\bar{u}+u'$, $v=\bar{v}+v'$, $w=\bar{w}+w'$, where $\bar{u}$, $\bar{v}$, and $\bar{w}$ are the mean velocities averaged over the turbulence time scale (Eq. 1), and u', v', w' are their fluctuations. Velocity magnitude, *V*, and standard deviation, σ, (root mean square fluctuation) of the velocity components were quantified with the following equations:

$$\bar{i} = \frac{\sum i}{n} \quad where\ i=u,\ v,\ and\ w \tag{1}$$

$$V = \sqrt{\bar{u}^2 + \bar{v}^2 + \bar{w}^2} \tag{2}$$

$$\sigma_i = \sqrt{\frac{\sum (i - \bar{i})^2}{n-1}} \quad where\ \ i = u, v\ and\ w \tag{3}$$

Turbulence intensity (Lacey et al., 2012) were quantified as

$$I_i = \frac{\sigma_i}{U} \quad \textit{where i=u, v, and w} \tag{4}$$

where U is the mean flow velocity through the slot, turbulent kinetic energy, *TKE* (Lacey et al., 2012):

$$TKE = 0.5(\sigma_u^2 + \sigma_v^2 + \sigma_w^2) \tag{5}$$

We proposed to define a new biologically meaningful turbulent intensity, which we quantified as the ratio between the root mean of the *TKE* and the velocity that lamprey have been observed attaching:

$$I_{Bio} = \frac{\sqrt{TKE}}{U_{Bio}} \quad \textit{where } U_{Bio}\textit{=1.8 m·s}^{-1}\textit{ for Pacific lamprey} \tag{6}$$

This provides the turbulence intensity scaled by the average velocity for which lamprey initiate saltation. We expect that we can redefine this index for other aquatic species by using any suitable velocity that induces threshold response in behavior.

We also quantified Reynolds shear stresses (Goodwin, 2004)

$$\tau_{uv} = -\rho\overline{u'v'} \tag{7}$$

where ρ is the fluid density, in this case water.

Mathworks MATLAB software was used to interpolate a 30 by 30 point grid to create contour maps for $\overline{u}$, $\overline{v}$, $\overline{w}$, σ_u, σ_v, σ_w, I_u, I_v, I_w, and *TKE*, which were used to interpret fish swimming behavior in the slot using data from the 99 measurement points per treatment combination.

We estimated the easiest path by implementing a simulated path algorithm that assumes Pacific lamprey always move upstream and select the smallest value of the hydraulic quantity of the nearby cells. For each metric evaluated for the easiest path

(average velocity, TKE, power, and work), the algorithm ran all possible options where the first cell is chosen and the 2 cells to the right, the forward cell, and the 2 cells to the left are evaluated to find the lowest value. This repeats from that cell until the flume traverse is completed. This is completed for every possible path and the path with the lowest possible value is the "easy path". The sum of the values from the simulated path algorithm was used to calculate the total of each metric evaluated to swim through the flume.

To analyze the effort required for a fish to travel through the flume we calculated the power used by the lamprey passing the vertical slot with the equation proposed in the work of McElroy et al. (2012):

$$P = \frac{1}{2}\rho C_D S\left[\frac{d}{t}\cos\theta + V\right]^3 \quad (8)$$

where C_D (0.0077) is the drag coefficient induced by the fish shape, S is the surface area of an average size adult fish (0.074 m^2), d is the distance traveled (m), t is the time to pass through the slot (s), θ is the angle between the fish path direction and the flow direction, and V is the water velocity (m/s).

We also proposed a work equation, W, which incorporates both turbulence and mean velocity:

$$W = \int \sqrt{TKE} + V \; dx \quad (9)$$

where dx is the infinitesimal distance traveled by the fish within the flume.

Turbulence periodicity was estimated using a Fast Fourier Transform (FFT) at several points within the flume. Orientation and scale of turbulence eddies were qualitatively assessed within the flume during measurements.

In our analysis of the fish swimming paths we chose to focus on the hydrodynamics of the flow near the bottom of our experimental flume for Pacific lamprey because lamprey generally swim near the bottom of structures in areas of high velocity and have a 2-dimensional swim path.

Results

The turbulence-inducing wall increased heterogeneity of both velocity and turbulence besides increasing turbulence magnitude. The average velocity was higher in the downstream section of the vertical slot for the control treatment but in the upstream section for the turbulence treatment. The turbulence follows the same pattern of being higher at the downstream end of the slot for all treatments and elevations for all calculated turbulence metrics (TKE, Root Mean TKE Normalized by Lamprey Saltation Velocity, TKE Normalized by the Velocity at the Upstream end of the Slot). The turbulence was approximately the same at the upstream and downstream end for the turbulence treatments and the turbulence at the downstream end is approximately 4 times that of the upstream end for the control treatment. Table 1 summarizes the spatially averaged variables measured for the 18 scenarios at the downstream (D/S) and upstream (U/S) ends of the slot near the bottom of the flume.

Table 1: Summary of measurements within the flume slot at the floor level, with D/S is downstream end, and U/S upstream end of the slot

Hydraulic quantity	Location	Control Treatment	Turbulence Treatment
Turbulent Kinetic Energy, k ($cm^2 \cdot s^{-2}$)	D/S	1326.05	2959.65
	U/S	321.78	2084.65
Root Mean TKE, k	D/S	7.37	16.44
Normalized by 180 cm/s	U/S	1.79	11.58
Turbulent Kinetic Energy, k ($cm \cdot s^{-1}$)	D/S	23.91	36.84
Normalized by Entrance Velocity	U/S	4.50	28.11
Average Velocity, Vavg ($cm \cdot s^{-1}$)	D/S	70.85	44.52
	U/S	59.49	89.79
x-component of Velocity, Vx ($cm \cdot s^{-1}$)	D/S	-39.93	-54.91
Positive is D/S	U/S	-47.51	-20.98
y-component of Velocity, Vy ($cm \cdot s^{-1}$)	D/S	-7.63	-16.87
Positive is up on plots	U/S	-6.40	-53.45
z-component of Velocity, Vz ($cm \cdot s^{-1}$)	D/S	2.82	3.89
Positive is towards bottom	U/S	1.54	3.02
x-component of Turbulence Intensity	D/S	0.46	0.93
	U/S	0.18	0.80
y-component of Turbulence Intensity	D/S	0.31	0.66
	U/S	0.19	0.39
z-component of Turbulence Intensity	D/S	0.13	0.20
	U/S	0.07	0.15
Reynolds Stress	D/S	21.42	44.76
	U/S	41.87	122.71

Table 2: Summary of measurements within the flume slot at 0.3 m and 0.65m above the floor with D/S is downstream end, and U/S upstream end of the slot

Hydraulic quantity	**Location**	**Control Treatment @ 0.3m**	**Turbulence Treatment @ 0.3m**	**Control Treatment @ 0.65 m**	**Turbulence Treatment @ 0.65 m**
Turbulent Kinetic Energy, TKE ($cm^2 \cdot s^{-2}$)	D/S	1380.48	2506.00	1053.40	2805.66
	U/S	382.58	2430.60	225.94	3116.71
Root Mean TKE, k	D/S	7.67	13.92	5.85	15.59
Normalized by 180 cm/s	U/S	2.13	13.50	1.26	17.32
Turbulent Kinetic Energy, k ($cm \cdot s^{-1}$)	D/S	21.16	37.68	14.80	48.14
Normalized by Entrance Velocity	U/S	5.06	38.17	2.89	56.88
Average Velocity, Vavg ($cm \cdot s^{-1}$)	D/S	76.81	56.83	86.45	53.78
	U/S	64.88	78.16	74.08	69.11
x-component of Velocity, Vx ($cm \cdot s^{-1}$)	D/S	53.13	28.36	55.24	28.45
	U/S	59.14	-2.25	65.76	6.53

Velocity

The velocity field near the bottom of the flume was more homogenous for most, but not all scenarios for the control (Figure 4) than turbulence treatment (Figure 5). The average velocity was highest near the middle of the slot for the control treatment, but at the upstream end of the slot near the wall of the slot for the turbulence treatment. The turbulence-inducing wall created an eddy at the upstream end of the slot and the resultant of the three components is much higher than in the control treatment, where $\bar{u}$ was by-far the largest component of V. The eddy varied the flow similarly for the other 2 water depths (0.30 and 0.65 m) (figures in Appendix).

The x-component of the velocity, $\bar{u}$, is highest at the upstream end for many of the control treatments and more consistently at the downstream end for the turbulence treatment. The turbulence-inducing wall created a vertical-axis eddy that primarily varies the flow in the y-direction, $\bar{v}$, with minimal variation in the z-direction, $\bar{w}$ (Figure 6). The x-component

of the velocity has an area where it recirculates near the bottom of the flume creating flow fields that move upstream in the flume. The $\bar{u}$ recirculation only occurs near the bottom of the flume. Additional contour plots are included in the appendix.

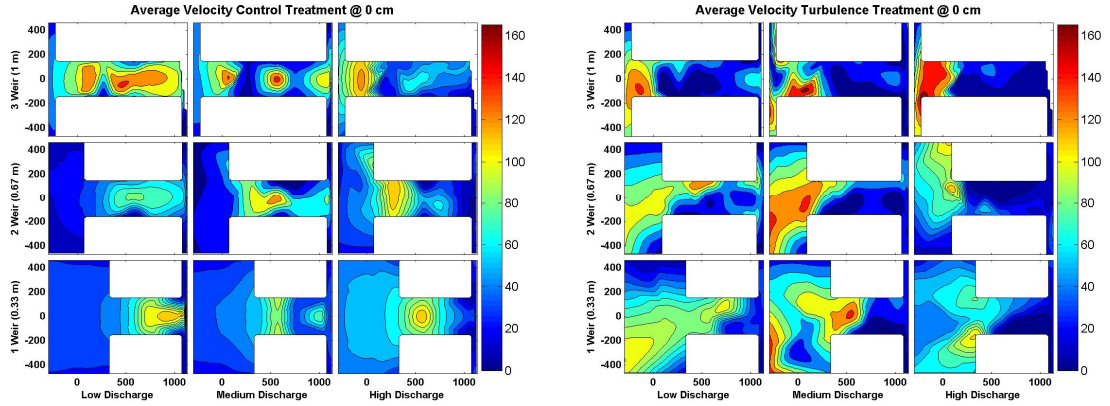

Figure 4: Contour plots of average velocity ($cm \cdot s^{-1}$) for the control treatment and turbulence treatment for each slot discharge and length treatments at 0 cm from the floor. Bulk flow direction is left to right.

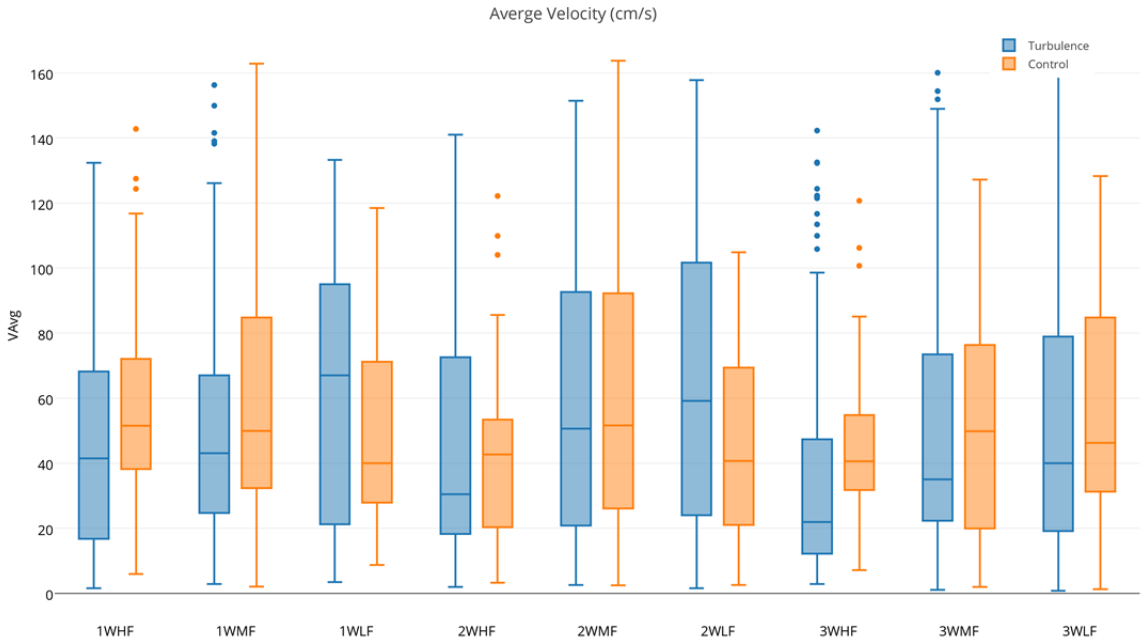

Figure 5: Box plot of average velocity for the control treatment and turbulence treatment for each slot discharge and length treatments. First two characters represent slot length and last two represent discharge. (Low, Medium, High)

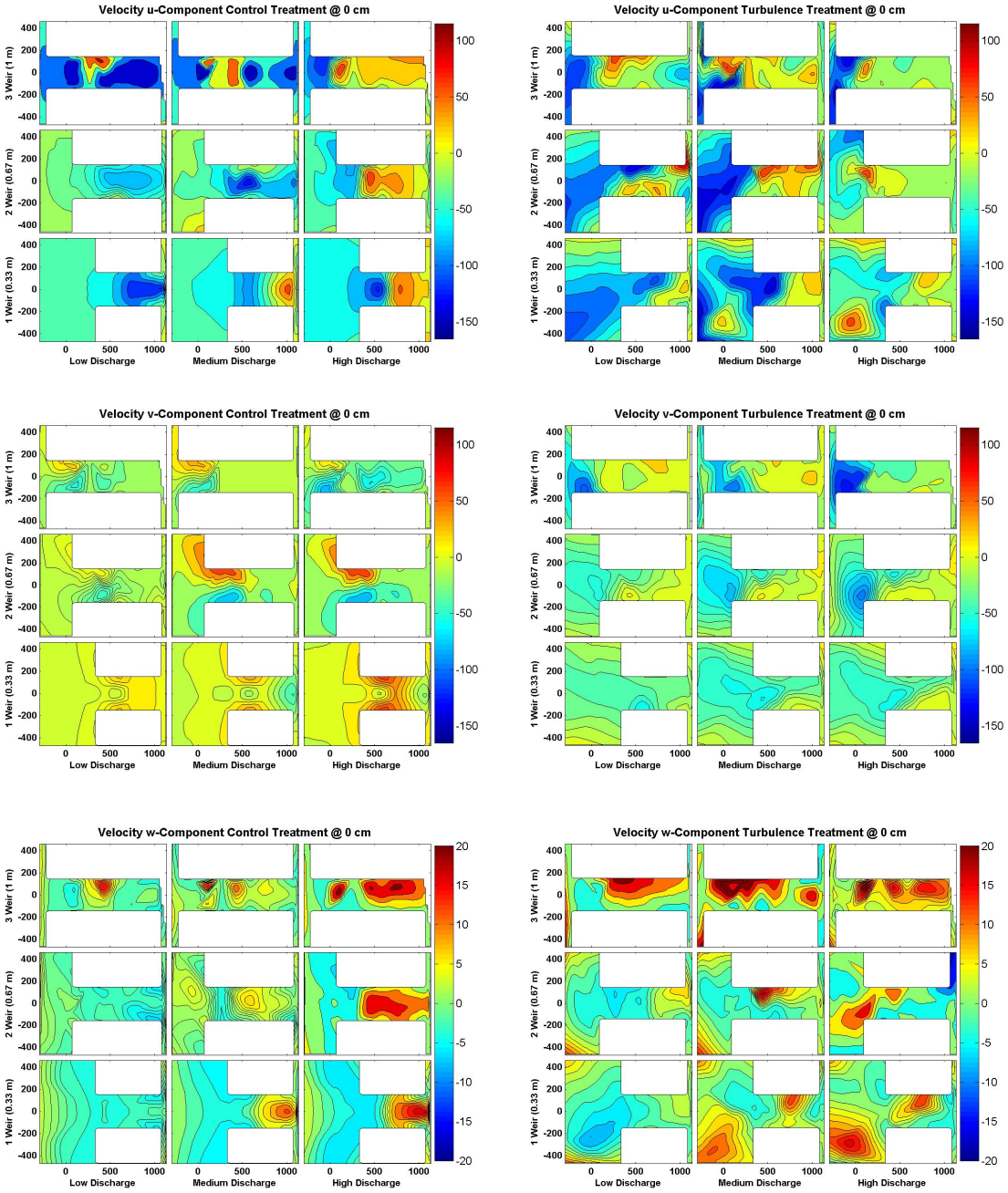

Figure 6: Contour plots of velocity, u, v, w (flow, lateral, vertical) for the control treatment (left panel) and turbulence treatment (right panel) for each slot discharge and length treatments at 0 cm from the floor. Bulk flow direction is left to right.

Root-Mean Square of the turbulent velocity fluctuations, σ_i

The largest turbulence standard deviation from the mean is in the *x*-direction for both the control and turbulence treatments. The control treatments have nearly zero fluctuation in

the *y*- and *z*-directions (Figure 7). Increases in discharge caused higher velocity fluctuations within the slot at all three elevations of measurement. Longer slot lengths did create more velocity fluctuations with a few exceptions. Patterns and magnitude are similar at the other two depths, whose contour plots are included in the additional materials.

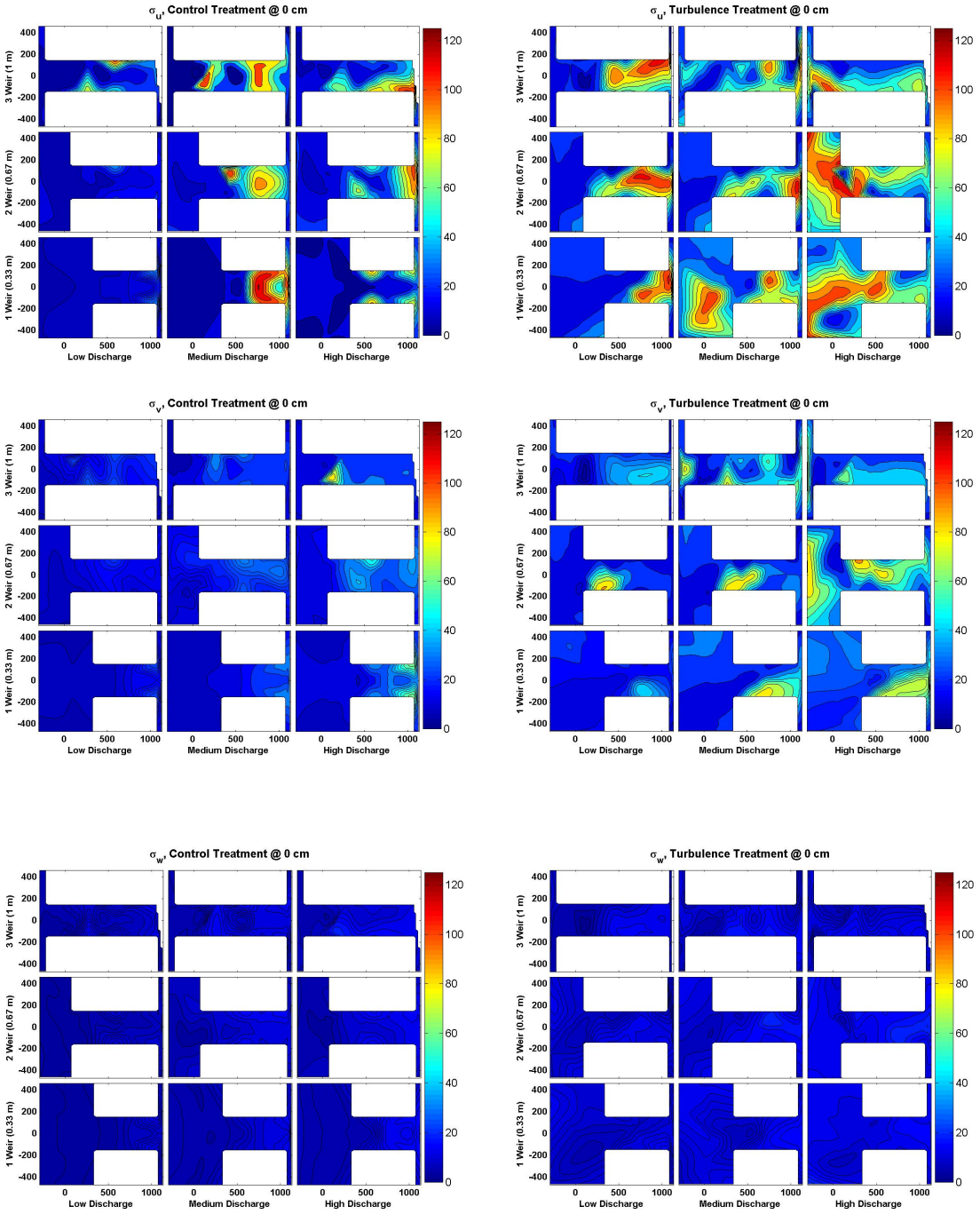

Figure 7: Contour plots of the Root-Mean Square of the turbulent velocity fluctuations, σ_u, σ_v, and σ_w, for the control treatment (left panel) and turbulence treatment (right panel) for each slot discharge and length treatments at 0 cm from the floor. Bulk flow direction is left to right.

Turbulence intensity

The mean *x*-component of the turbulence intensity, I_u, was much lower for the control than the turbulence treatment (Figure 8) and larger at the upstream end of the slot with the introduction of the turbulence-inducing wall than without it. The turbulence-inducing wall increases the turbulence intensity at the wall of the slot. The *y*- and *z*-components follow similar patterns as in the turbulence fluctuations for all 3 depths. Contour plots at 0.3 and 0.65 m are included in the additional materials.

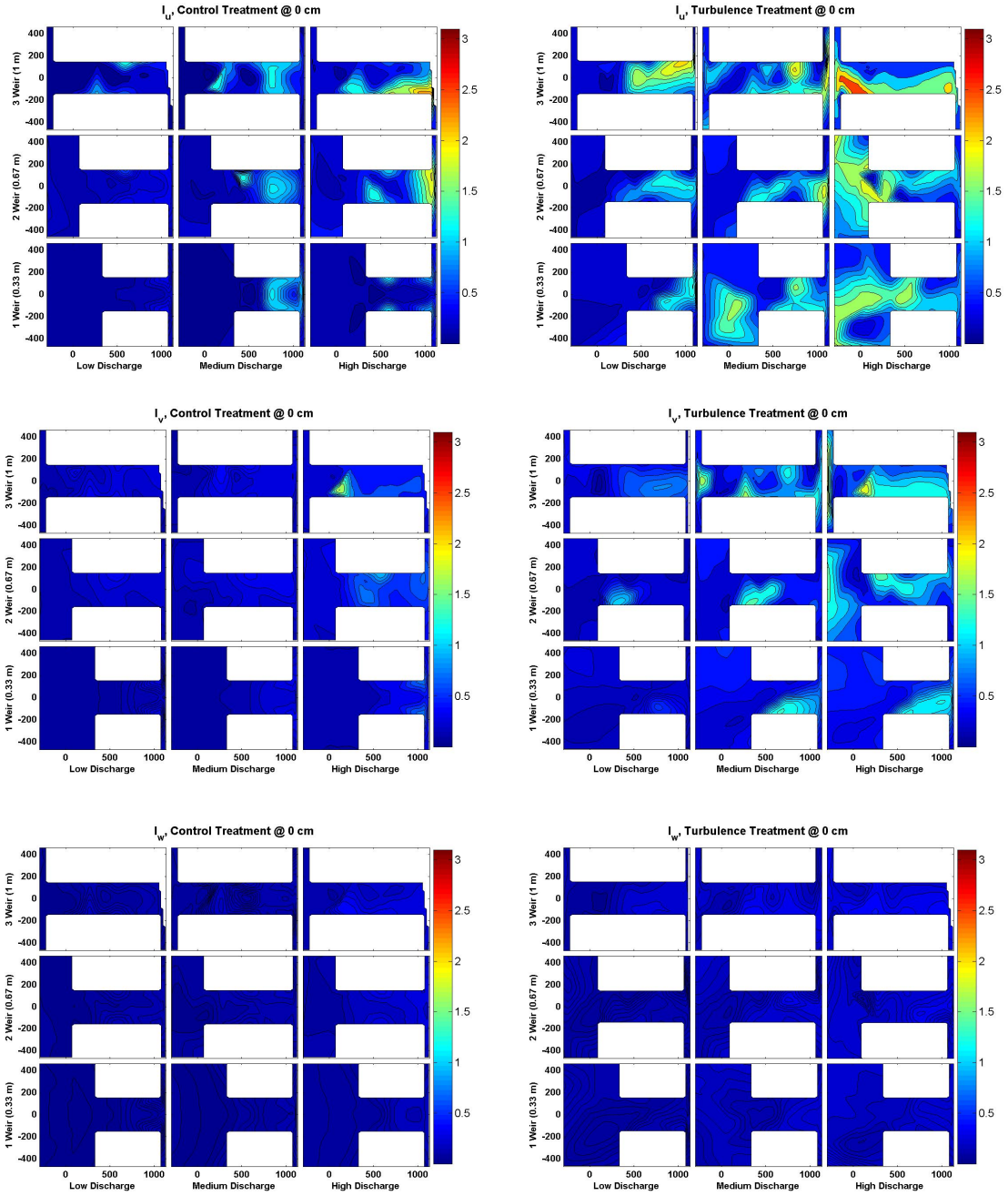

Figure 8: Contour plots of the *x*, *y*, and *z*- component of the turbulence intensity, I_u, I_v, I_w, for the control treatment (left panel) and turbulence treatment (right panel) for each slot discharge and length treatments. Bulk flow direction is left to right.

Reynolds shear stresses

Reynolds shear stresses do not appear to have a clear pattern through the varying treatments, scenarios, or depths (Figure 9). The increase in shear stress created by the

turbulence-inducing wall is shown in the upstream end of the slot. The shear stress is higher in the downstream end of the slot for the control treatment and the upstream end in the turbulence treatment. Increases in discharge increase the Reynolds shear stresses.

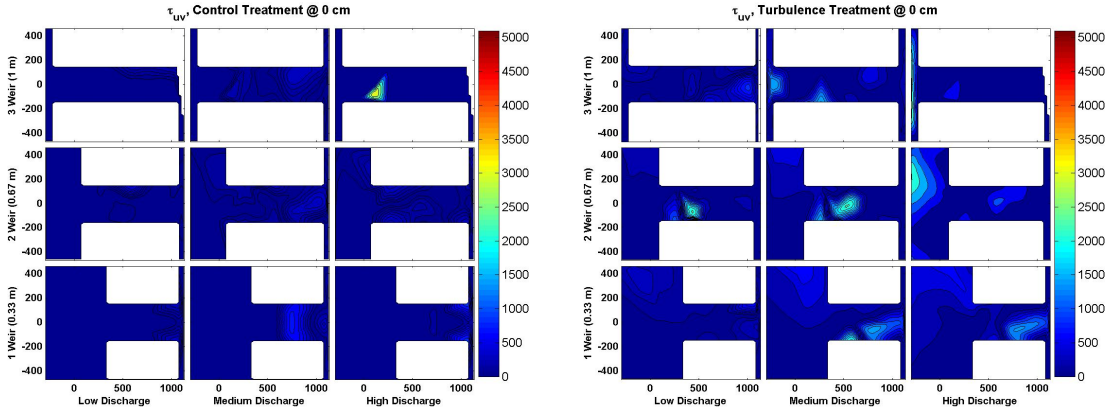

Figure 9: Contour plots of Reynolds Shear Stress, τ, for the control treatment and turbulence treatment for each slot discharge and length treatments. Bulk flow direction is left to right.

Turbulent Kinetic Energy

The turbulent kinetic energy, *TKE*, presents patterns similar to that of I_u. The *TKE* at the bottom of the flume increases at higher discharge and longer treatment lengths (Figure 10). The area of higher *TKE* shifts from the downstream end of the slot in the control treatment to the upstream end in the turbulence treatment. This shift is due to the large vertical eddy created by the turbulence-inducing wall. A similar pattern is found at the 0.3-m and 0.65-m depths from the bottom of the flume (Figures in supplemental material). *TKE* distribution was more heterogeneous for all scenarios of the turbulent than control treatments (Figure 11). We selected *TKE* as the best metric of turbulence for our evaluation of swim paths within the flume because it accounts for the variation in velocity in all three directions.

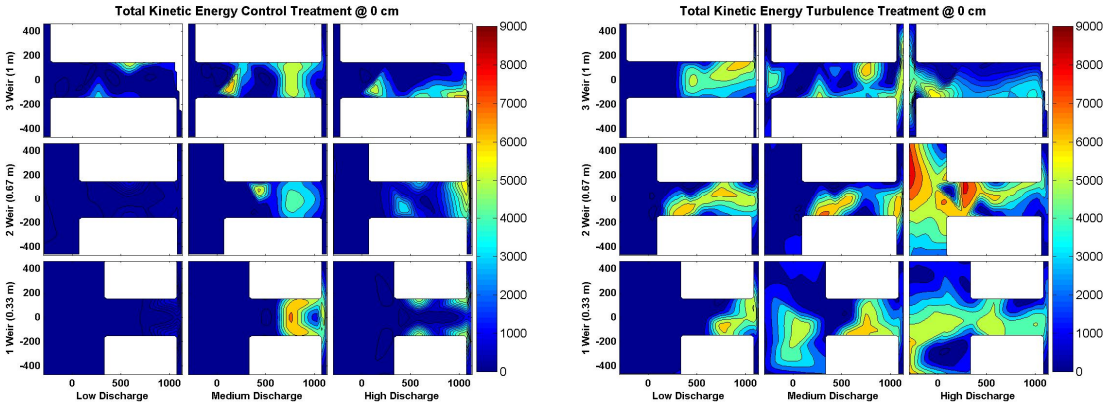

Figure 10: Contour plots of turbulent kinetic energy, *TKE,* for the control treatment and turbulence treatment for each slot discharge and length treatments. Bulk flow direction is left to right.

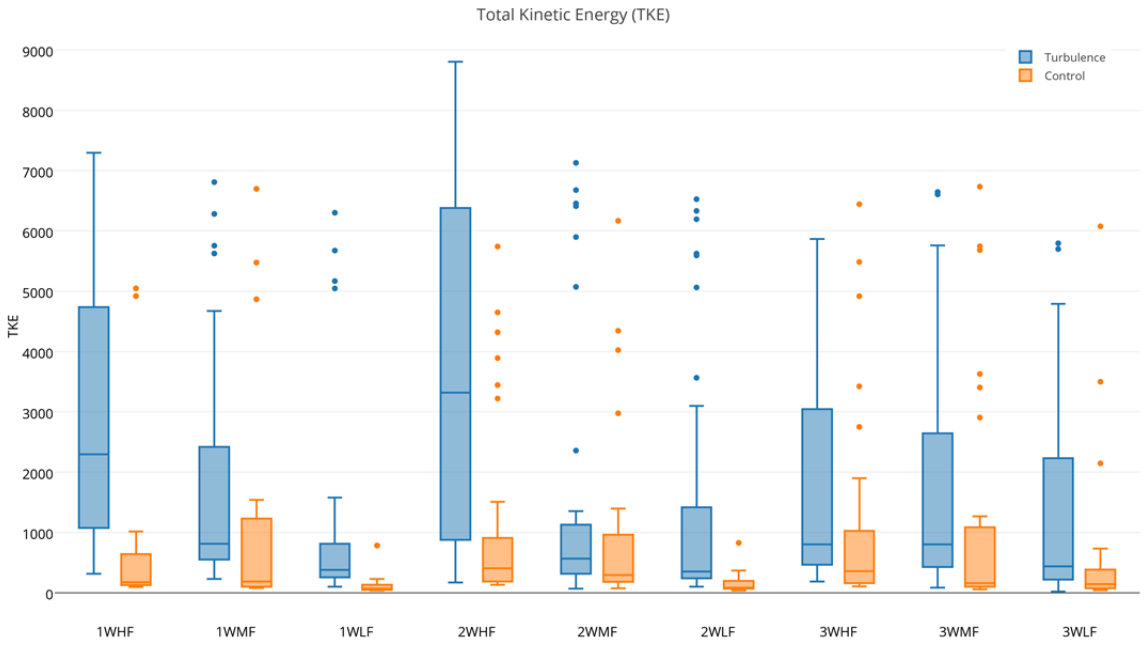

Figure 11: Box plot of *TKE* for the control treatment and turbulence treatment for each slot velocity and length treatments. First two characters represent slot length and last two represent discharge. (Low, Medium, High)

Normalized Root Mean TKE

The ratio of the root of the TKE to the velocity that saltation of lamprey has been observed (1.8 m/s) follows the same pattern as TKE alone. The value provides an important metric of a unitless turbulence (Figure 12).

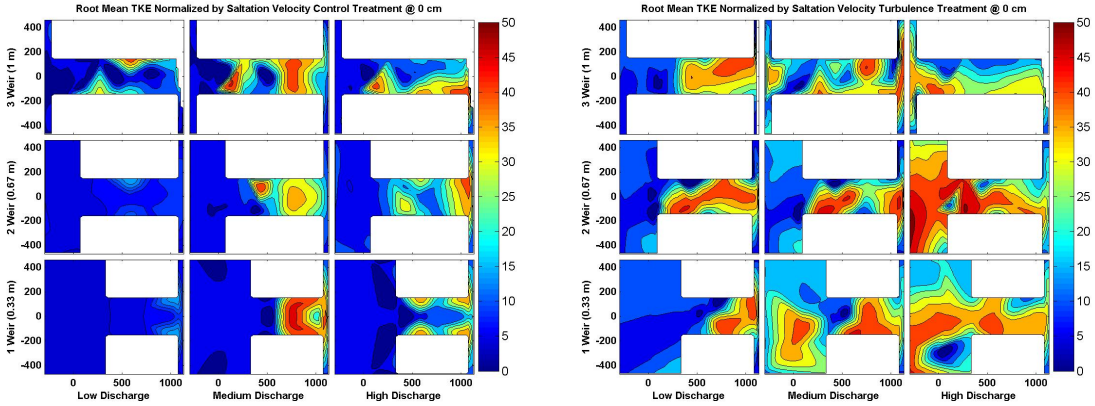

Figure 12: Contour plots of the ratio of the root of turbulent kinetic energy, *TKE,* to the lamprey saltation velocity for the control treatment and turbulence treatment for each slot discharge and length treatments. Bulk flow direction is left to right.

Turbulence periodicity, orientation, and scale

The Fast Fourier Transform (FFT) analysis did not find a dominant frequency in any location within the slot regardless of treatment. We observed secondary flow eddies at the entrance and exit of the vertical slot within the control treatment. The turbulence-inducing wall created a large eddy at the upstream end of the slot that rotated counterclockwise extending the entire width of the slot, ~0.46m, throughout all of the turbulence treatments in addition to the secondary flow eddies.

Power required to travel through the vertical slot

The power required to travel through the slot on the path of least resistance increased by an order of magnitude across treatment and ranged from 7,539 $g \cdot cm^{-2} \cdot s^{-3}$ in the medium-length low-discharge control treatment to 76,186 $g \cdot cm^{-2} \cdot s^{-3}$ in the long-length high-discharge turbulence treatment.

Work required to travel upstream through the vertical slot

The work required to travel the path of least work ranged from 63,444 $cm^2 \cdot s^{-2}$ in the medium length low discharge control treatment to 138,326 $cm^2 \cdot s^{-2}$ in the medium length medium discharge turbulence treatment.

Relationship of Attachment Time

Nearly all Pacific lamprey used within trials successfully passed the vertical slot as reported in the work of Kirk et al., 2015 and passage success did not provide a good metric for comparison. The most significant difference among treatments was the attachment time and the path location within the flume. Quantitatively, the lamprey attached in most instances at the upstream end of the slot in the high discharge simulations. This was more evident with the high discharge and turbulence treatment. In the other discharges, the lampreys did not have a clear pattern of attachment location. The measured attachment times were compared to average velocity, turbulent kinetic energy, root mean *TKE* normalized by saltation velocity, power, and work. Values of the correlation coefficient, R^2, were 0.07 for average velocity, 0.06 for *TKE*, 0.03 for power, and 0.18 for work. The attachment time provides a predictor of the amount of energy expended within the vertical slot since the Pacific lamprey attach once they reach physical exhaustion.

There was no association between attachment time recorded for Pacific lamprey and the power required to travel through the flume on the path of least resistance (Eq. 8). (Figure 13; Eq. 8; two-way ANOVA $P_{power} = 0.517$; $P_{treatment} = 0.554$; $P_{powerXtreatment} = 0.481$)

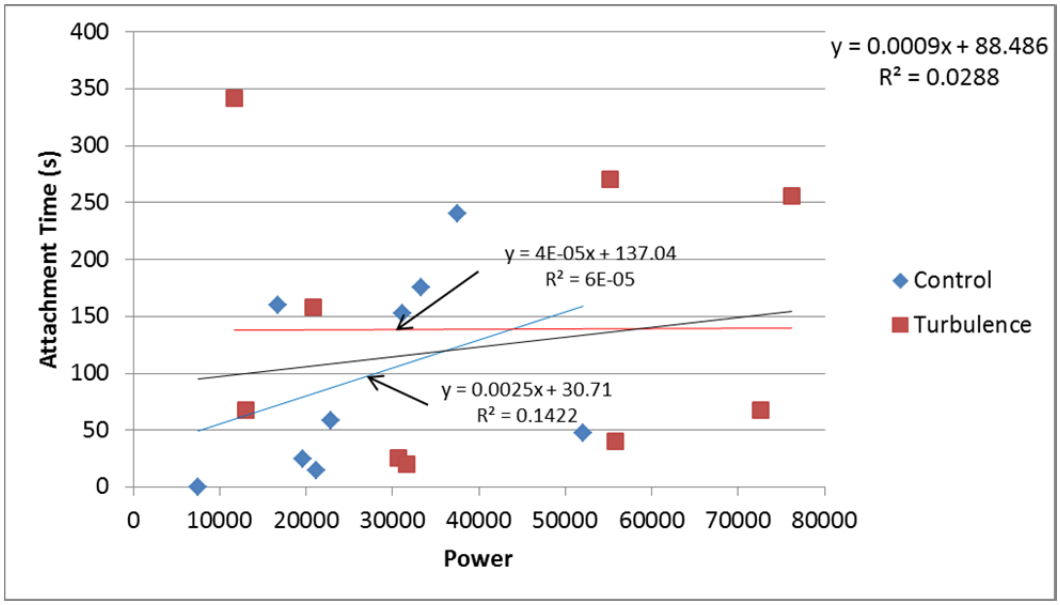

Figure 13: Correlation between attachment time and power required to travel through the path of least resistance Eq. 8.

There was some evidence of a relationship between attachment time and estimated work to move through the slot along the path of least resistance (Two-way ANOVA P_{work} = 0.094; $P_{treatment}$ = 0.913; $P_{workXtreatment}$= 0.510; Figure 14).

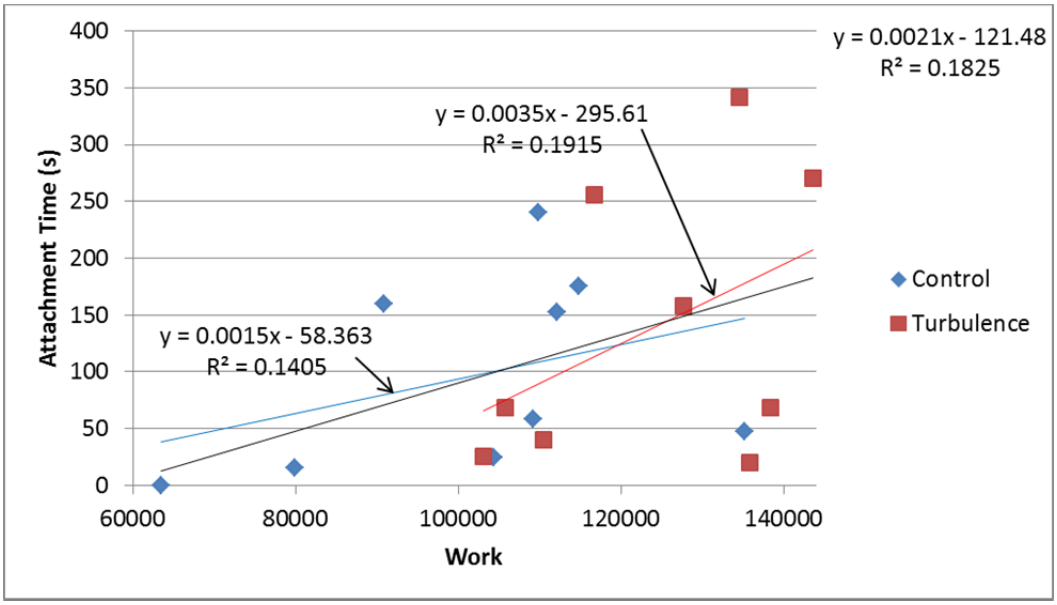

Figure 14: Attachment time correlation to work, Eq. 9, required traveling through the path of least resistance.

The association between attachment time and normalized TKE was highly significant and stronger than for work or power (Two-way ANOVA $P_{NTKE} = 0.009$; $P_{treatment} = 0.113$; $P_{NTKEXtreatment} = 0.850$; Figure 15). Notably, the treatment and control conditions were nearly discontinuous, but there was no evidence that the relationship differed within treatment or control condition (i.e., test for differences in intercept and slopes had $P > 0.05$).

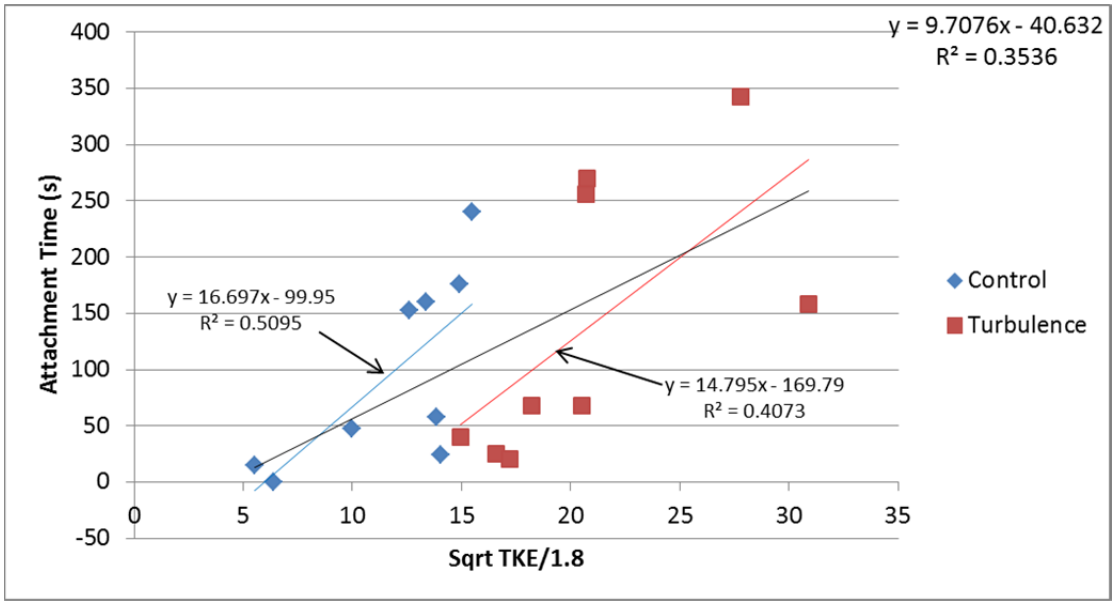

Figure 15: Attachment time correlation to Normalized Root Mean of TKE, Eq. 6, required traveling through the path of least resistance.

The normalized TKE provides the highest correlation coefficient to attachment time over all of the flow scenarios. This metric provided the best fit and thus may be the most biologically important metric of lamprey behavior.

Swim Path Prediction

The path analysis algorithm was computed for average velocity, total kinetic energy, and our work equation. The algorithm mostly predicts that the path of least resistance for velocity and turbulence will be near the walls of the flume. The path is not always on the

same wall for turbulence or velocity. The work equation incorporates both velocity and turbulence to find the path of least resistance. It appears that at low discharges turbulence does not affect fish path and at higher discharges turbulence becomes the control in the work equation (Figure 16).

These swim paths were compared to actual observed swim paths for Pacific lamprey (Kirk et al., 2015). Velocity appears to be a good predictor of Pacific lamprey swim path for the low velocity and low turbulence scenarios. Once the velocity becomes higher or the turbulence is increased, the turbulence appears to be the best predictor of swim paths. Of the variables we evaluated, the work equation we developed incorporates this apparent threshold that was observed at bulk velocities greater than 1.2 m/s the turbulence becomes high and becomes the control for the Pacific lamprey and would be the best final predictor of swim paths.

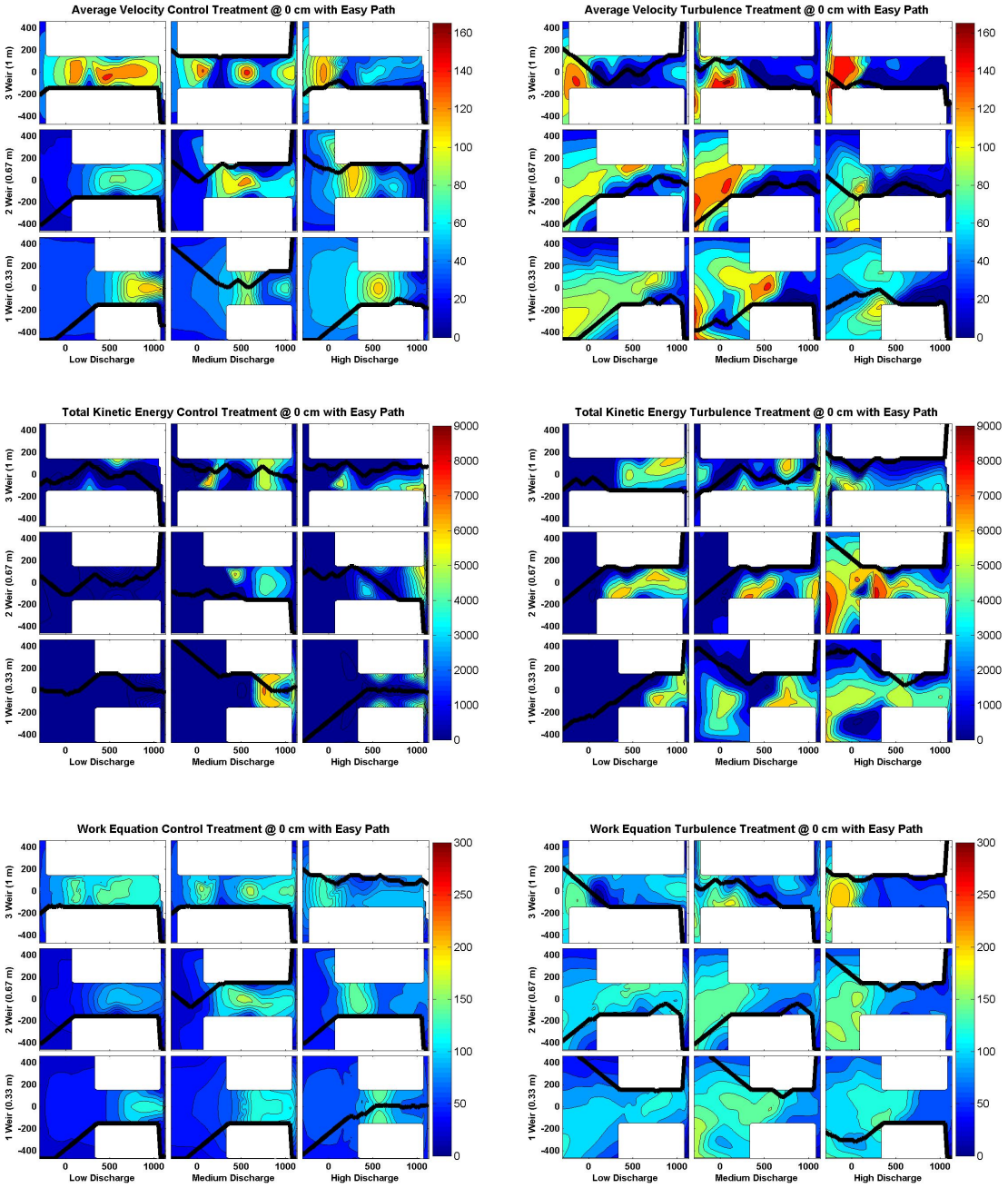

Figure 16: Contour plots of the easy path analysis (Average Velocity, TKE, and Work) for the control treatment (left panel) and turbulence treatment (right panel) for each slot discharge and length treatments at 0 cm from the floor.

Discussion

The introduction of the turbulence-inducing wall altered the flow field for all scenarios. For all of the hydrodynamic measured and calculated variables, the higher values were at the downstream end or middle of the slot for the control treatment. The higher values moved to the upstream end of the slot near one of the walls once the turbulence inducing wall was installed. The location of the higher values would move up or downstream depending on the location of the wall, but the concentration of high values would remain. The flow field had values of an order of magnitude higher with the turbulence-inducing wall installed than without. This shift in higher values occurred at all three (0, 0.3 and 0.65 m from the flume bottom) elevations. The change in location of the higher velocity and turbulence may hinder passage of some fish species. Vertical slot fishways that are parallel to the flow, as our control case without the turbulence-inducing wall, allow fish to burst through the most difficult hydrodynamic condition and the end of the passage at the upstream end of the slot has easier conditions to traverse. The turbulence-inducing wall may fatigue the fish and prevent them from completing passage due to the increasing turbulence through the slot (Theodore Castro-Santos et al., 2009). The 90 degree flow change that is simulated by the turbulence-inducing wall occurs within the serpentine section of the fishway at the Bonneville Dam (Matthew L. Keefer, Caudill, Clabough, et al., 2013) and other fishways throughout the world (Vianney-Legendre Vertical Slot Fishway, Quebec, Canada; Sariakandi Fishway, India; Charles River Dam, Massachusetts; Rainbow Dam, Connecticut).

At low discharge (1.2 $m \cdot s^{-1}$ bulk velocity), the turbulence-inducing wall does not create the higher velocities and turbulence observed at medium (1.8 $m \cdot s^{-1}$ bulk velocity) and

high (2.4 $m \cdot s^{-1}$ bulk velocity) discharges. Low discharges within in fishway areas that are not required to have attraction flows for salmonids, but where some velocity is needed for guidance (~1-1.5 $m \cdot s^{-1}$), do not appear to prevent the passage of non-salmonids (Matthew L. Keefer, Caudill, Clabough, et al., 2013). We measured velocities greater than 2.2 $m \cdot s^{-1}$ throughout the Bonneville serpentine weir. Passage on the River Mondego in Portugal seems to validate that low discharges no matter the turbulence provides good passage for all species (Mateus et al., 2015).

The flume conditions were very noisy (Doppler Noise) and turbulent during our measurements. The Signal to Noise Ratio (SNR) ranged from 5 dB to 26 dB in all of the treatments. Most of the measurements had SNR greater than 15 dB and is considered acceptable for high frequency velocity measurements (Sontek, 1997). The correlation coefficient for the ADV beams was below 60% in nearly all conditions. The ADV was tested at very low flow and the SNR was greater than 30 dB with correlation coefficients higher than 80% prior to every day's experiments. The measured values of SNR and Confidence interval were not as good as we would have liked, but were not unexpected given the observed turbulent conditions found in our flume and in the serpentine fishway.

With definite limitations, our work equation and root of *TKE* normalized by the observed saltation velocity provides a good predictor of the difficulty to travel through a fishway for Pacific lamprey. Our work equation has a weak relationship to attachment time with a correlation coefficient of 0.18, but better with the normalized root mean of TKE, 0.35, for our evaluation with attachment time length of Pacific lamprey. The correlation to turbulence, velocity, and power through the slot were an order of magnitude less and did not appear to follow a clear trend. It is logical that with increased work required to travel

through the slot, the attachment time of the lamprey increases. The root mean of the turbulence normalized by saltation velocity provides a metric of when the variation of velocity reaches the velocity at which lamprey begin saltation. Measurements taken along precise paths taken by fish will likely show that work provides a better metric of attachment time.

Other unmeasured factors such as sensory cues and prior experience likely contributed to the observed variation in attachment time that was not accounted for using work alone. In their study, the energy analysis proposed by Guiny et al., 2005 was not a good predictor of swim path due to the complexities of the equations. McElroy et al., (2012) had similar results with their cost based equation. Neither of these studies incorporates turbulence into their equations. The addition of turbulence adds a complexity to the swim path analysis that is challenging to quantify. A decision must be made of how intensity is calculated, and if the other metrics such as scale will be incorporated (Lacey et al., 2012). After review of standard deviation of velocity, turbulence intensity, Reynolds shear stresses, and *TKE* all of the intensity values followed a similar trend. We chose *TKE* to quantify intensity because it incorporates turbulence in all three directions. Although our work equation is simple, it may provide an additional metric for fish path analysis in otherwise challenging hydrodynamic conditions and overall we recommend a multivariate approach. Further, behavior of fish will be limited by the sensory information available to them, and while our minimum path model attempts to account for this, whether lamprey or other fish have sufficient information to follow optimal paths in reality is unknown. Additionally, observed versus optimal paths likely deviate in part because we estimated optimal paths based on time-averaged hydraulic parameters, but fish respond to near-instantaneous

variation in hydraulic conditions. For this reason, we expect the deviation between optimal and observed paths to increase with increasing turbulence (i.e., between turbulence and control treatments in our experiments). The use of the proposed work equation on a large fishway has the challenge of measuring turbulence at a fine grid but of easy integration into a CFD model such as that presented in Goodwin, et al. (2006).

We collected a small sample of measurements within the serpentine weirs of the Cascade Island fishway at the Bonneville Dam (Appendix Figure 99 & Figure 100). Our measurements of the velocity and turbulence within the fishway were higher than those within our experimental flume. This was due to the limitations of the experimental flume. Our experiments do provide data on the difficulties of passage of vertical slot fishways and the added difficulty with increased turbulence. The passage of the actual serpentine weirs will be much more difficult with the increased velocity, turbulence, and depth.

The Pacific lamprey are anguilliform swimmers that move to a burst and attach method of swimming when they encounter velocity barriers or reach physiological exhaustion (Matthew L. Keefer et al., 2010). In our experiments, the lamprey normally swam near the bottom and side of the flume. This may affect our path tracking because the lamprey may not be avoiding areas of high turbulence or velocity and may generally swim near walls for guidance due to their lack of visual cues swimming nocturnally. Pacific lamprey my also attach when they reach a velocity barrier. Although we cannot completely eliminate this possibility, the attachment of lamprey provides a good metric of when the lamprey reached exhaustion. Longer attachment time suggests that lamprey required a longer rest or conditions were too challenging to move forward.

There may be other behavioral cues that cause lamprey to not pass the serpentine weirs that include: lamprey largely travel nocturnally and depend more on hydraulic cues than visual cues as opposed to diurnal fishes (Matthew L. Keefer, Caudill, Peery, et al., 2013); no motivation to travel around 180° bends; or not having the energy budget to travel through a series of serpentines.

Further research should analyze how other fish species are affected by the parameters outlined in this paper. A biologically important swim speed for sub-carangiform swimmers could be when they move to burst and rest behavior. Our measurements provide the changes in velocity and turbulence throughout the water column around turbulence-inducing structures. It may be found that strong swimmers such as salmonids, the turbulence has little effect due to swim speed, fish size, or fish density on swimming capability and the work equation we developed should be adjusted to account for the change.

Conclusion

Historically fishways have been designed to facilitate upstream migration at migration barriers by reducing flow velocity by adding hydraulic structures with the drawback of forming high turbulence. Our results showed that turbulence created by a turbulence-inducing structure presented more than doubled root mean square values of the velocity fluctuations in all directions and turbulent kinetic energy (*TKE*) increased on average 150%. Structures built within fishways that are designed for a target species based on velocity and depth requirements have potentially the negative side effect to increase turbulence within the fishway. Consequently, we suggest that in designing fish passage all hydraulic values should be considered such to avoid that when velocity is not a limiting factor turbulence may become the limiting factor.

Correlation between velocity magnitude and *TKE* is mostly negative especially in the turbulent treatment cases supporting the observation that high turbulence is the mechanism to consume hydrodynamic energy and thus reduce velocity within hydraulic structures. Flow field analysis shows that turbulence increases with length of the slot with constant velocity and with velocity for constant slot length for the control turbulence treatment. High turbulence is mostly present toward the entrance (downstream end) of the slot. Conversely, high turbulence is distributed through the entire length of the slot in the turbulence treatment. Large recirculating flow cells develop near the bottom of the slot with intense upstream flow direction velocity magnitudes (longitudinal flow components). These cells are larger and stronger in the control than turbulent treatment scenarios.

Our equation that integrates both velocity and *TKE* over the pathway to find the work required to travel upstream within the structure shows that the attachment time of lamprey increases with total work and turbulence required through the flume. Our results suggest that turbulence requires fish to find the lower work pathway. The lowest total work path was in general equivalent to the lowest total velocity path for the control treatment. The lowest total work path was in general equivalent to the lowest total turbulence path for the turbulence treatment. We note that higher turbulence likely affect the sensory cues available to lamprey as well, particularly during the nocturnal migration. Future work could disentangle the effects of turbulence conditions on sensory cues and behavior by manipulating turbulence while experimentally or statistically controlling for the effect of work required for passage. The increased work required to travel through the flume diminishes the total energy budget for the migration of fish.

References

Barton, M. (2007). *Bond's Biology of Fishes* (3rd ed.). Belmont, Ca: Brooks/ Cole.

Castro-Santos, T. (2005). Optimal swim speeds for traversing velocity barriers: an analysis of volitional high-speed swimming behavior of migratory fishes. *Journal of Experimental Biology*, *208*(3), 421–432. http://doi.org/10.1242/jeb.01380

Castro-Santos, T., Cotel, A., & Webb, P. (2009). Fishway Evaluations for Better Bioengineering : An Integrative Approach A Framework for Fishway. *American Fisheries Society Symposium*, *69*(November 2015), 557–575.

Clay, C. H. (1961). *Design of Fishways and other Fish Facilities* (Vol. 24). Ottawa: The Department of Fisheries of Canada. http://doi.org/10.1577/1548-8659(1962)24[15:DOFAOF]2.0.CO;2

Clay, C. H. (1995). *Design of fishways and other fish facilities.* (2nd Editio). Boca Raton: Lewis Publishers, CRC Press, Inc.

Goettel, M. T., Atkinson, J. F., & Bennett, S. J. (2015). Behavior of western blacknose dace in a turbulence modified flow field. *Ecological Engineering*, *74*, 230–240. http://doi.org/10.1016/j.ecoleng.2014.10.012

Goodwin, R. A. (2004). *Hydrodynamics and Juvenile Salmon Movement Behavior at Lower Granite Dam: Decoding the Relationship Using 3-D Space-Time Simulation*. Cornell University.

Goodwin, R. A., Nestler, J. M., Anderson, J. J., Weber, L. J., & Loucks, D. P. (2006). Forecasting 3-D fish movement behavior using a Eulerian-Lagrangian-agent method (ELAM). *Ecological Modelling*, *192*, 197–223.

http://doi.org/10.1016/j.ecolmodel.2005.08.004

Goring, D. G., & Nikora, V. I. (2002). Despiking Acoustic Doppler Velocimeter Data. *Journal of Hydraulic Engineering*, *128*(1), 117–126. http://doi.org/10.1061/(ASCE)0733-9429(2002)128:1(117)

Guiny, E. ., Ervine, D. A. ., & Armstrong, J. D. . (2005). Hydraulic and biological aspects of fish passes for Atlantic salmon. *Journal of Hydraulic Engineering*, *131*(7), 542–553. http://doi.org/10.1061/(ASCE)0733-9429(2005)131:7(542)

Katopodis, C. (1992). Introduction to fishway design. *Oceans*, (January), 67. Retrieved from http://www.wra.gov.tw/public/attachment/41110254871.pdf

Katopodis, C., & Gervais, R. (2012). Ecohydraulic analysis of fish fatigue data. *River Research and Applications*, *28*(4), 444–456. http://doi.org/10.1002/rra.1566

Keefer, M. L., Caudill, C. C., Peery, C. A., & Moser, M. L. (2013). Context-dependent diel behavior of upstream-migrating anadromous fishes. *Environmental Biology of Fishes*, *96*(6), 691–700. http://doi.org/10.1007/s10641-012-0059-5

Keefer, M. L., Caudill, C., Clabough, T. S., Jepson, M. A., Johnson, E. L., Peery, C. A., … Moser, M. L. (2013). Fishway passage bottleneck identification and prioritization: a case study of Pacific lamprey at Bonneville Dam. *... Journal of Fisheries ...*, *1565*(August), 1551–1565. http://doi.org/10.1139/cjfas-2013-0164

Keefer, M. L., Clabough, T. S., Jepson, M. A., Johnson, E. L., Boggs, C. T., & Caudill, C. C. (2013). Adult Pacific lamprey passage: data synthesis and fishway improvement prioritization tools. UI FERL report 2012-8 for the US Army Corps of Engineers, Portland District.

Keefer, M. L., Daigle, W. R., Peery, C. a., Pennington, H. T., Lee, S. R., & Moser, M. L. (2010). Testing Adult Pacific Lamprey Performance at Structural Challenges in Fishways. *North American Journal of Fisheries Management*, *30*(November), 376–385. http://doi.org/10.1577/M09-099.1

Keefer, M. L., Peery, C. a., Lee, S. R., Daigle, W. R., Johnson, E. L., & Moser, M. L. (2011). Behaviour of adult Pacific lamprey in near-field flow and fishway design experiments. *Fisheries Management and Ecology*, *18*, 177–189. http://doi.org/10.1111/j.1365-2400.2010.00772.x

Kemp, P. S. (2012). Bridging the Gap Between Fish Beahaviour, Performance and Hydrodynamics: An Ecohydraulics Approach to Fish Passage Research. *River Research and Applications*, *28*(4), 403–406. http://doi.org/10.1002/rra.1599

Kemp, P. S., Tsuzaki, T., & Moser, M. L. (2009). Linking behaviour and performance: Intermittent locomotion in a climbing fish. *Journal of Zoology*, *277*(2), 171–178. http://doi.org/10.1111/j.1469-7998.2008.00525.x

Kim, J. H. (2001). Hydraulic characteristics by weir type in a pool-weir fishway. *Ecological Engineering*, *16*, 425–433. http://doi.org/10.1016/S0925-8574(00)00125-7

Kirk, M. A., Caudill, C. C., Tonina, D., & Syms., J. C. (2015). Effects of water velocity, turbulence, and obstacle length on the swimming capabilities of adult Pacific lampreys. *Fisheries Management and Ecology. (In Revision)*.

Lacey, R. W. J., Neary, V. S., Liao, J. C., Enders, E. C., & Tritico, H. M. (2012). The IPOS Framework: Linking fish swimming performance in altered flows from laboratory experiments to rivers. *River Research and Applications*, *28*(4), 429–443.

http://doi.org/10.1002/rra.1584

Mallen-Cooper, M., & Brand, D. a. (2007). Non-salmonids in a salmonid fishway: What do 50 years of data tell us about past and future fish passage? *Fisheries Management and Ecology*, *14*(5), 319–332. http://doi.org/10.1111/j.1365-2400.2007.00557.x

Mateus, C., Alexandre, C. M., Cardoso, G., Pereira, E., Ganhão, E., Adão, H., … Félix, P. (2015). Installing an eel passage in River Mondego. Retrieved January 4, 2016, from http://www.rhpdm.uevora.pt/action2.html

McElroy, B., DeLonay, A., & Jacobson, R. (2012). Optimum swimming pathways of fish spawning migrations in rivers. *Ecology*, *93*(1), 29–34. http://doi.org/10.1890/11-1082.1

Moser, M. L., Keefer, M. L., Pennington, H. T., Ogden, D. a., & Simonson, J. E. (2011). Development of Pacific lamprey fishways at a hydropower dam. *Fisheries Management and Ecology*, *18*(3), 190–200. http://doi.org/10.1111/j.1365-2400.2010.00773.x

NMFS, N. (2008). Anadromous Salmonid Passage Facility Design. *NMFS, Northwest Region, Portland, Oregon*, (February), 1–127. Retrieved from http://scholar.google.com/scholar?hl=en&btnG=Search&q=intitle:Anadromous+salmonid+passage+facility+design#4

Orsborn, J. F. (1987). Fishways : historical assessment of design practices. *Fishways : Historical Assessment of Design Practices*.

Orsborn, J. F., & Powers, P. D. (1985). *Fishways: An Assessment of Their Development and Design : Final Project Report Part 3 of 4*. Bonneville Power Administration.

Rodríguez, T. T., Agudo, J. P., Mosquera, L. P., & González, E. P. (2006). Evaluating

vertical-slot fishway designs in terms of fish swimming capabilities. *Ecological Engineering*, *27*, 37–48. http://doi.org/10.1016/j.ecoleng.2005.09.015

Sontek. (1997). Pulse Coherent Doppler Processing and the ADV Correlation Coefficient, (November), 1–5.

Wahl, T. L. (2000). Analyzing ADV Data Using WinADV. *Joint Conference on Water Resources Engineering and Water Resources Planning & Management*, (1), 1–10. http://doi.org/10.1061/40517(2000)300

Zobott, H., Caudill, C. C., Keefer, M. L., Budwig, R., Frick, K., Moser, M. L., & Corbett., S. (2015). *Design guidelines for Pacific lamprey passage structures. UI FERL report 2015-5-DRAFT for the US Army Corps of Engineers, Portland District.*

Additional Plots

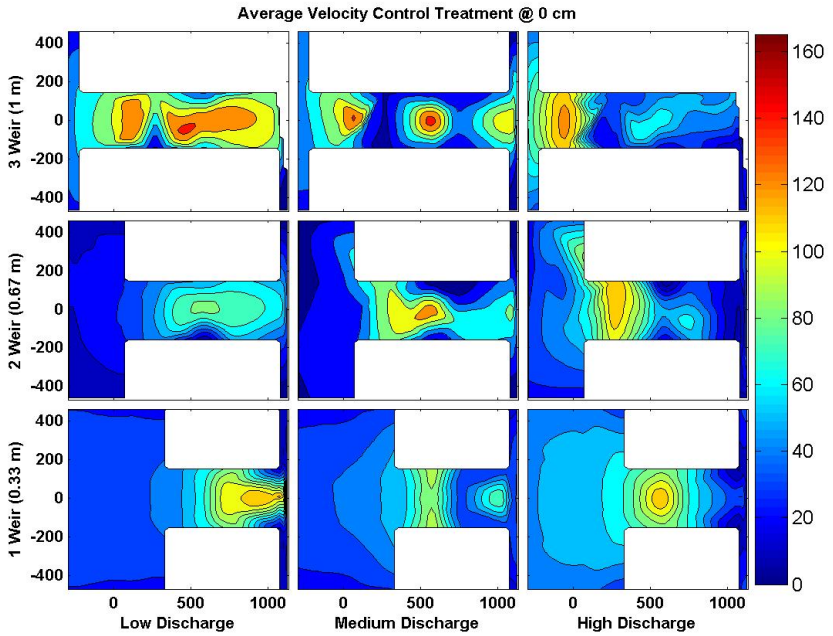

Figure 17: Contour plots of Average Velocity, V, for the control treatment at 0 cm for each slot discharge and length treatments.

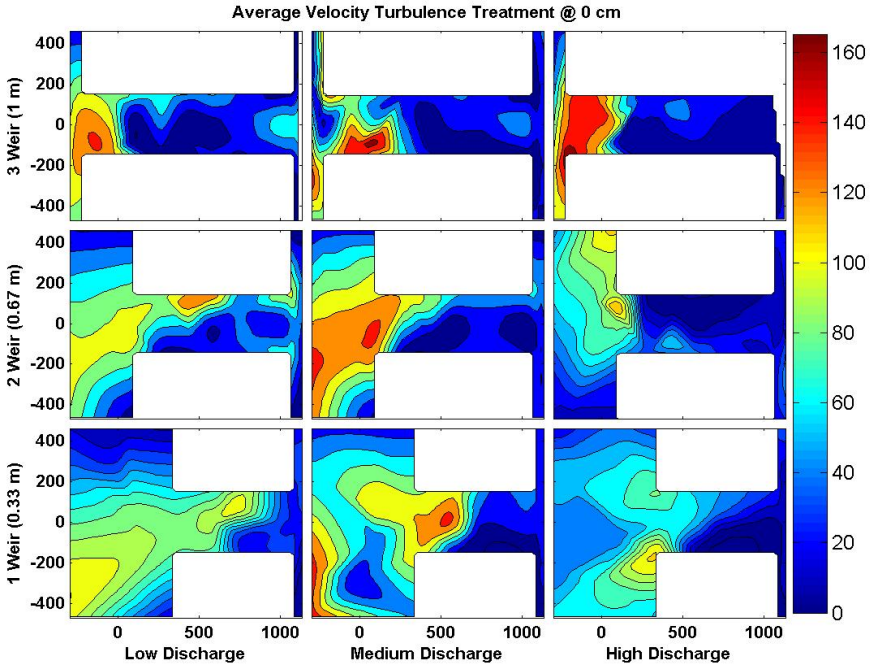

Figure 18: Contour plots of Average Velocity, V, for the turbulence treatment at 0 cm for each slot discharge and length treatments.

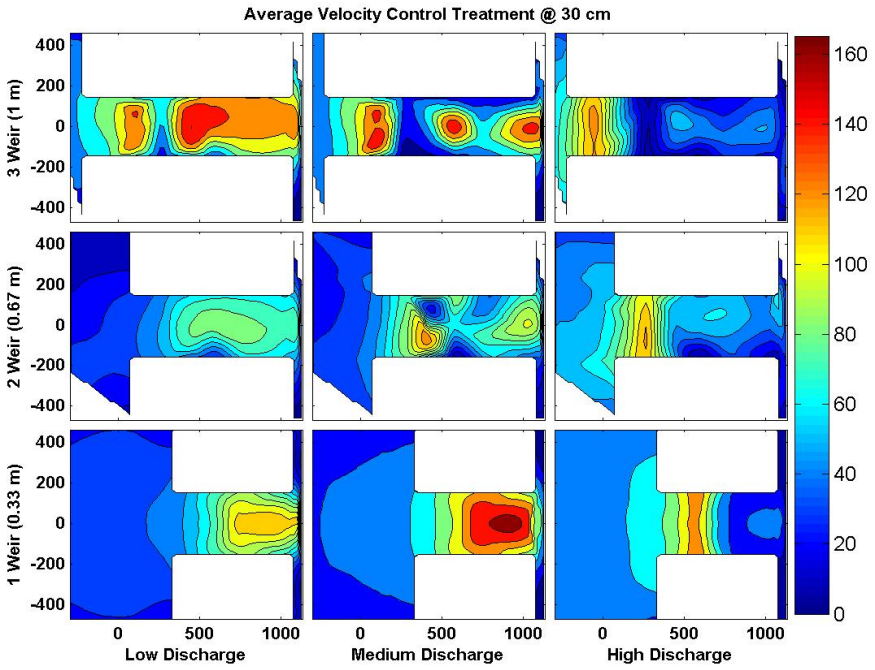

Figure 19: Contour plots of Average Velocity, V, for the control treatment at 30 cm for each slot discharge and length treatments.

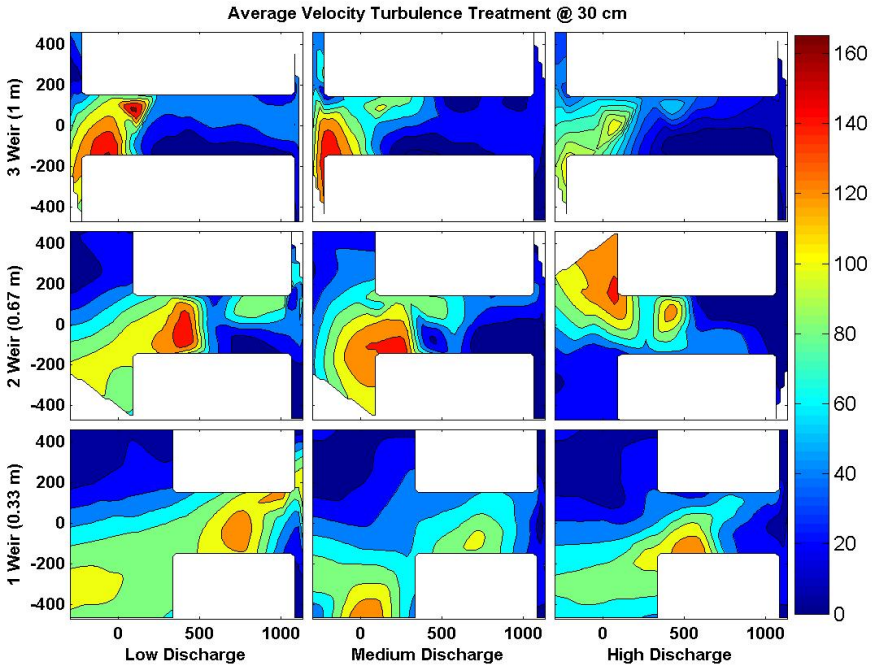

Figure 20: Contour plots of Average Velocity, V, for the turbulence treatment at 30 cm for each slot discharge and length treatments.

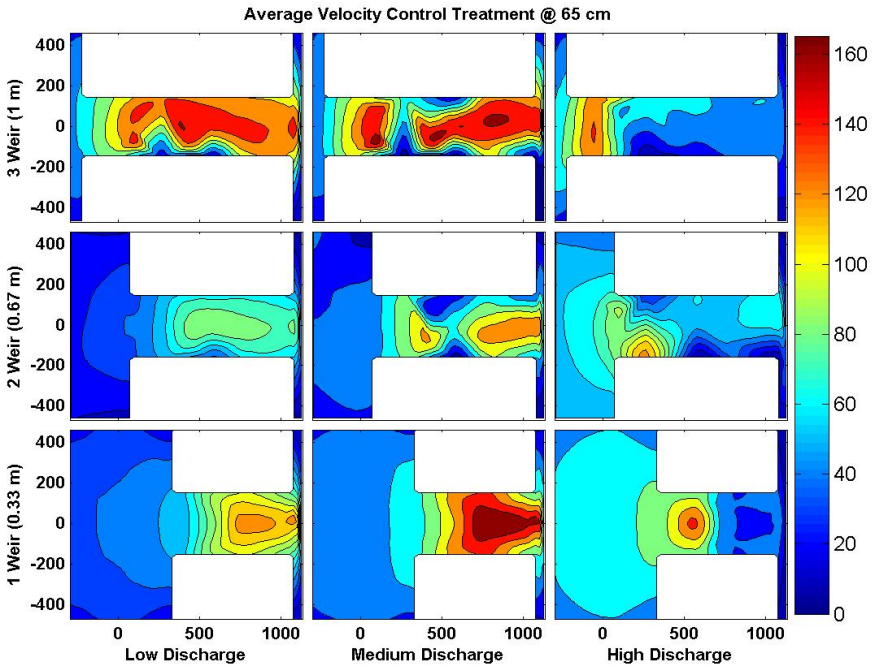

Figure 21: Contour plots of Average Velocity, V, for the control treatment at 65 cm for each slot discharge and length treatments.

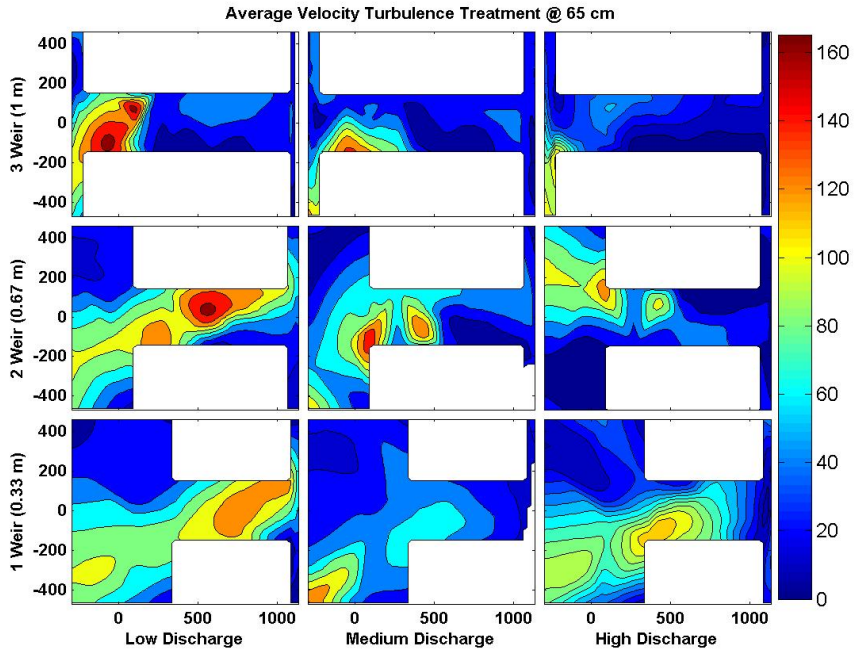

Figure 22: Contour plots of Average Velocity, V, for the turbulence treatment at 65 cm for each slot discharge and length treatments.

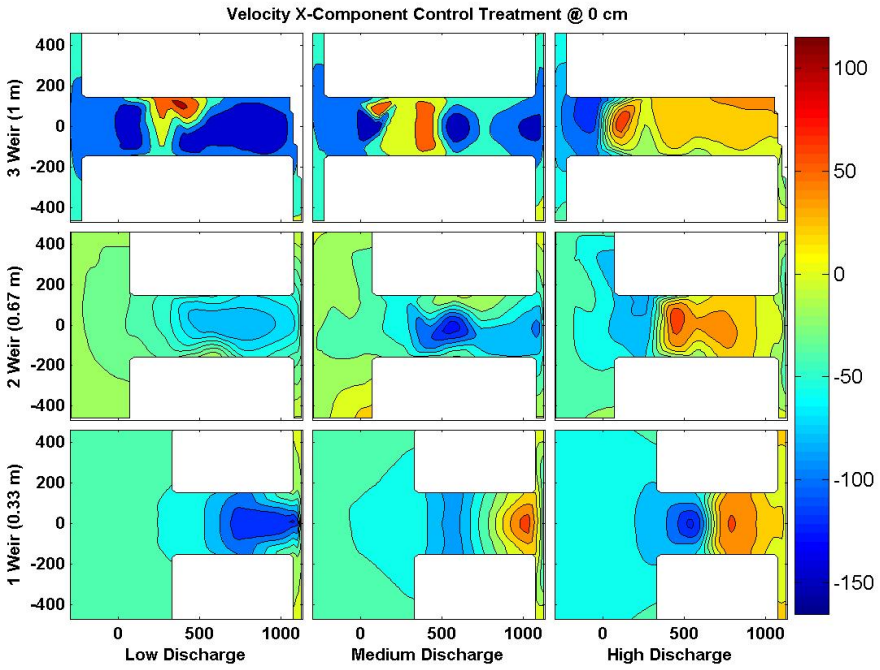

Figure 23: Contour plots of the velocity x-component, u, for the control treatment at 0 cm for each slot discharge and length treatments.

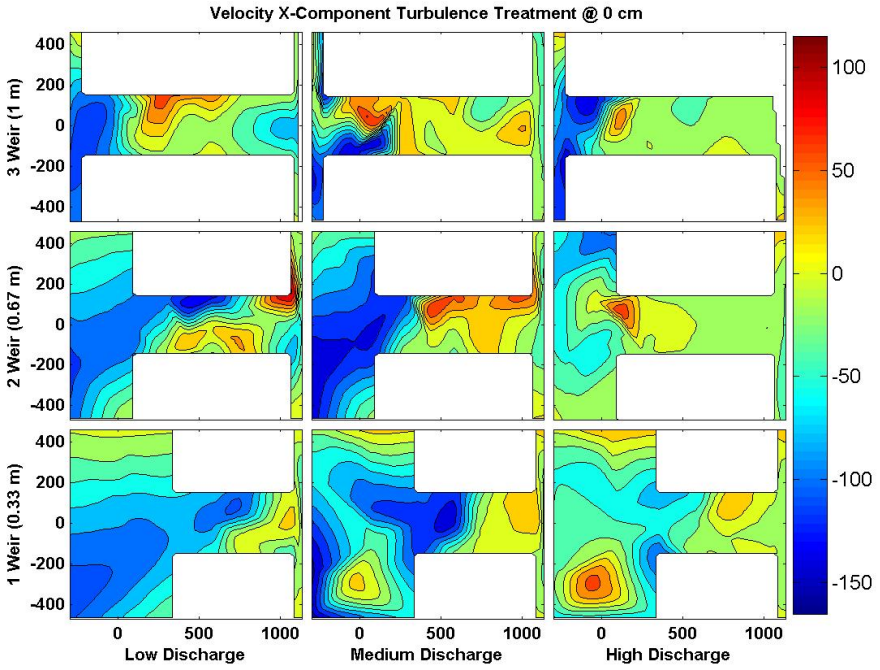

Figure 24: Contour plots of the velocity x-component, u, for the turbulence treatment at 0 cm for each slot discharge and length treatments.

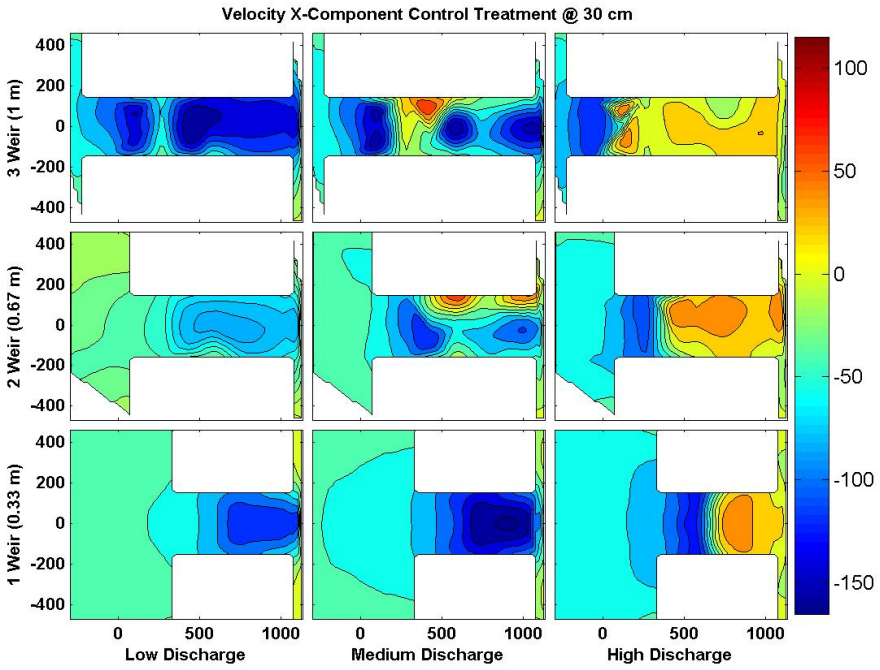

Figure 25: Contour plots of the velocity x-component, u, for the control treatment at 30 cm for each slot discharge and length treatments.

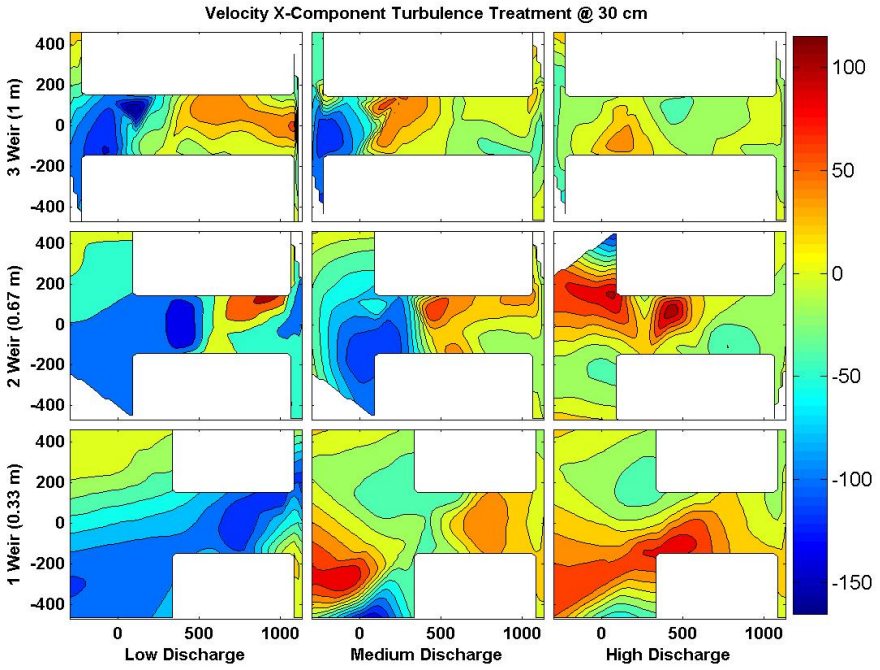

Figure 26: Contour plots of the velocity x-component, u, for the turbulence treatment at 30 cm for each slot discharge and length treatments.

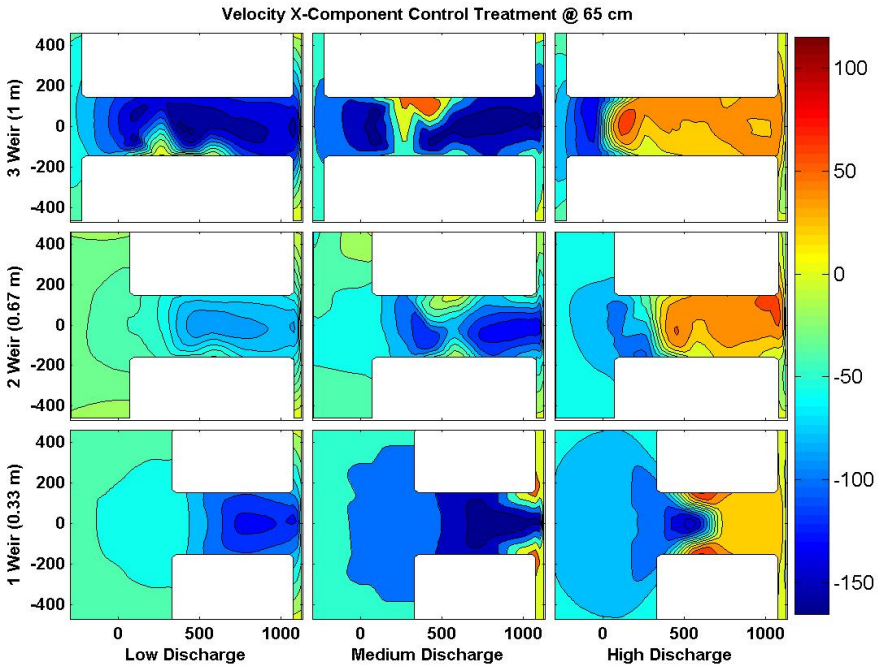

Figure 27: Contour plots of the velocity x-component, u, for the control treatment at 65 cm for each slot discharge and length treatments.

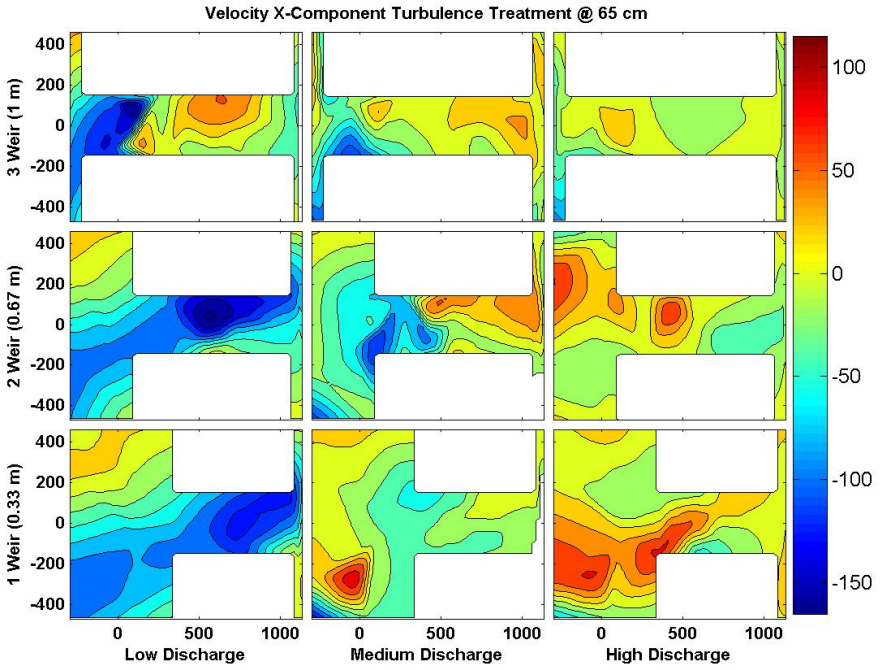

Figure 28: Contour plots of the velocity x-component, u, for the turbulence treatment at 65 cm for each slot discharge and length treatments.

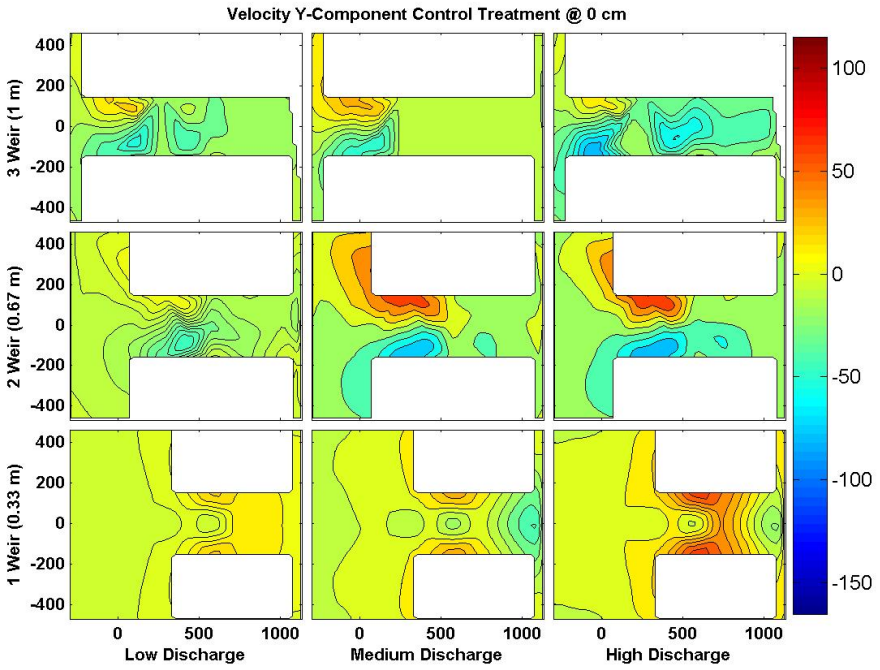

Figure 29: Contour plots of the velocity y-component, v, for the control treatment at 0 cm for each slot discharge and length treatments.

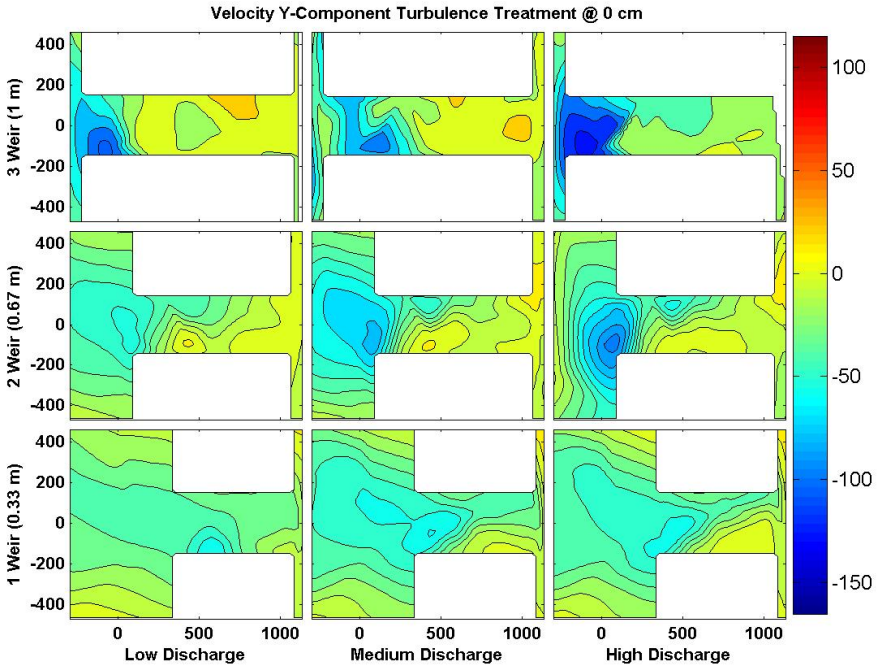

Figure 30: Contour plots of the velocity y-component, v, for the turbulence treatment at 0 cm for each slot discharge and length treatments.

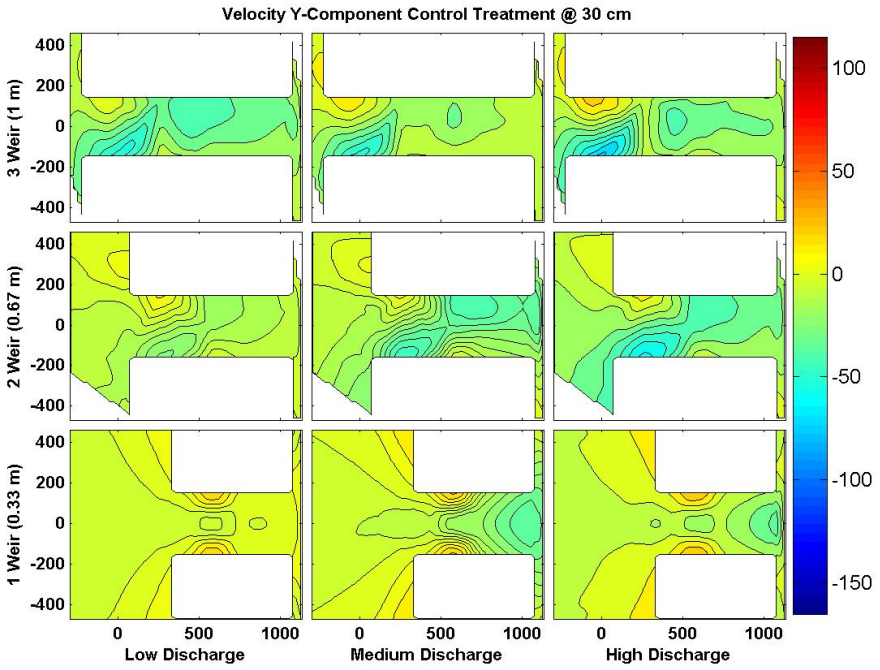

Figure 31: Contour plots of the velocity y-component, v, for the control treatment at 30 cm for each slot discharge and length treatments.

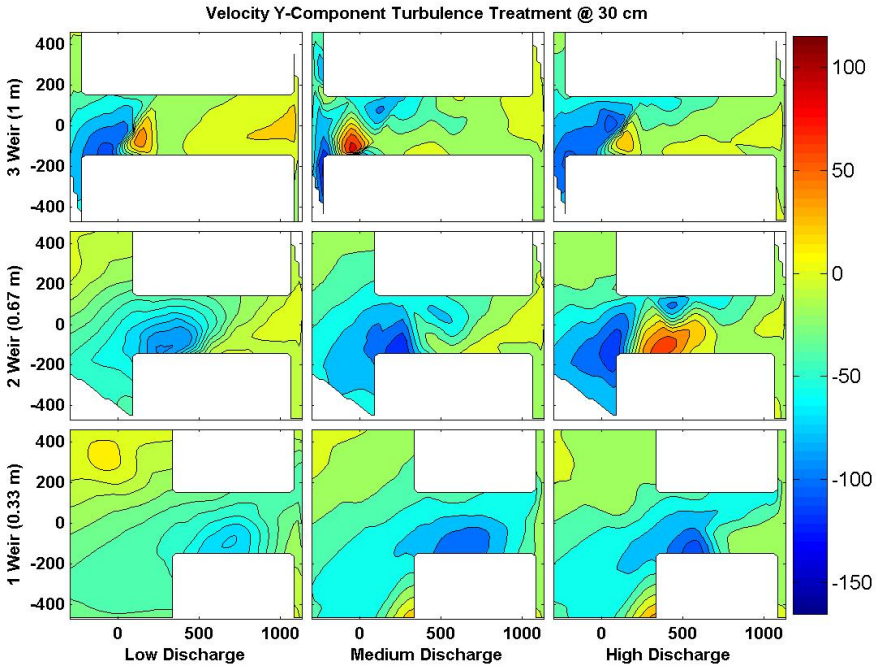

Figure 32: Contour plots of the velocity y-component, v, for the turbulence treatment at 30 cm for each slot discharge and length treatments.

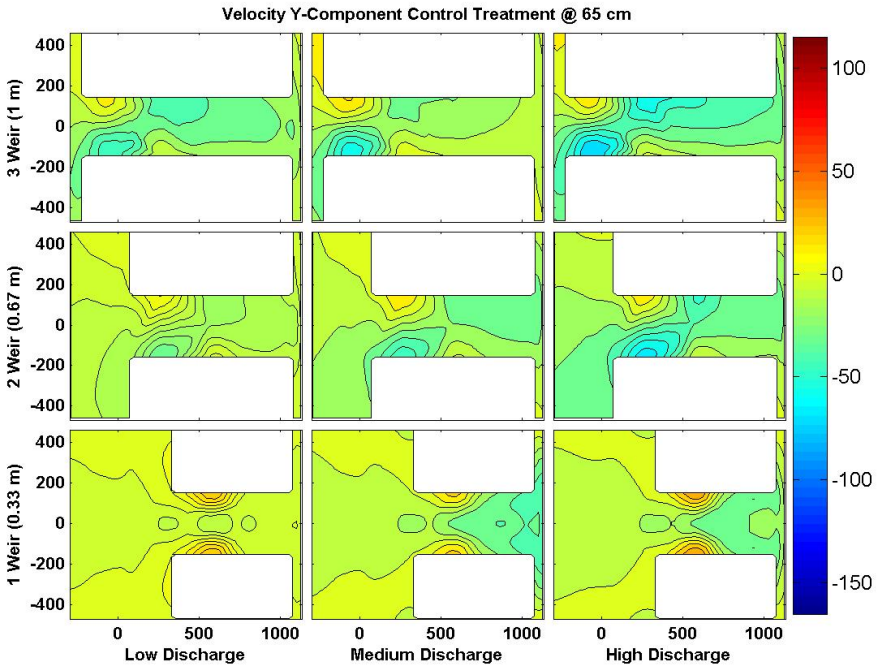

Figure 33: Contour plots of the velocity y-component, v, for the control treatment at 65 cm for each slot discharge and length treatments.

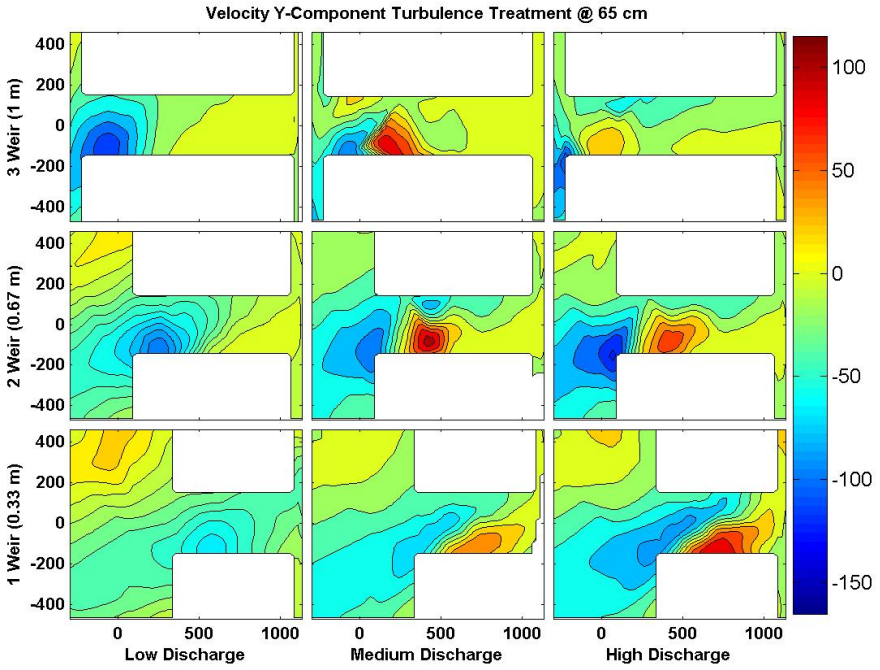

Figure 34: Contour plots of the velocity y-component, v, for the turbulence treatment at 65 cm for each slot discharge and length treatments.

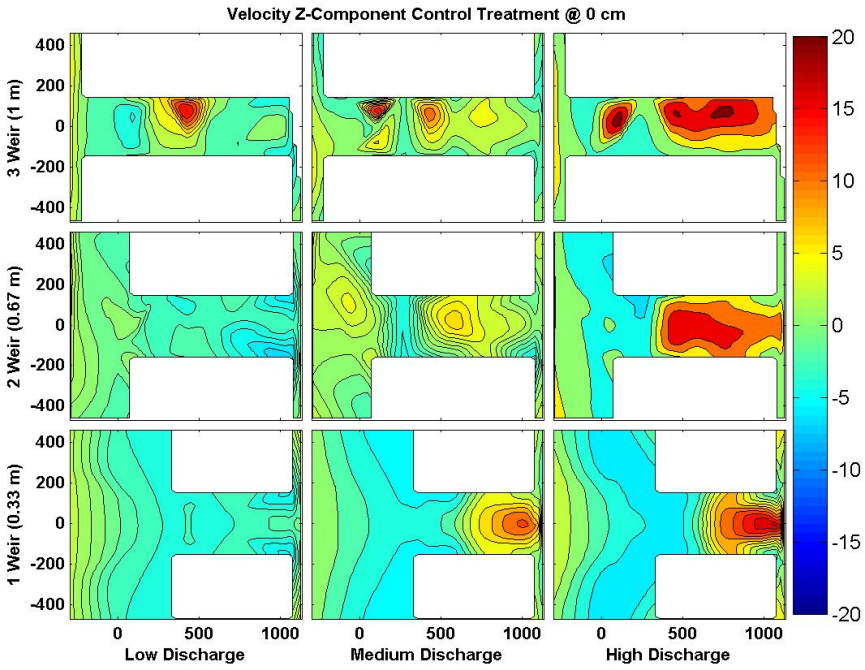

Figure 35: Contour plots of the velocity z-component, w, for the control treatment at 0 cm for each slot discharge and length treatments.

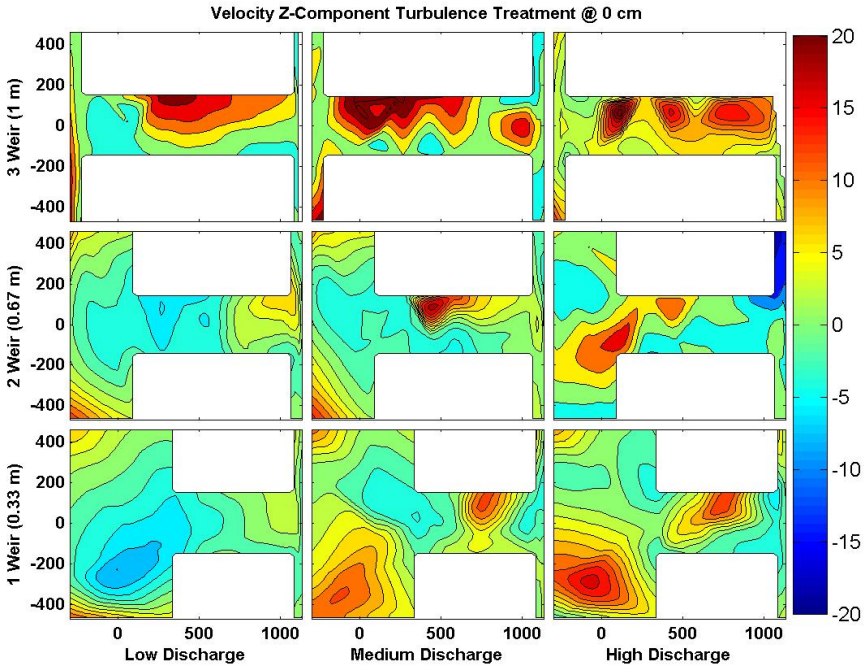

Figure 36: Contour plots of the velocity z-component, w, for the turbulence treatment at 0 cm for each slot discharge and length treatments.

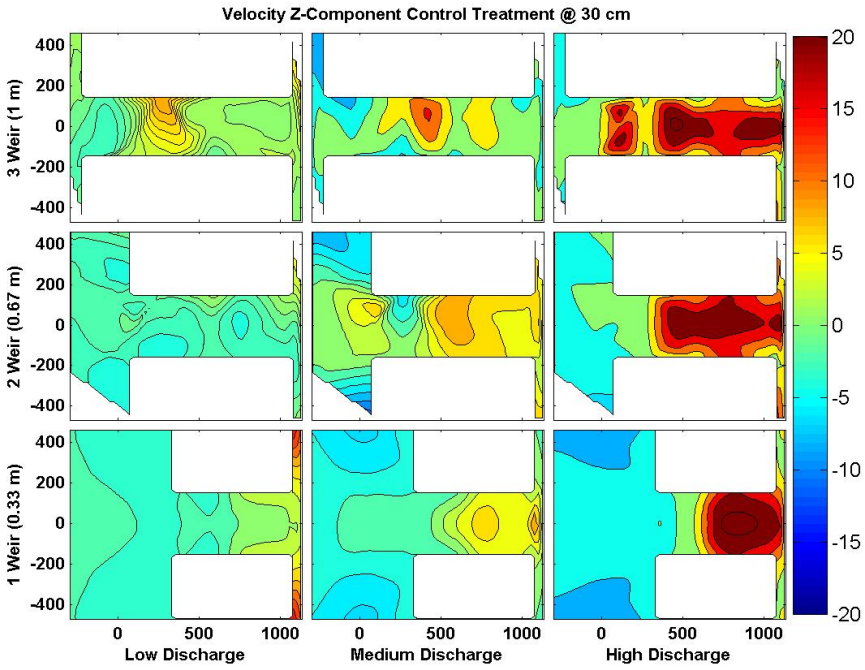

Figure 37: Contour plots of the velocity z-component, w, for the control treatment at 30 cm for each slot discharge and length treatments.

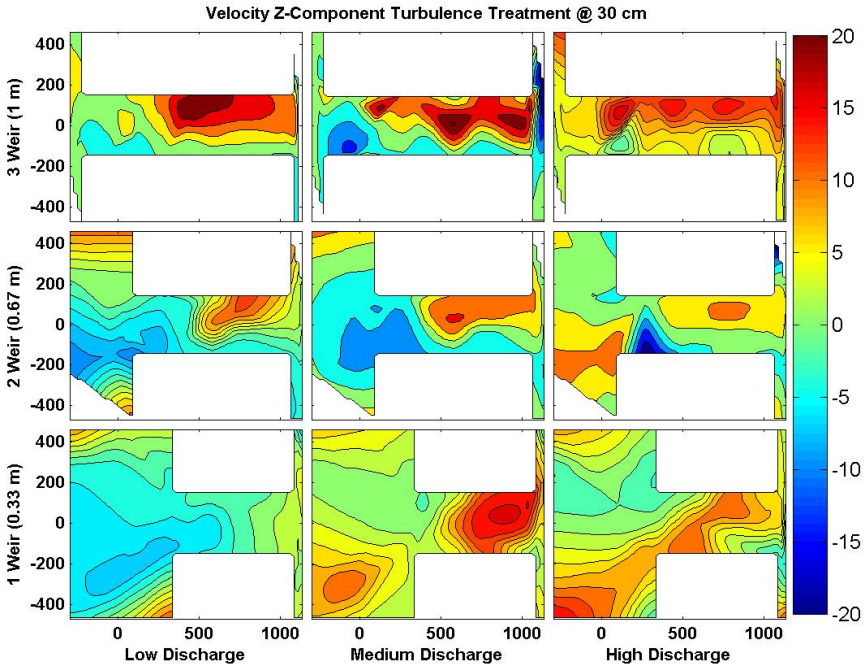

Figure 38: Contour plots of the velocity z-component, w, for the turbulence treatment at 30 cm for each slot discharge and length treatments.

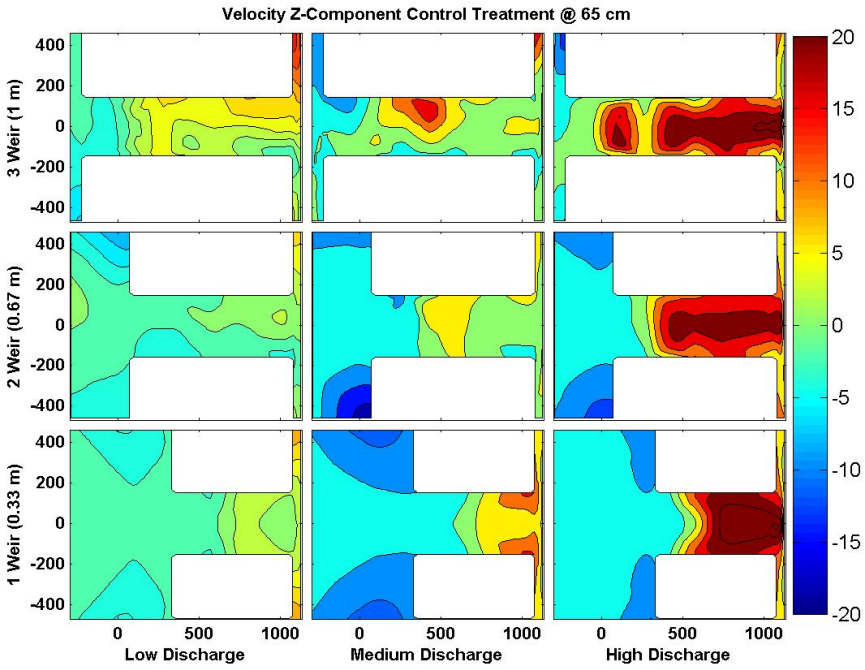

Figure 39: Contour plots of the velocity z-component, w, for the control treatment at 65 cm for each slot discharge and length treatments.

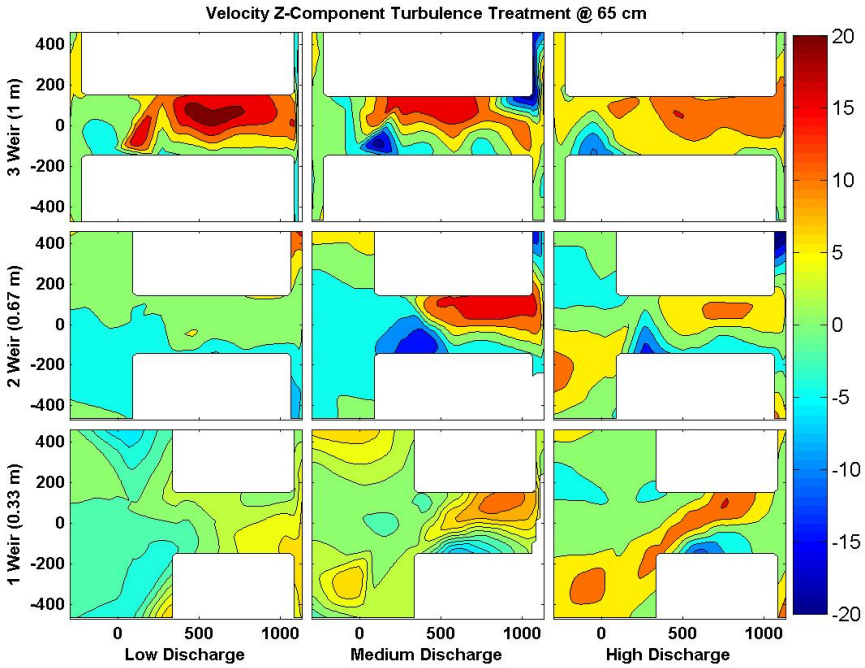

Figure 40: Contour plots of the velocity z-component, w, for the turbulence treatment at 65 cm for each slot discharge and length treatments.

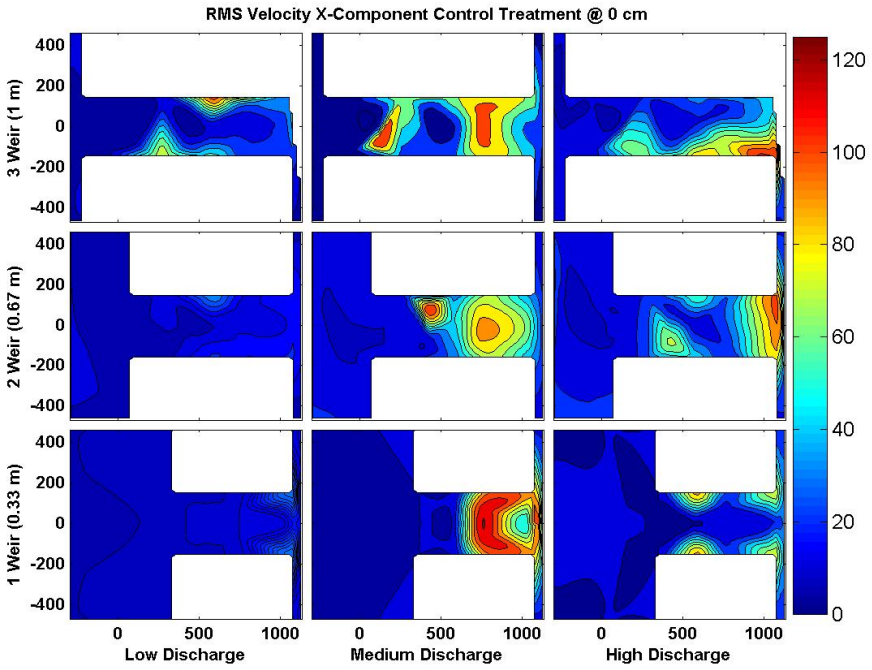

Figure 41: Contour plots of the RMS x-component for the control treatment at 0 cm for each slot discharge and length treatments.

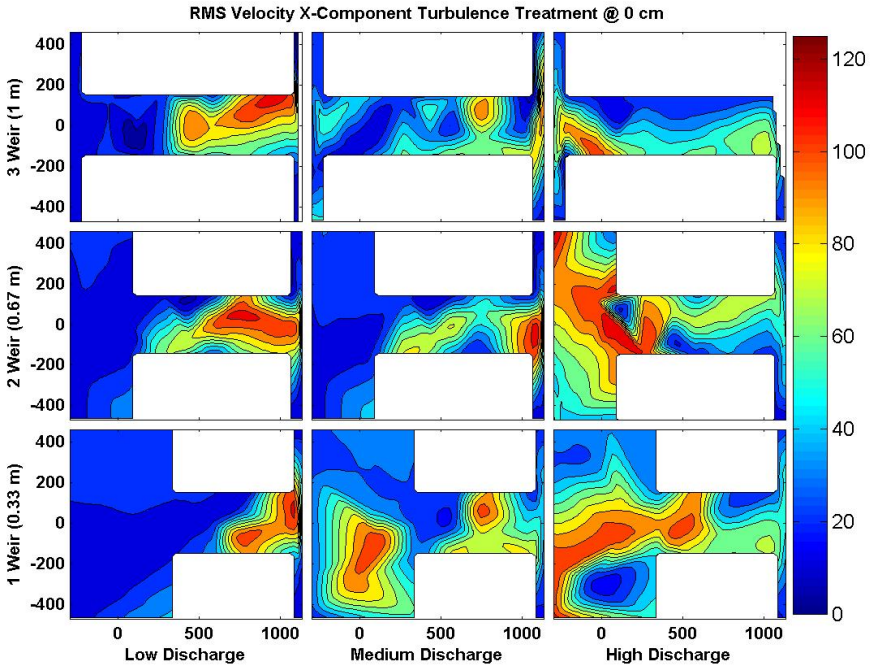

Figure 42: Contour plots of the RMS x-component for the turbulence treatment at 0 cm for each slot discharge and length treatments.

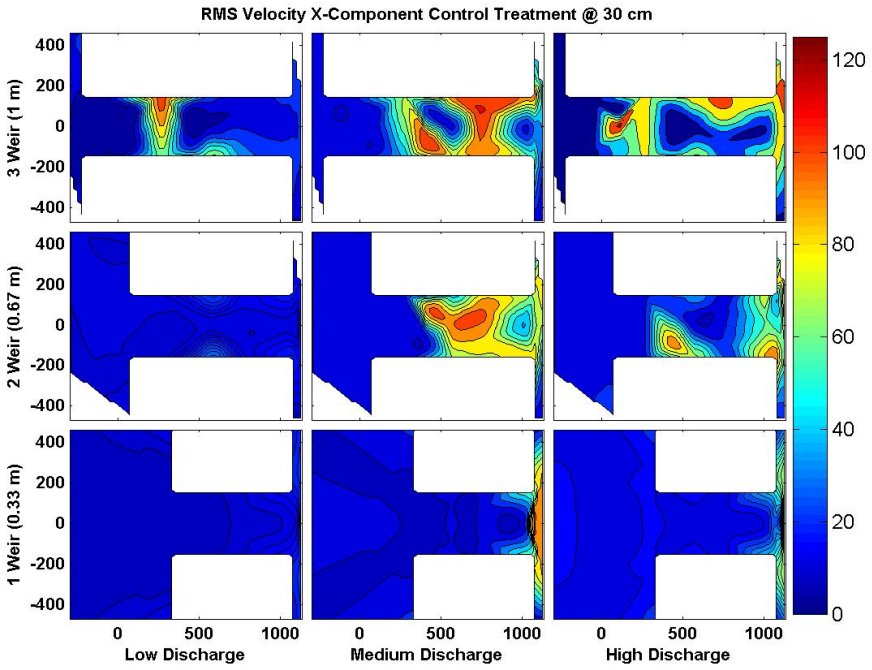

Figure 43: Contour plots of the RMS x-component for the control treatment at 30 cm for each slot discharge and length treatments.

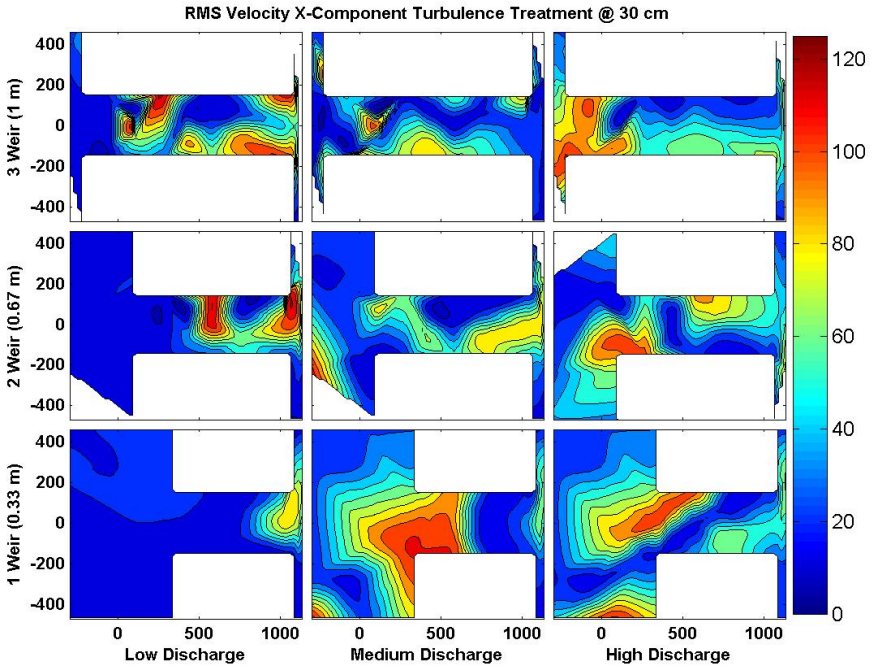

Figure 44: Contour plots of the RMS x-component for the turbulence treatment at 30 cm for each slot discharge and length treatments.

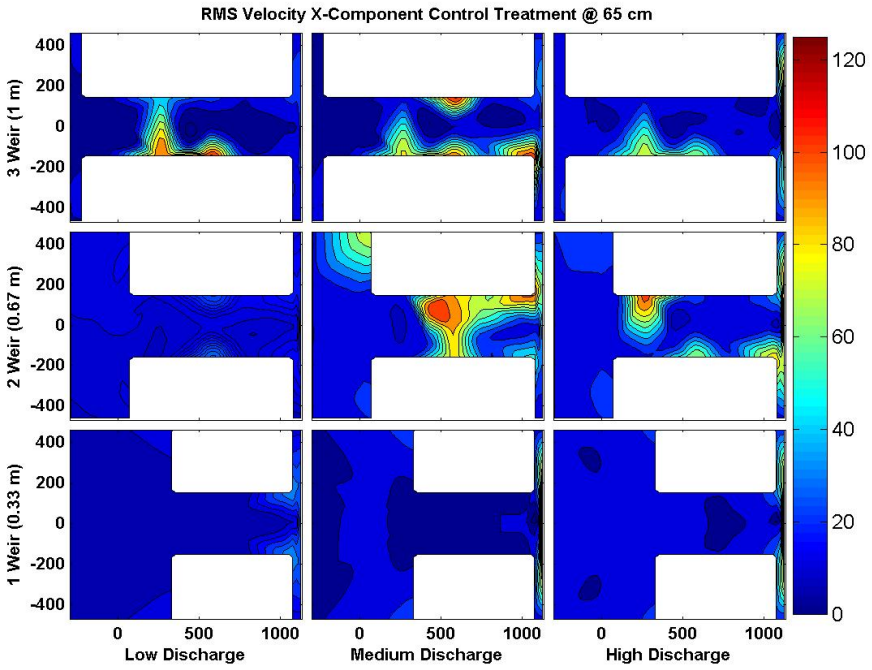

Figure 45: Contour plots of the RMS x-component for the control treatment at 65 cm for each slot discharge and length treatments.

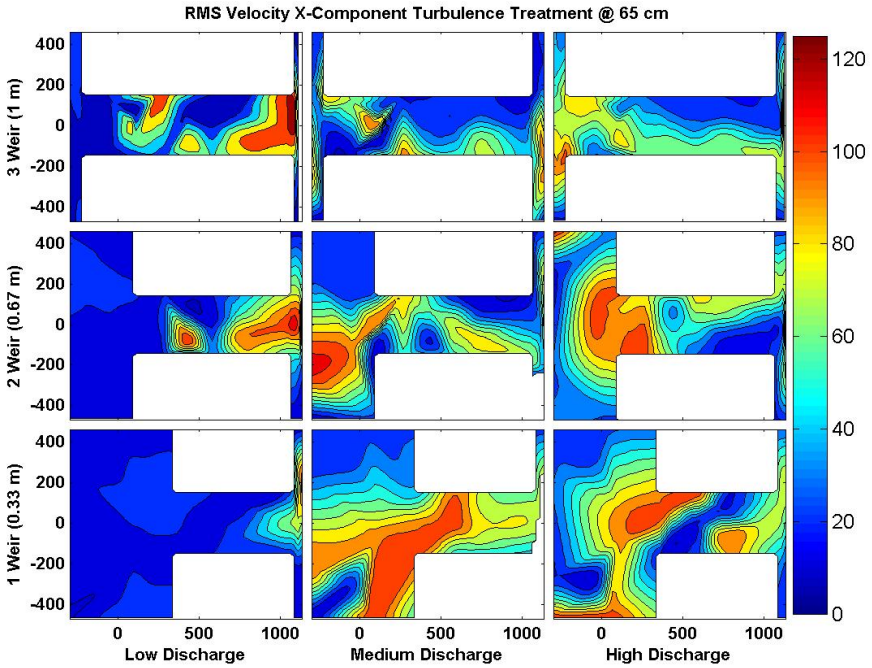

Figure 46: Contour plots of the RMS x-component for the turbulence treatment at 65 cm for each slot discharge and length treatments.

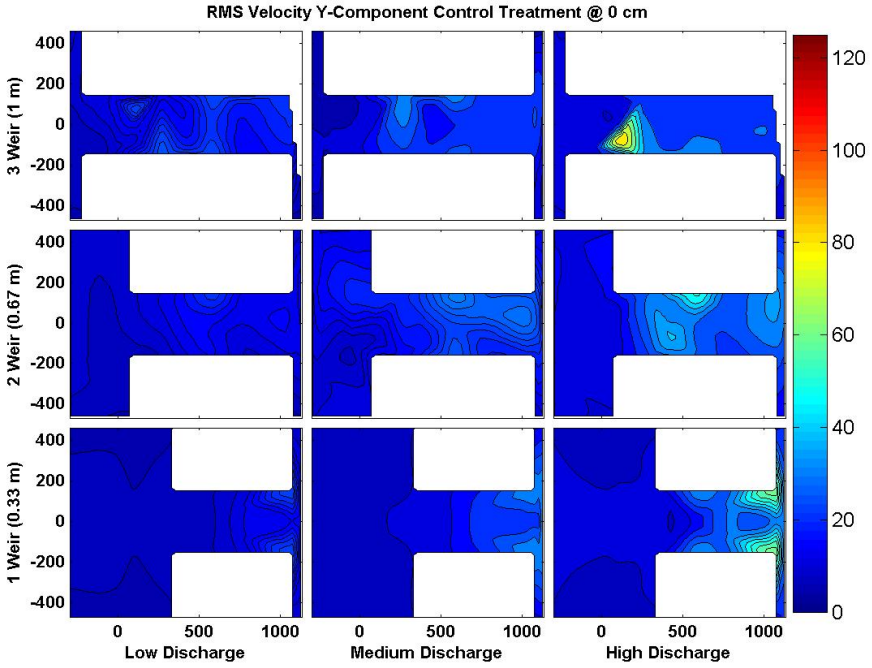

Figure 47: Contour plots of the RMS y-component for the control treatment at 0 cm for each slot discharge and length treatments.

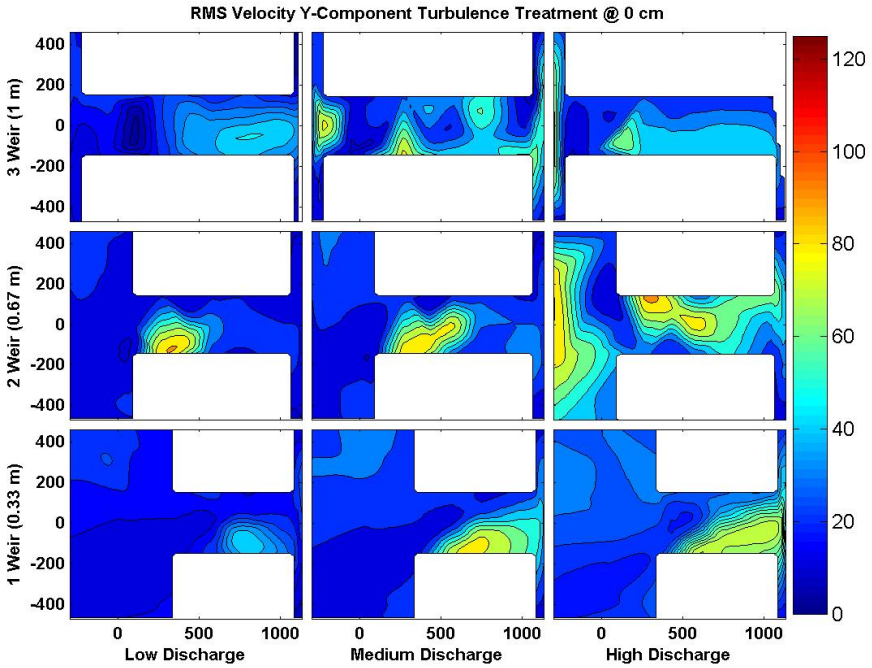

Figure 48: Contour plots of the RMS y-component for the turbulence treatment at 0 cm for each slot discharge and length treatments.

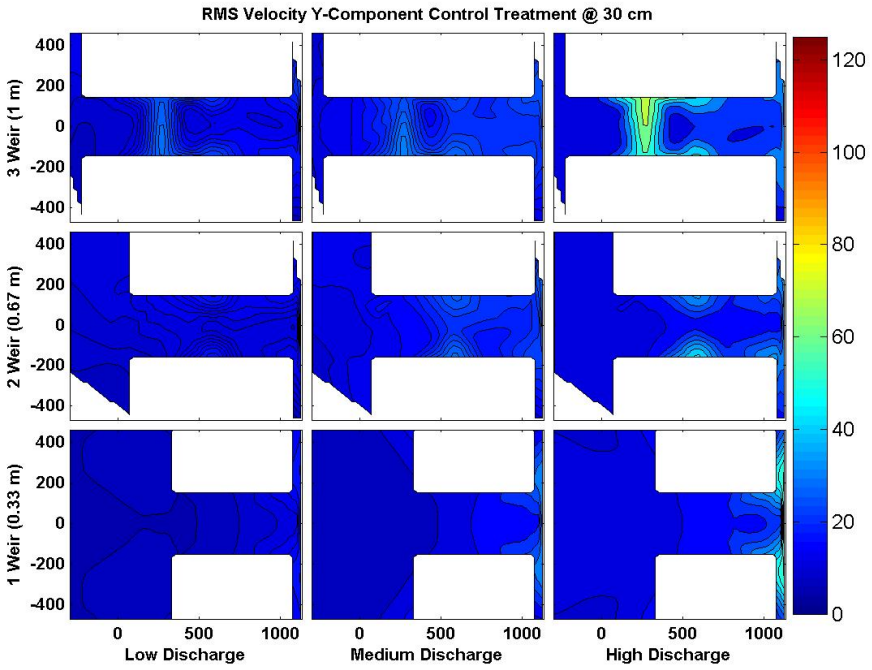

Figure 49: Contour plots of the RMS y-component for the control treatment at 30 cm for each slot discharge and length treatments.

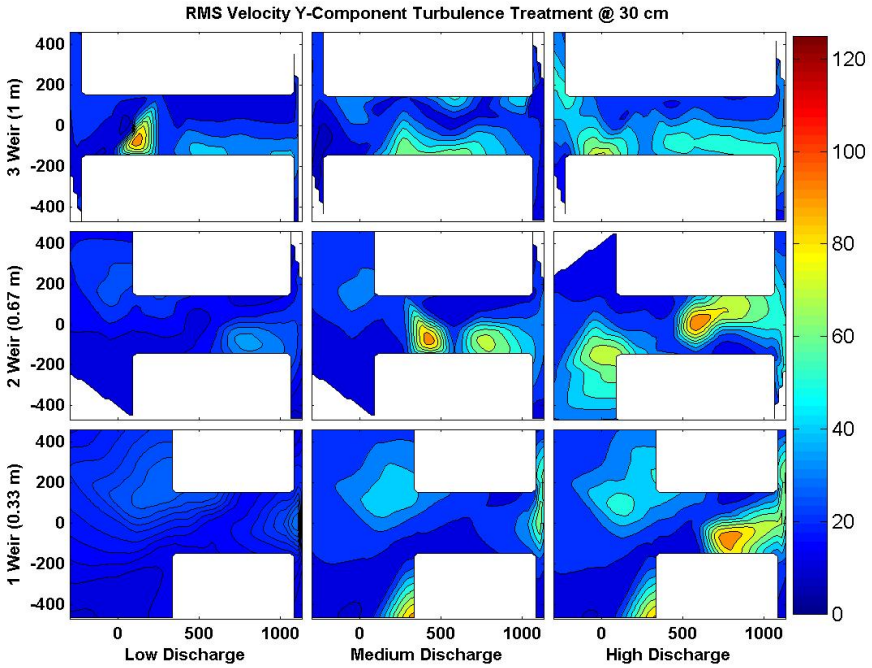

Figure 50: Contour plots of the RMS y-component for the turbulence treatment at 30 cm for each slot discharge and length treatments.

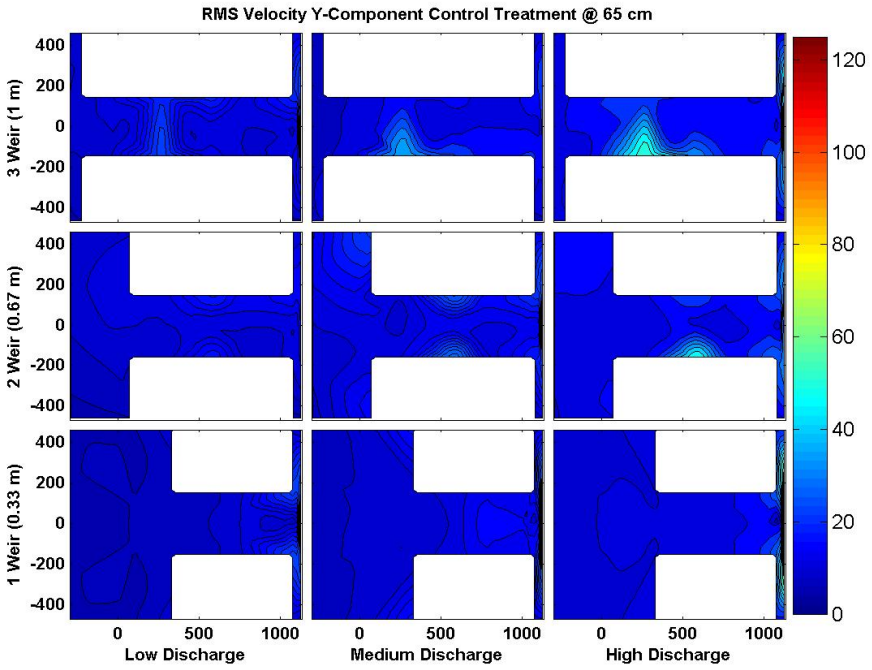

Figure 51: Contour plots of the RMS y-component for the control treatment at 65 cm for each slot discharge and length treatments.

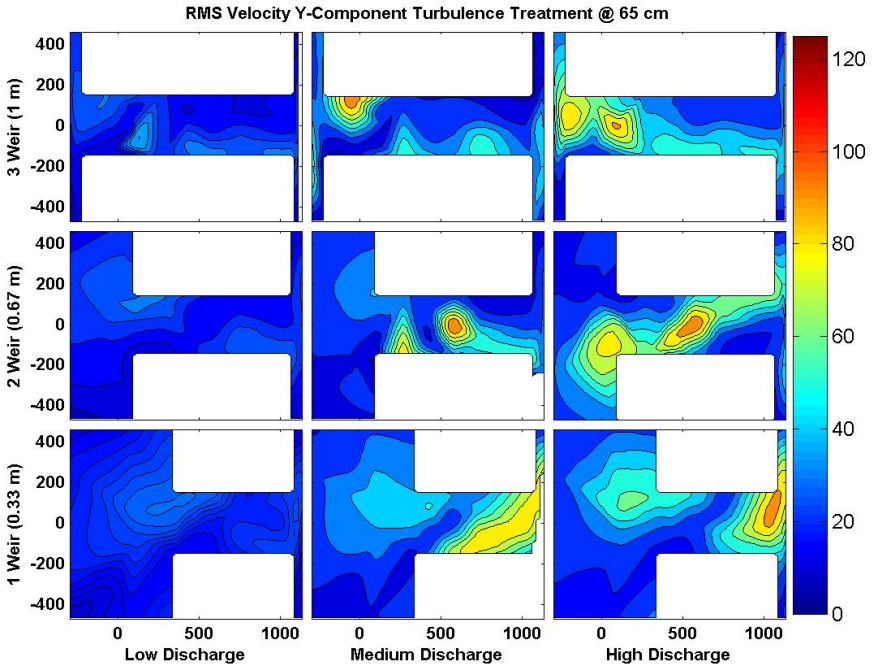

Figure 52: Contour plots of the RMS y-component for the turbulence treatment at 65 cm for each slot discharge and length treatments.

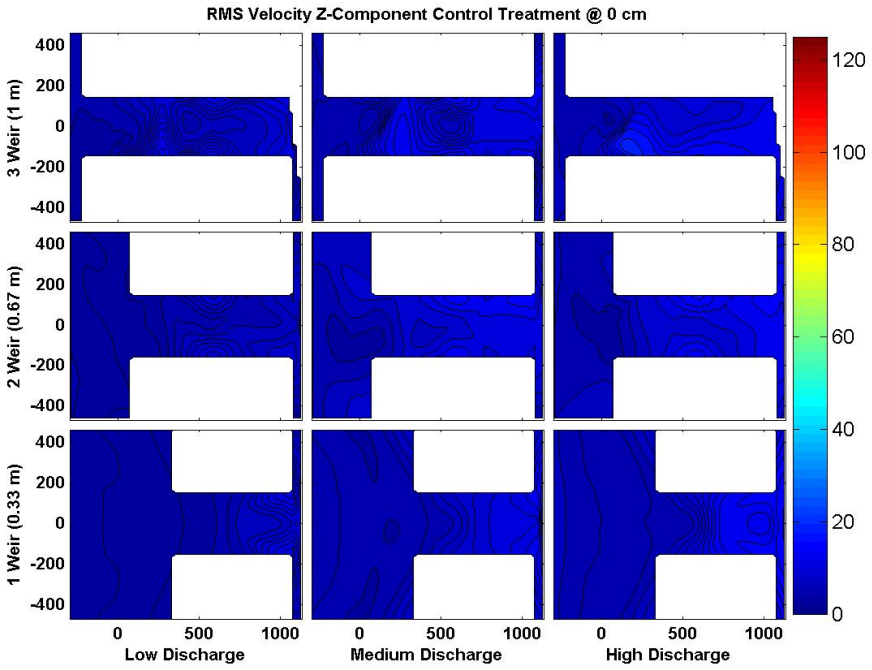

Figure 53: Contour plots of the RMS z-component for the control treatment at 0 cm for each slot discharge and length treatments.

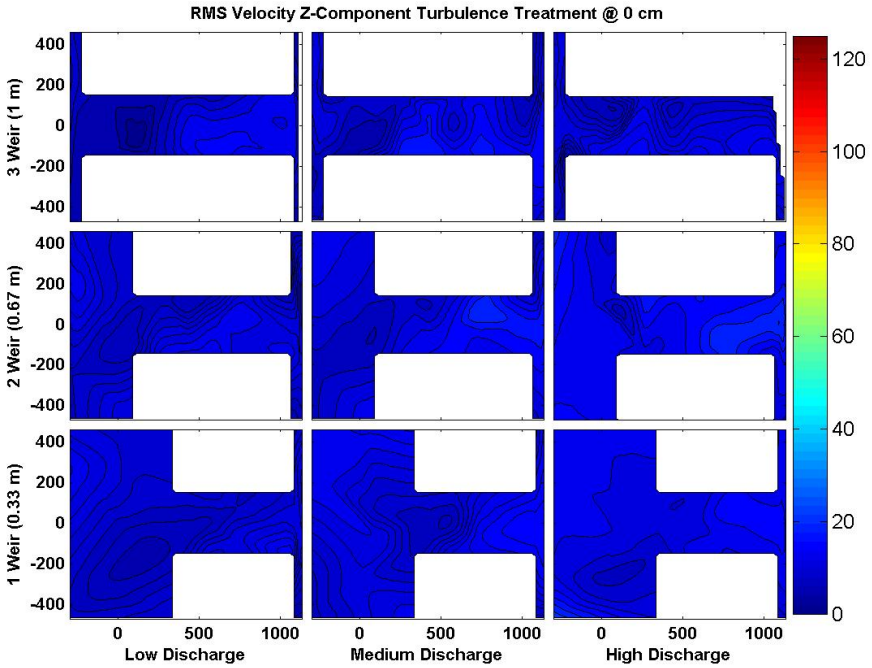

Figure 54: Contour plots of the RMS z-component for the turbulence treatment at 0 cm for each slot discharge and length treatments.

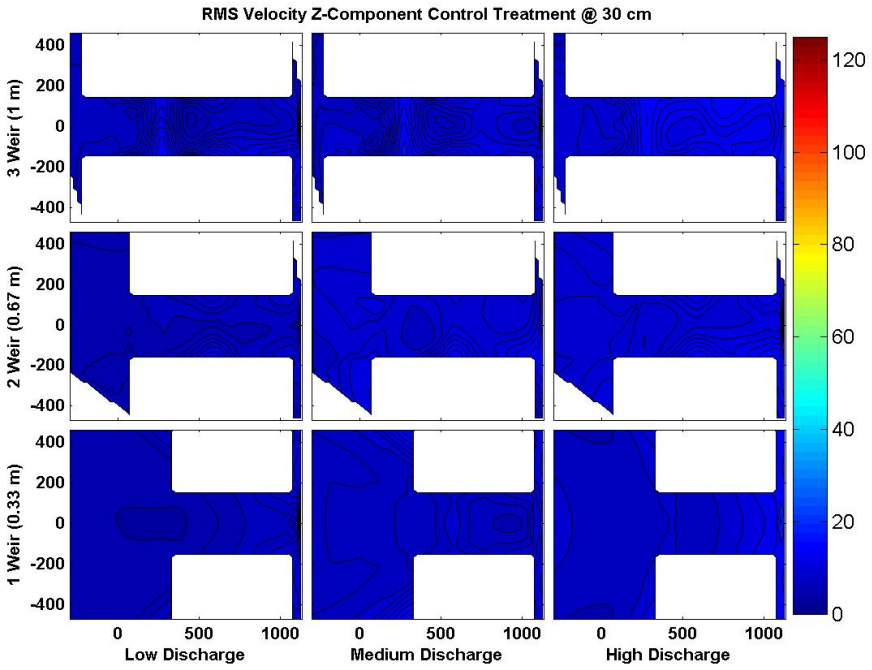

Figure 55: Contour plots of the RMS z-component for the control treatment at 30 cm for each slot discharge and length treatments.

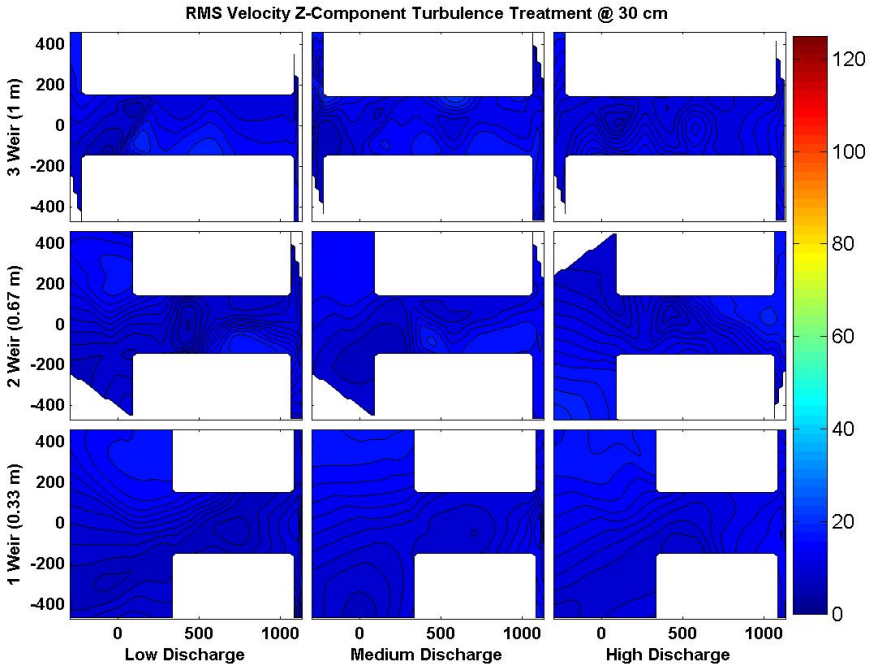

Figure 56: Contour plots of the RMS z-component for the turbulence treatment at 30 cm for each slot discharge and length treatments.

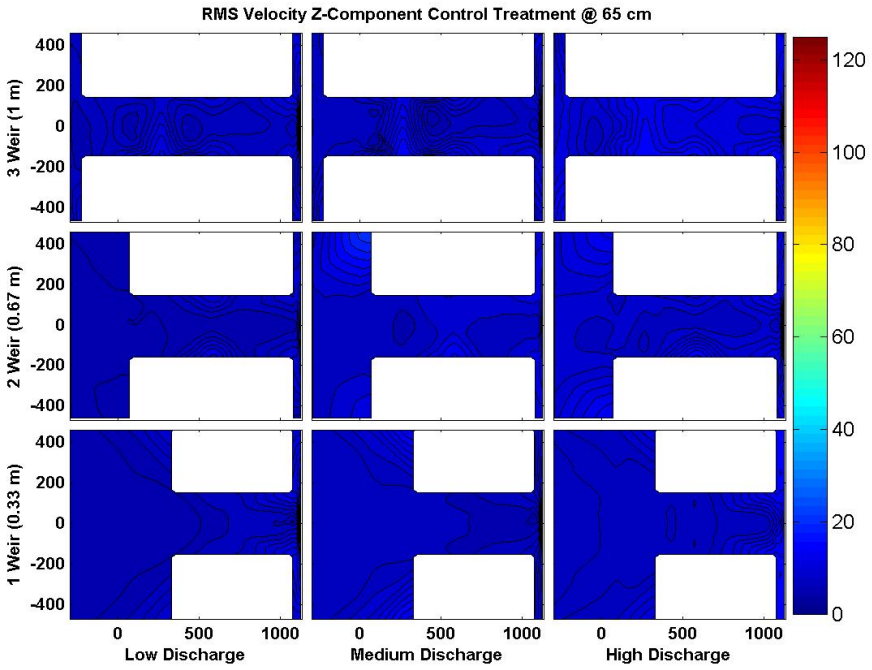

Figure 57: Contour plots of the RMS z-component for the control treatment at 65 cm for each slot discharge and length treatments.

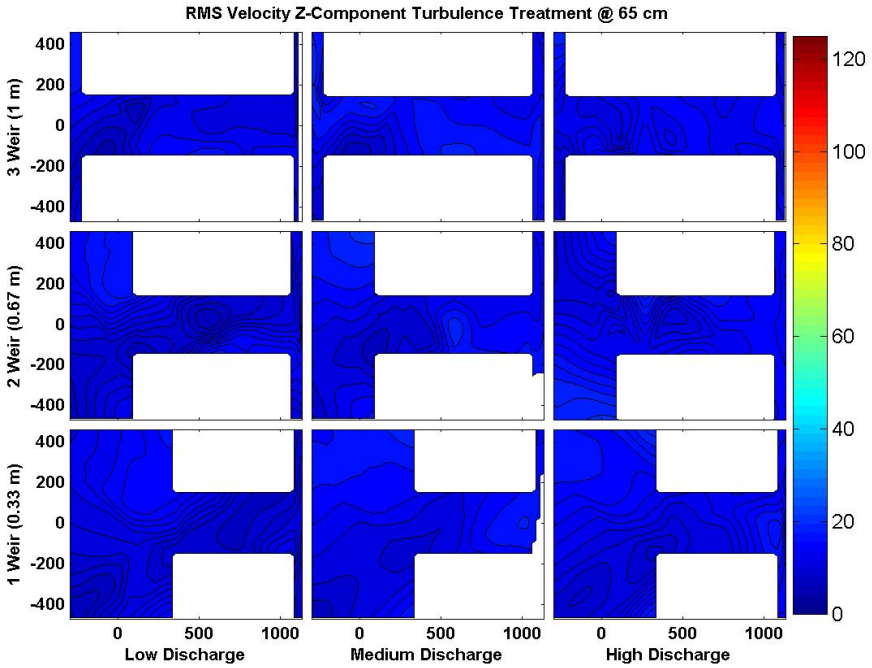

Figure 58: Contour plots of the RMS z-component for the turbulence treatment at 65 cm for each slot discharge and length treatments.

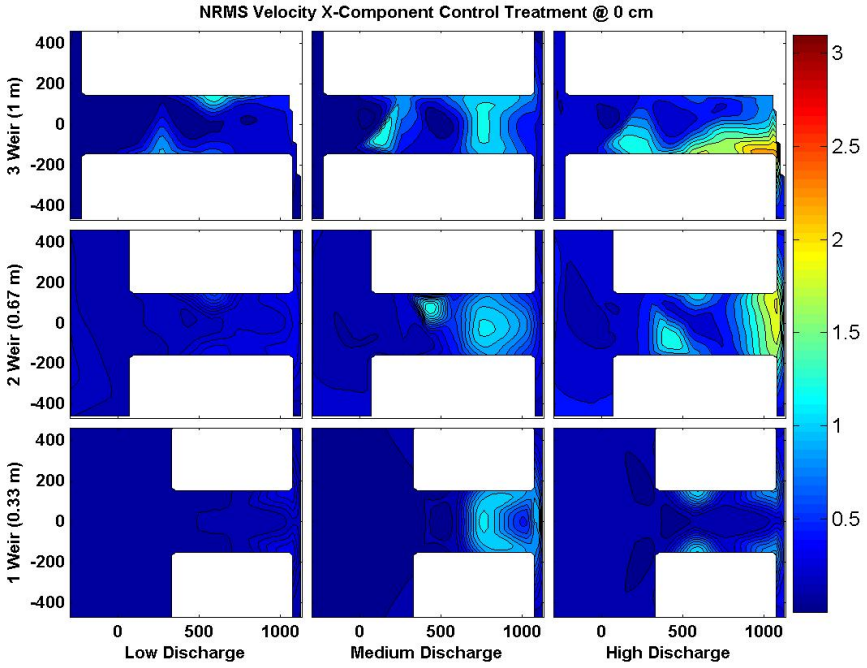

Figure 59: Contour plots of the NRMS x-component for the control treatment at 0 cm for each slot discharge and length treatments.

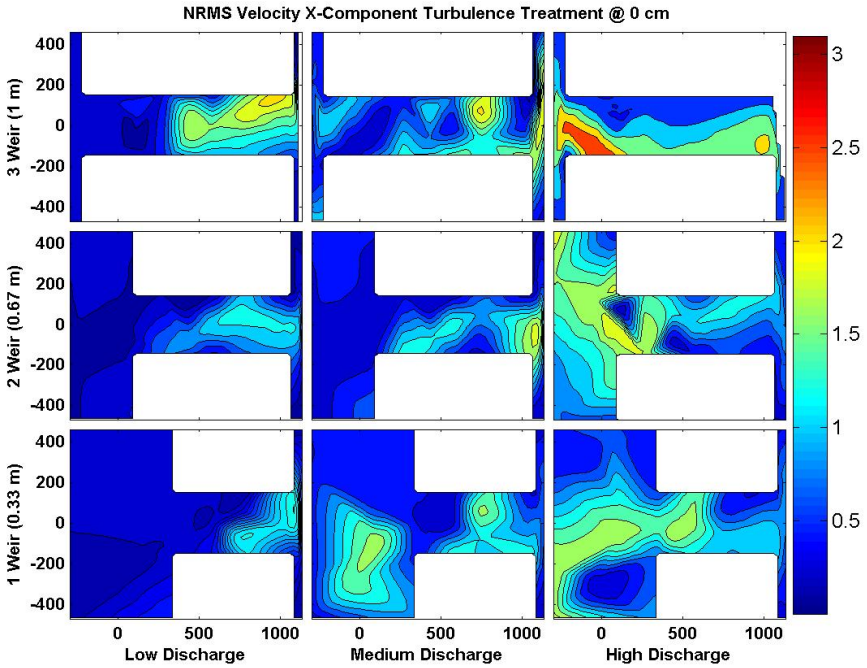

Figure 60: Contour plots of the NRMS x-component for the turbulence treatment at 0 cm for each slot discharge and length treatments.

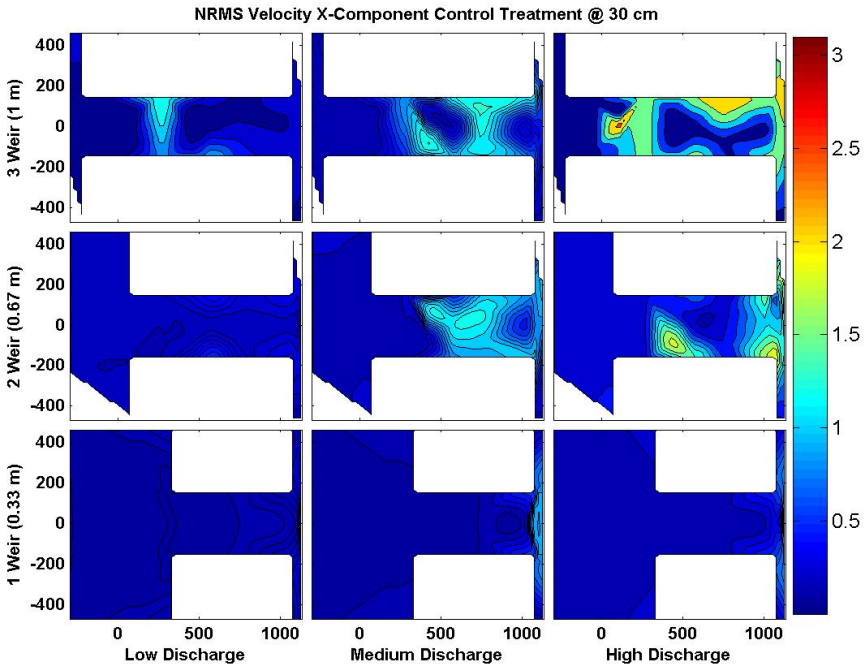

Figure 61: Contour plots of the NRMS x-component for the control treatment at 30 cm for each slot discharge and length treatments.

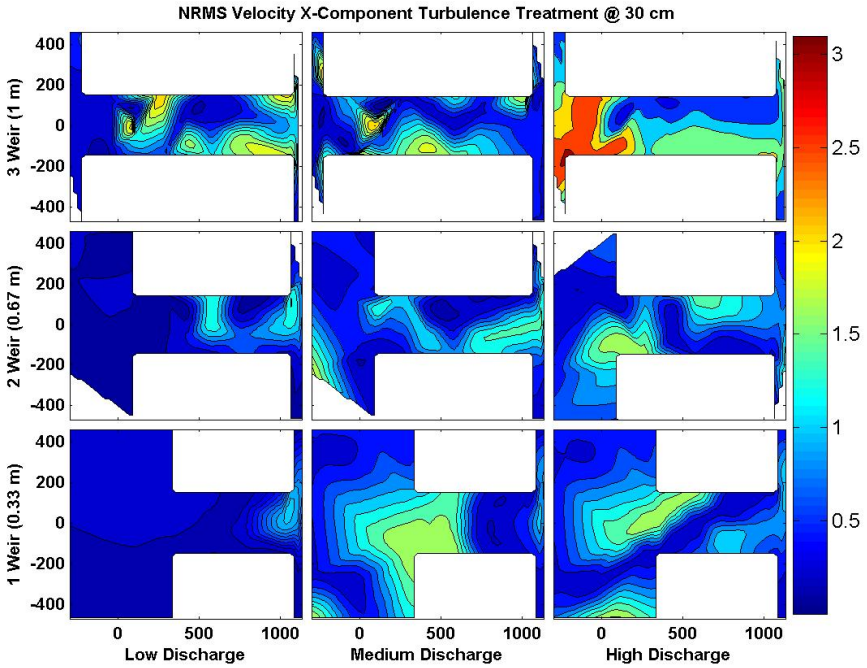

Figure 62: Contour plots of the NRMS x-component for the turbulence treatment at 30 cm for each slot discharge and length treatments.

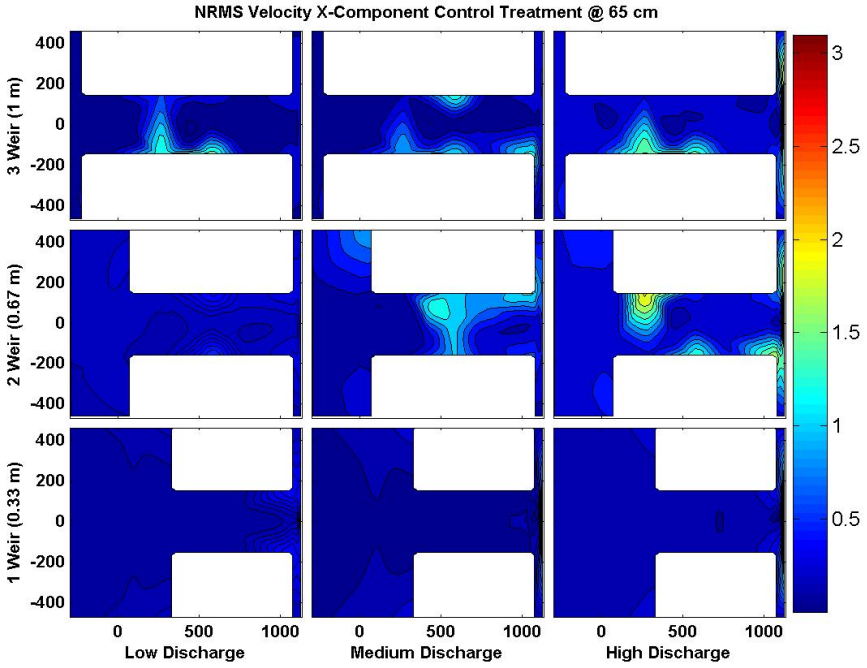

Figure 63: Contour plots of the NRMS x-component for the control treatment at 65 cm for each slot discharge and length treatments.

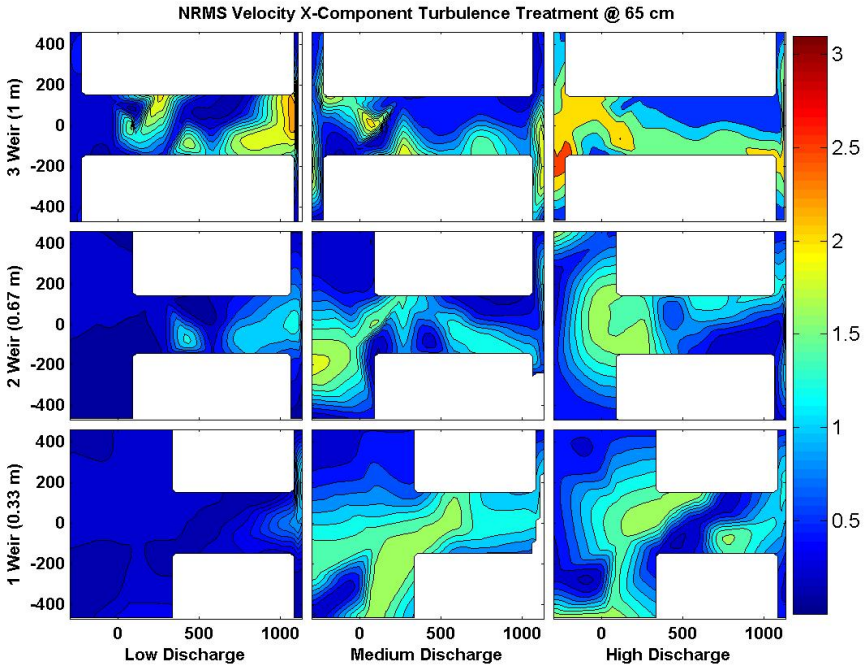

Figure 64: Contour plots of the NRMS x-component for the turbulence treatment at 65 cm for each slot discharge and length treatments.

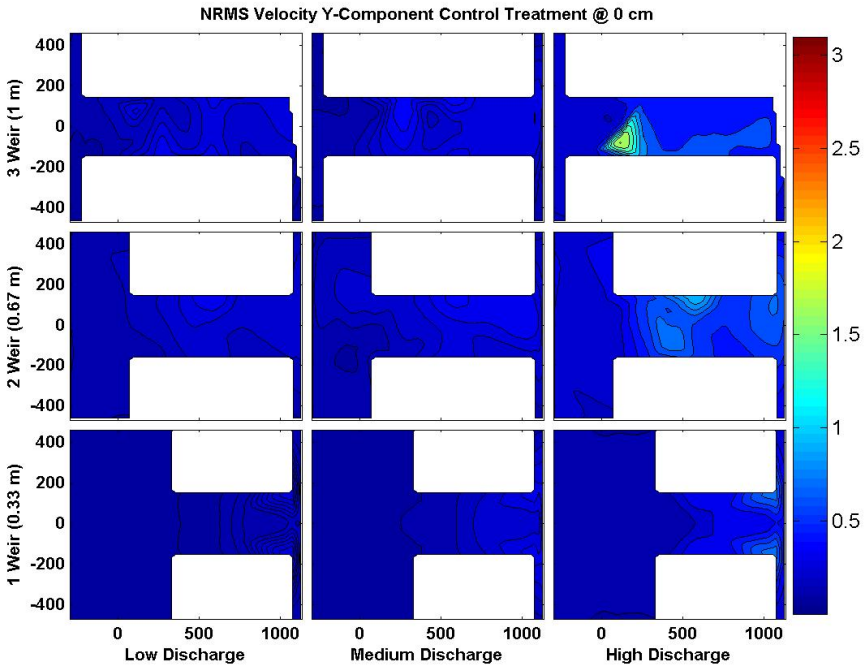

Figure 65: Contour plots of the NRMS y-component for the control treatment at 0 cm for each slot discharge and length treatments.

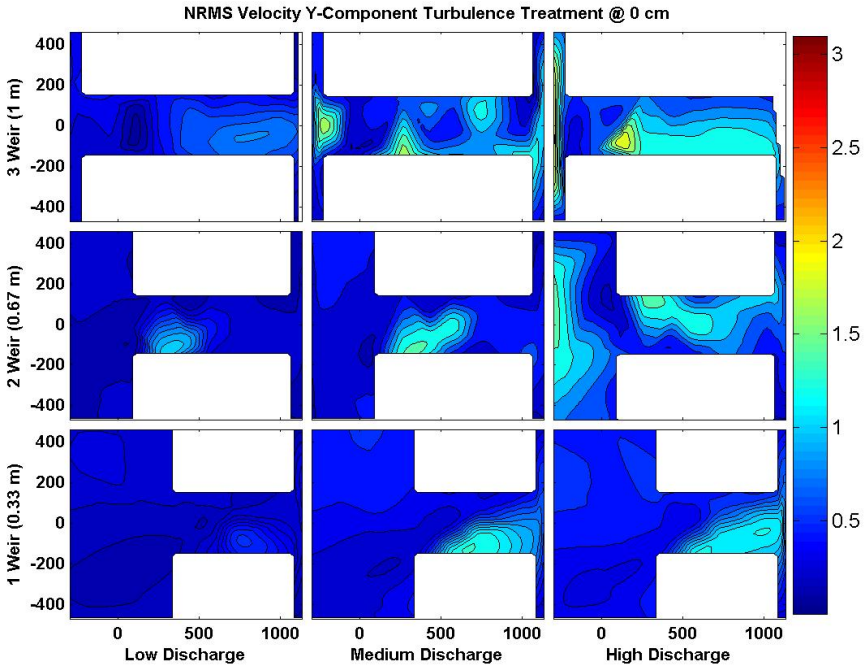

Figure 66: Contour plots of the NRMS y-component for the turbulence treatment at 0 cm for each slot discharge and length treatments.

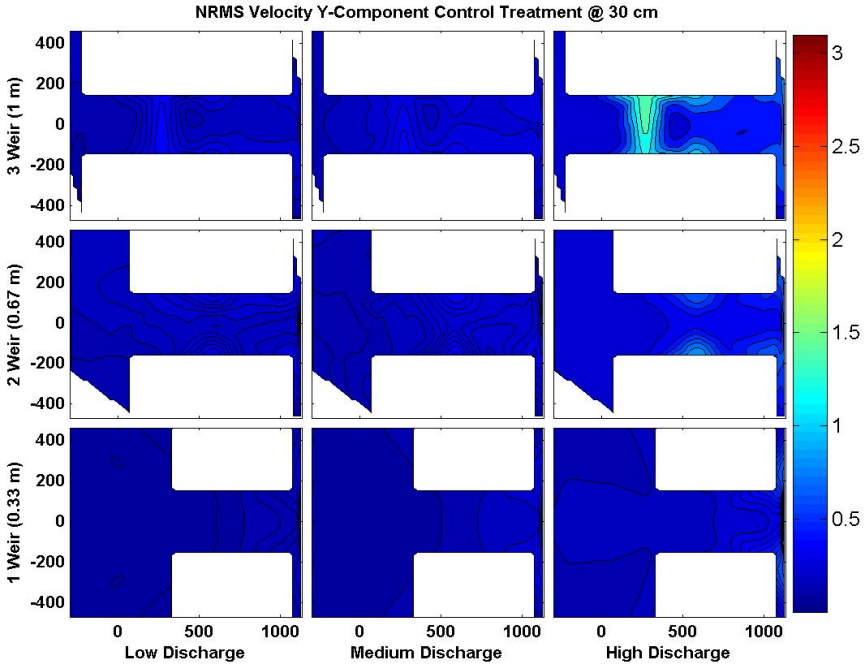

Figure 67: Contour plots of the NRMS y-component for the control treatment at 30 cm for each slot discharge and length treatments.

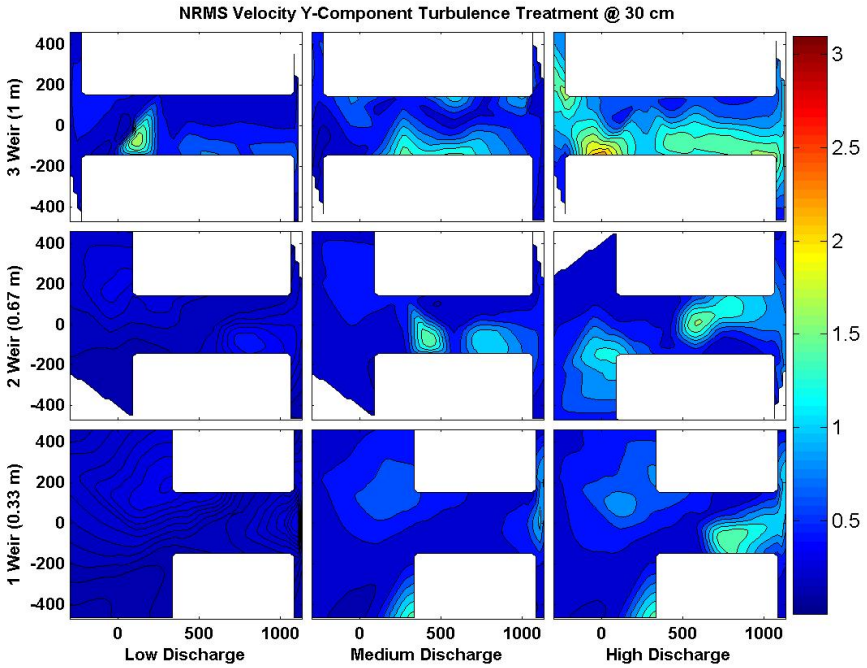

Figure 68: Contour plots of the NRMS y-component for the turbulence treatment at 30 cm for each slot discharge and length treatments.

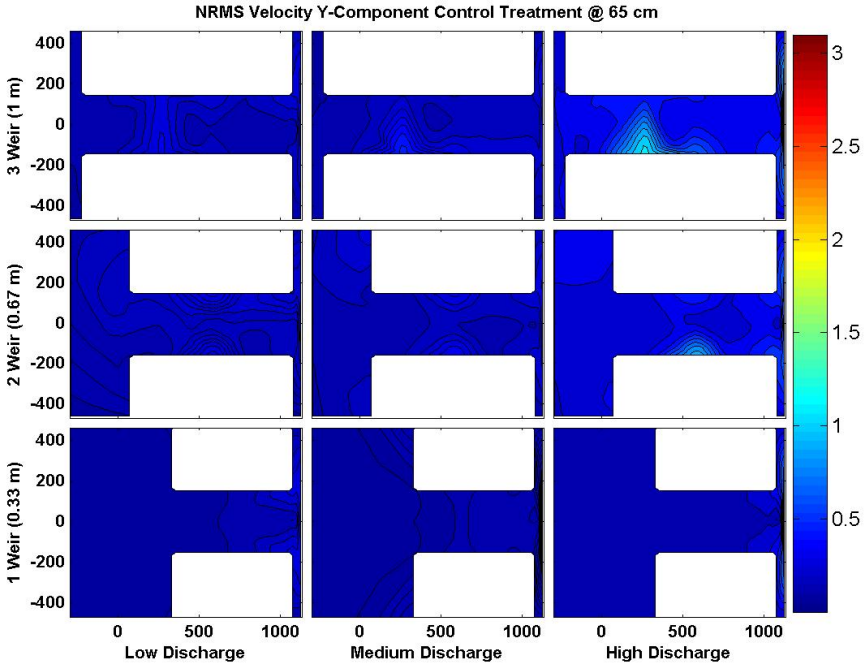

Figure 69: Contour plots of the NRMS y-component for the control treatment at 65 cm for each slot discharge and length treatments.

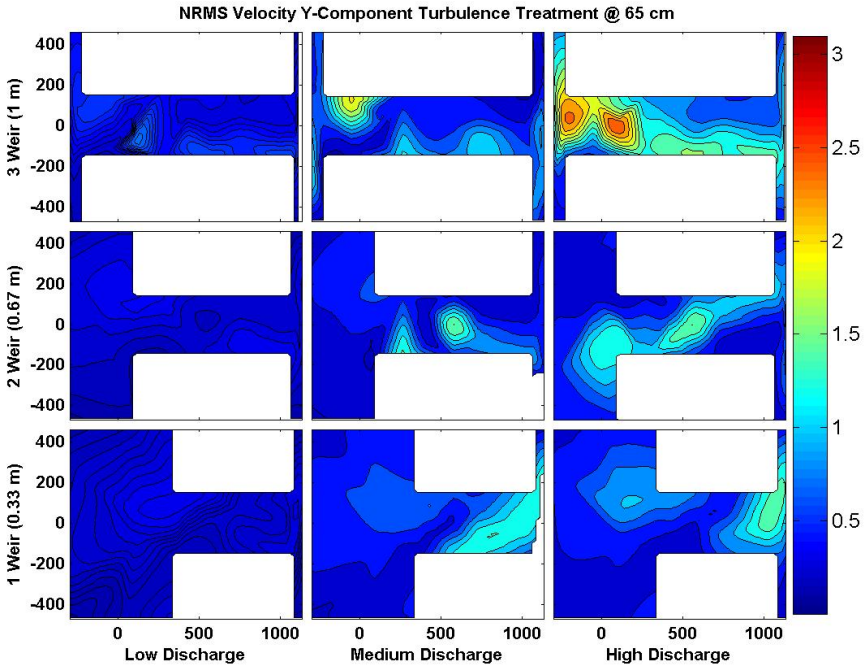

Figure 70: Contour plots of the NRMS y-component for the turbulence treatment at 65 cm for each slot discharge and length treatments.

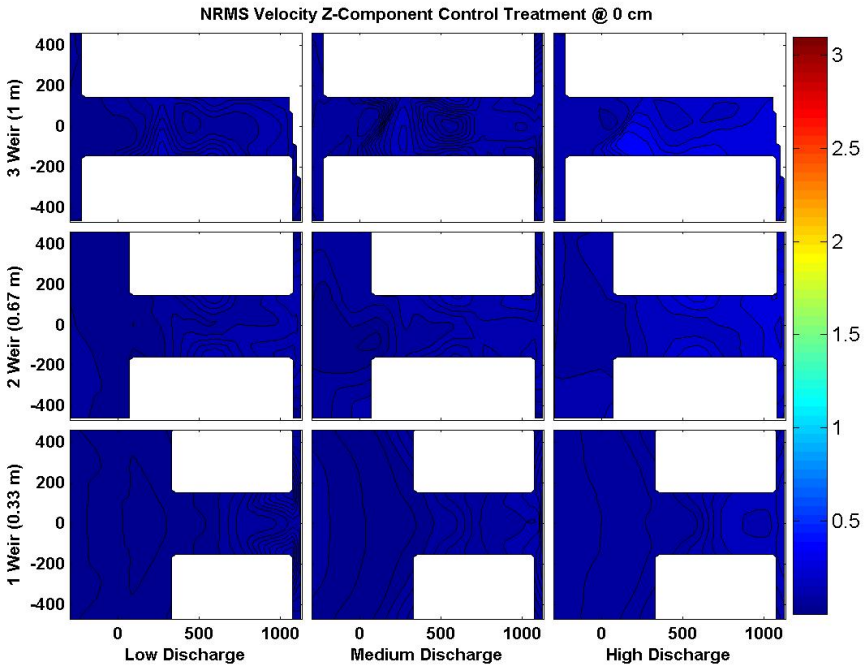

Figure 71: Contour plots of the NRMS z-component for the control treatment at 0 cm for each slot discharge and length treatments.

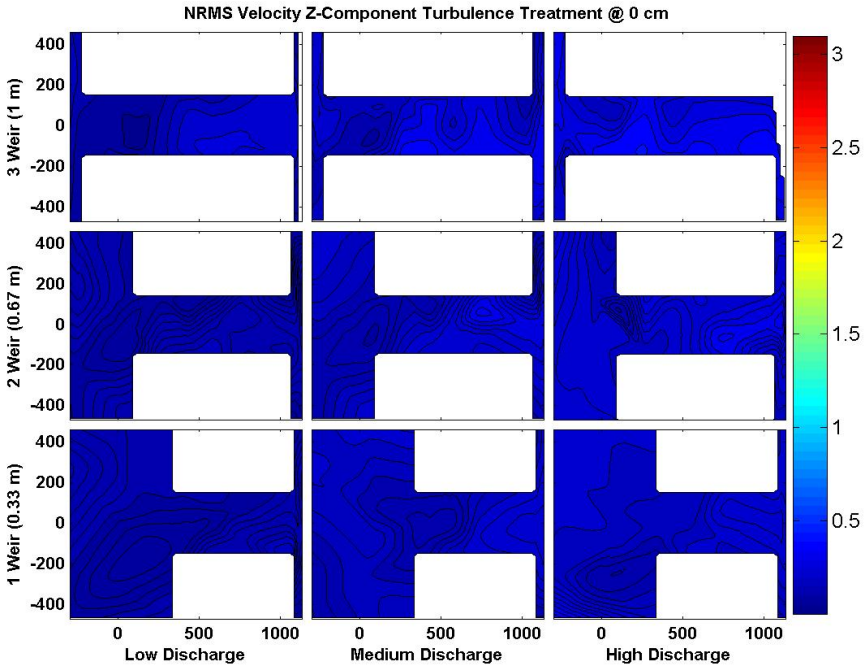

Figure 72: Contour plots of the NRMS z-component for the turbulence treatment at 0 cm for each slot discharge and length treatments.

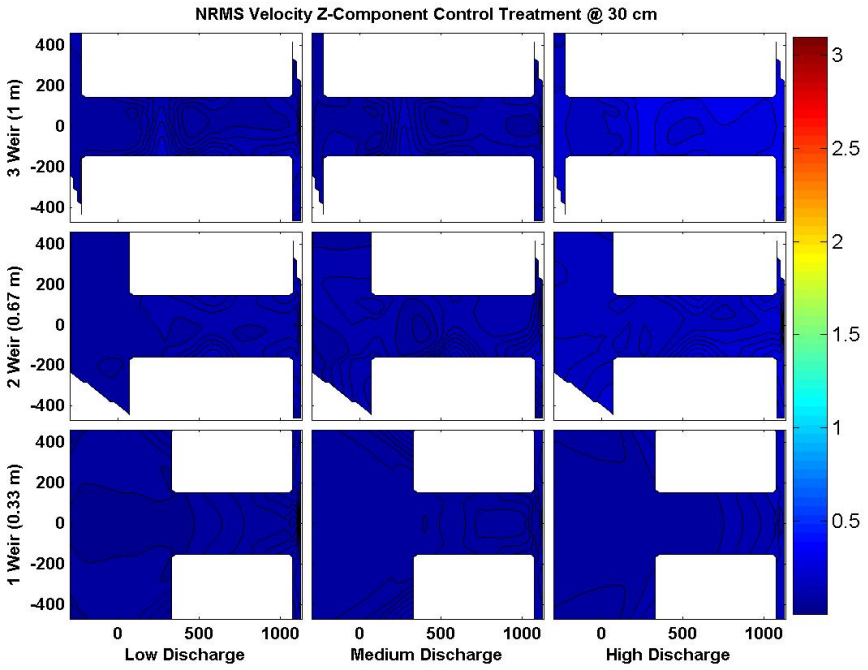

Figure 73: Contour plots of the NRMS z-component for the control treatment at 30 cm for each slot discharge and length treatments.

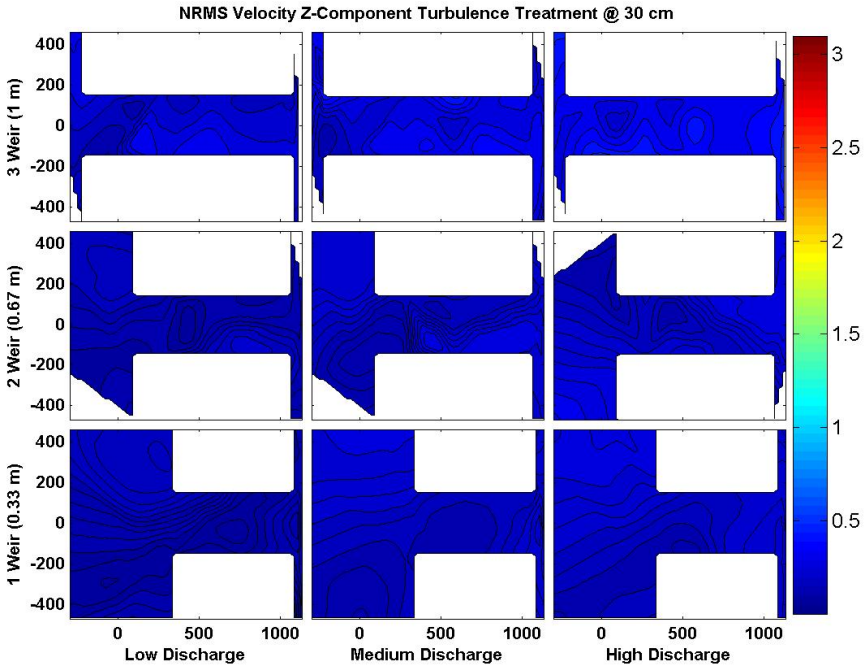

Figure 74: Contour plots of the NRMS z-component for the turbulence treatment at 30 cm for each slot discharge and length treatments.

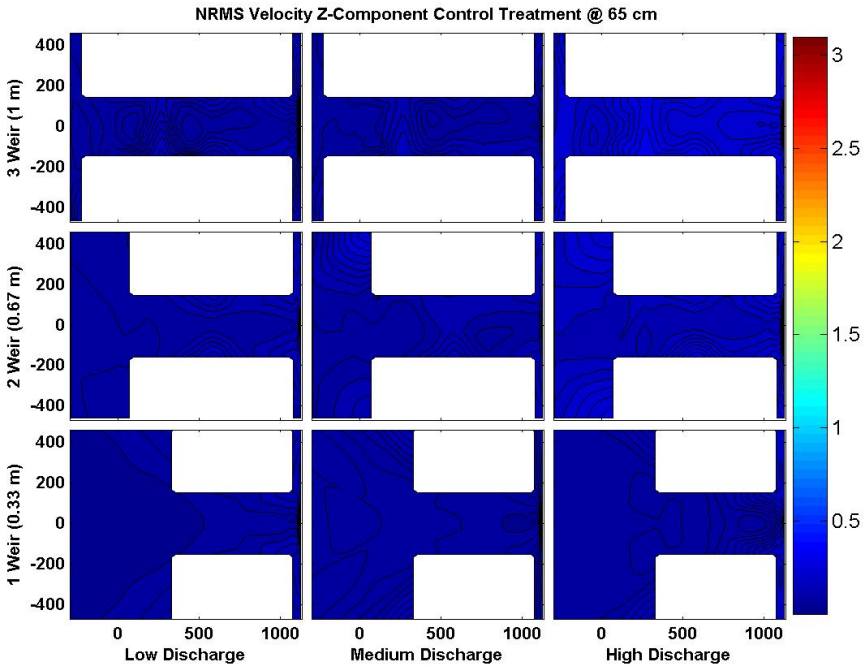

Figure 75: Contour plots of the NRMS z-component for the control treatment at 65 cm for each slot discharge and length treatments.

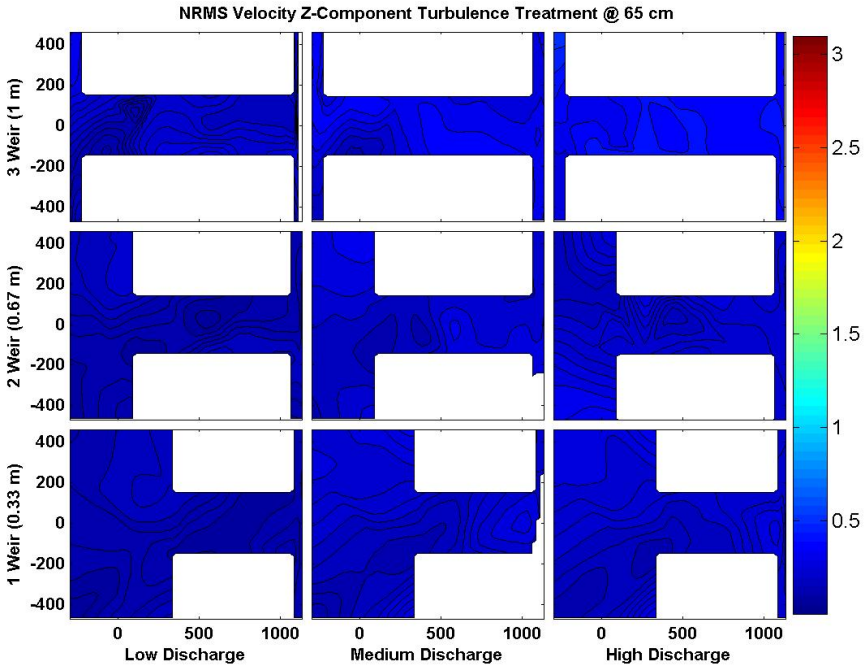

Figure 76: Contour plots of the NRMS z-component for the turbulence treatment at 65 cm for each slot discharge and length treatments.

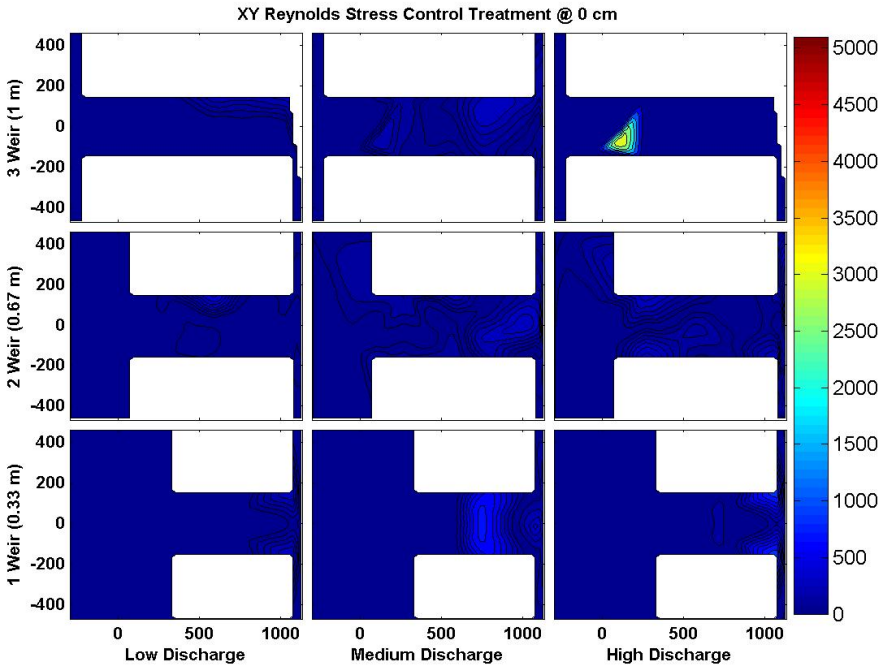

Figure 77: Contour plots of the X-Y Reynold's Stress for the control treatment at 0 cm for each slot discharge and length treatments.

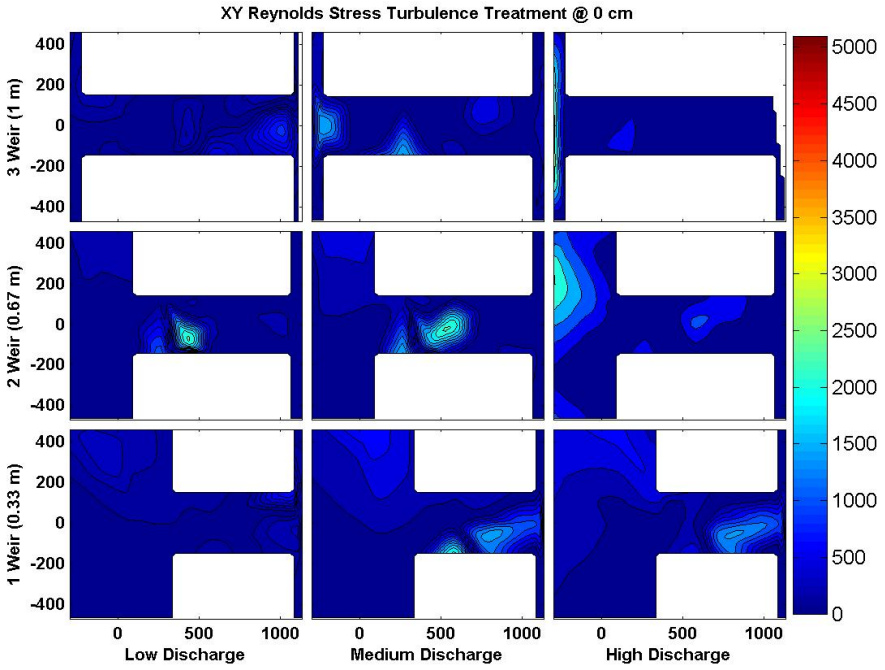

Figure 78: Contour plots of the X-Y Reynold's Stress for the turbulence treatment at 0 cm for each slot discharge and length treatments.

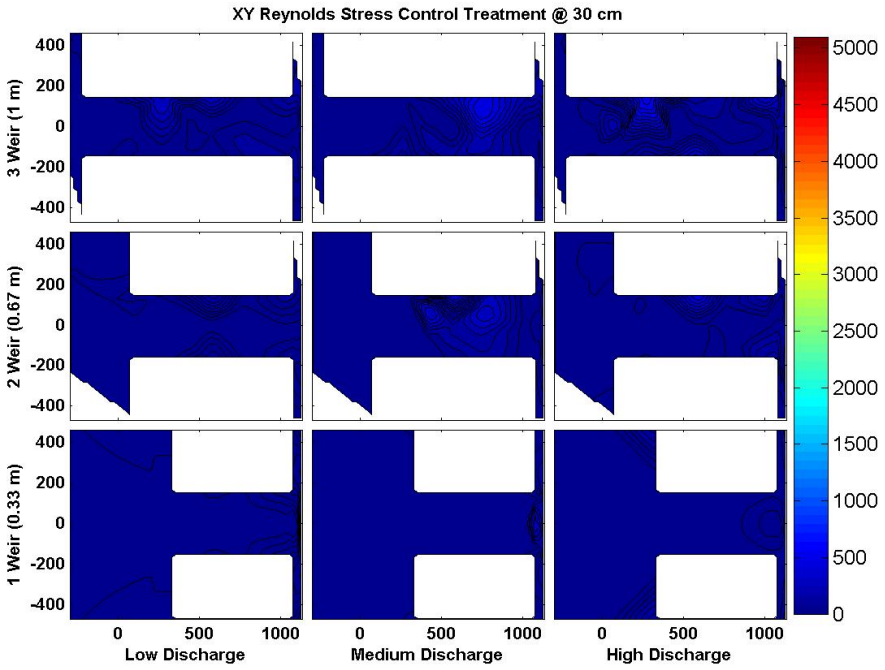

Figure 79: Contour plots of the X-Y Reynold's Stress for the control treatment at 30 cm for each slot discharge and length treatments.

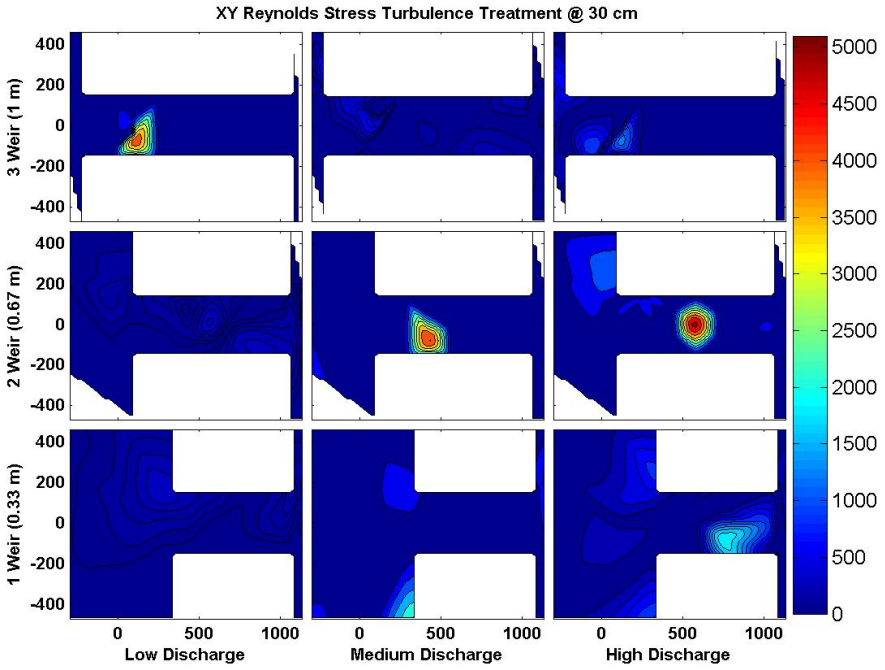

Figure 80: Contour plots of the X-Y Reynold's Stress for the turbulence treatment at 30 cm for each slot discharge and length treatments.

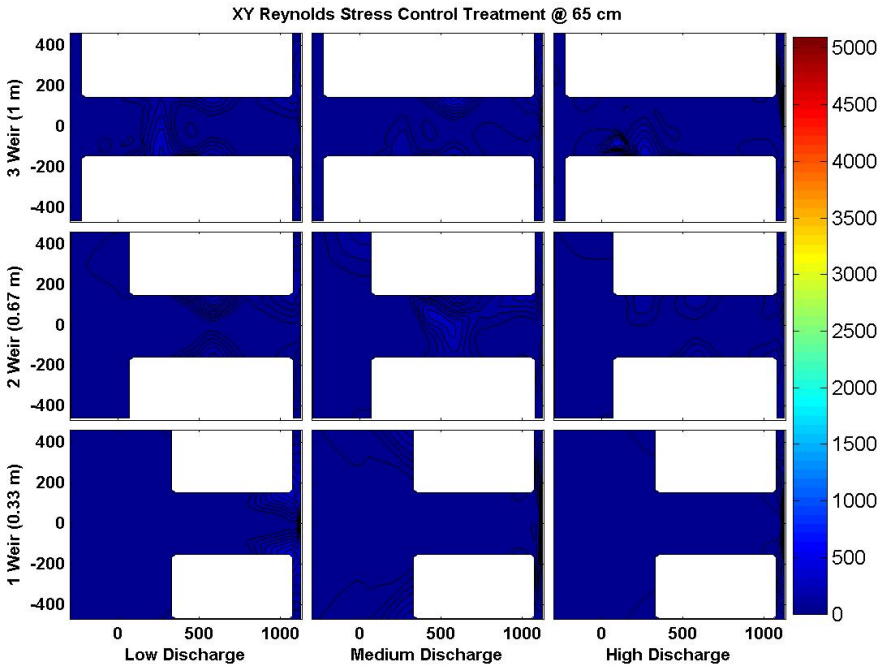

Figure 81: Contour plots of the X-Y Reynold's Stress for the control treatment at 65 cm for each slot discharge and length treatments.

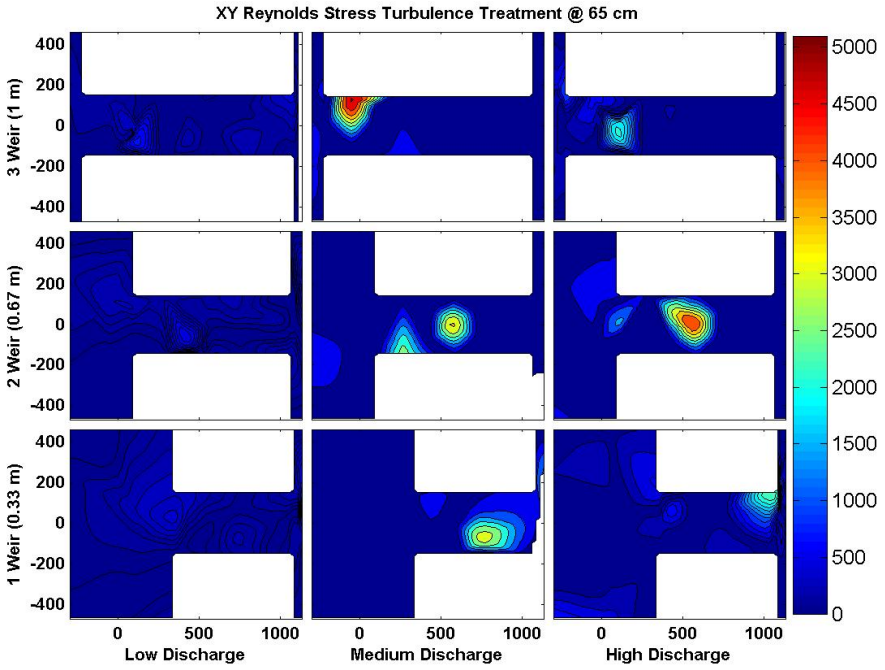

Figure 82: Contour plots of the X-Y Reynold's Stress for the turbulence treatment at 65 cm for each slot discharge and length treatments.

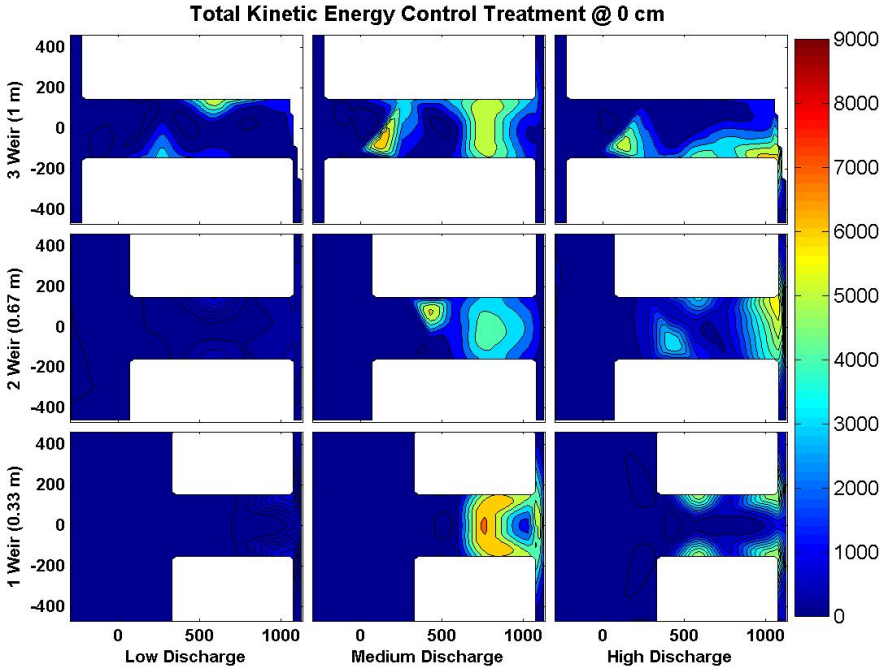

Figure 83: Contour plots of the turbulent kinetic energy, TKE, for the control treatment at 0 cm for each slot discharge and length treatments.

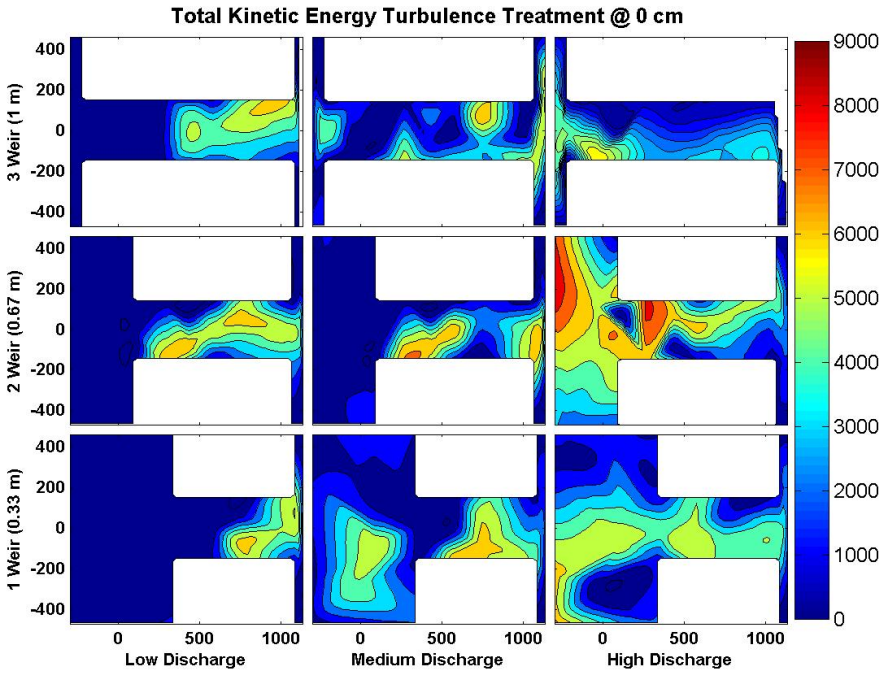

Figure 84: Contour plots of the turbulent kinetic energy, TKE, for the turbulence treatment at 0 cm for each slot discharge and length treatments.

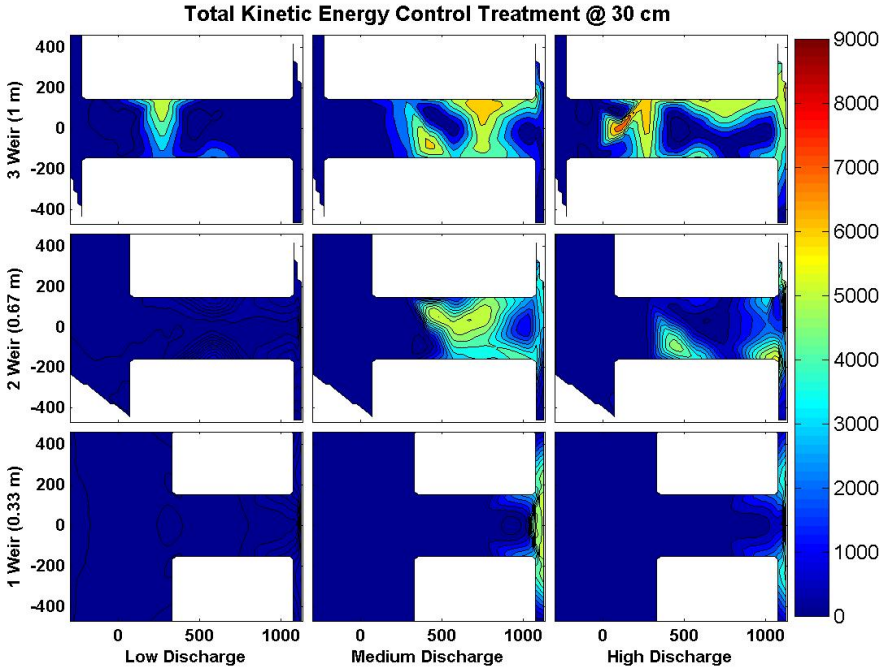

Figure 85: Contour plots of the turbulent kinetic energy, TKE, for the control treatment at 30 cm for each slot discharge and length treatments.

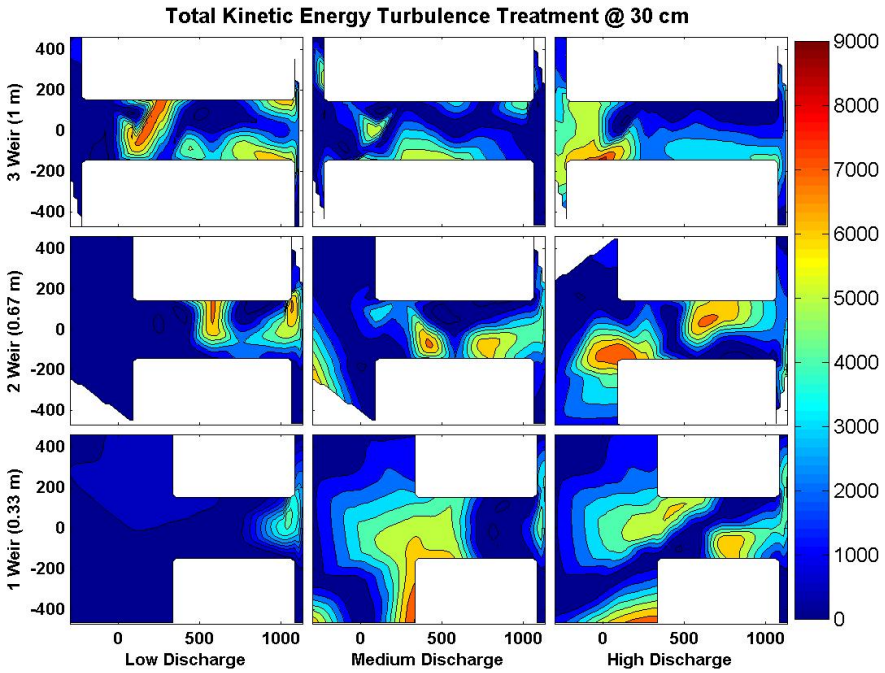

Figure 86: Contour plots of the turbulent kinetic energy, TKE, for the turbulence treatment at 30 cm for each slot discharge and length treatments.

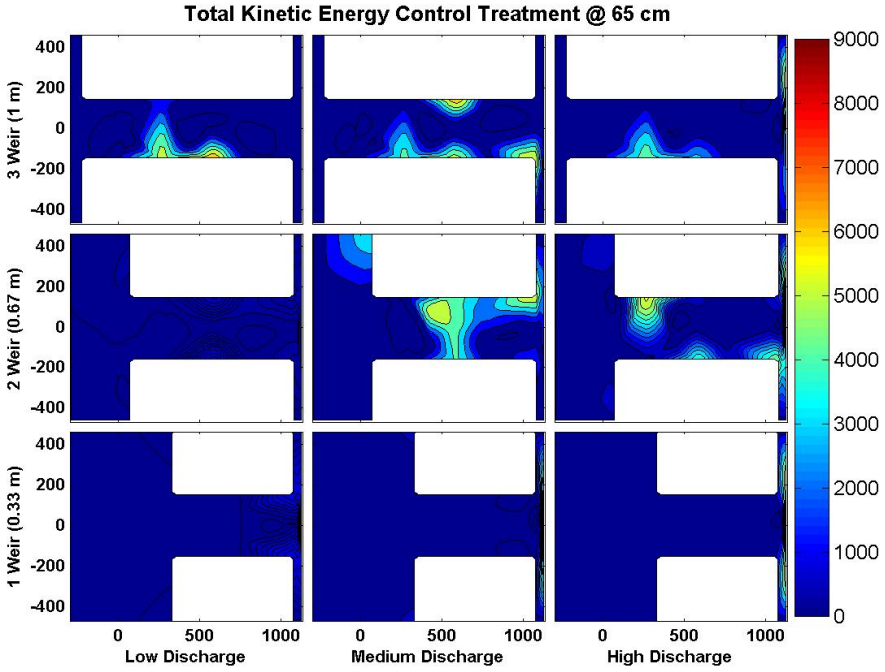

Figure 87: Contour plots of the turbulent kinetic energy, TKE, for the control treatment at 65 cm for each slot discharge and length treatments.

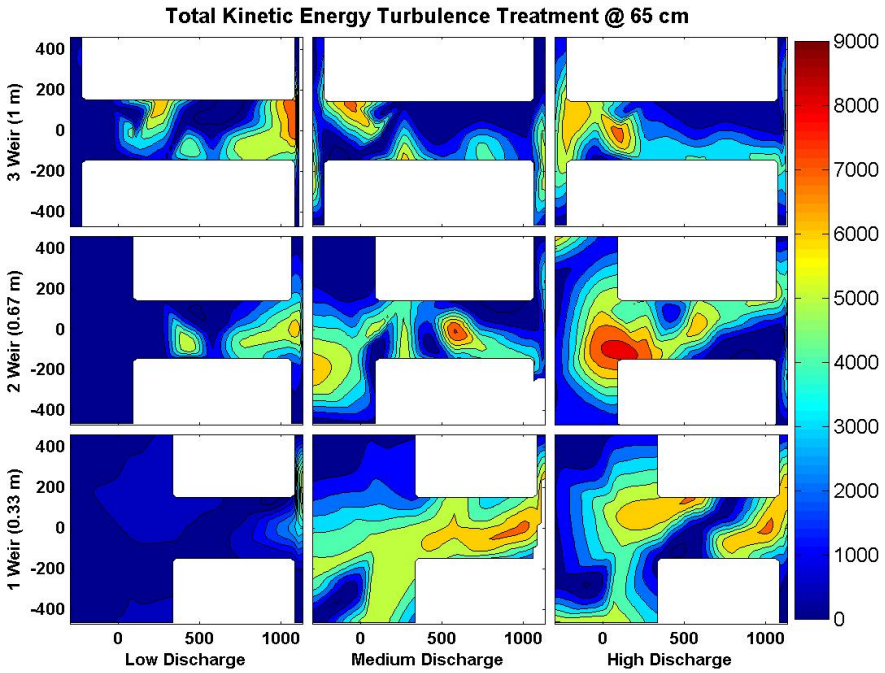

Figure 88: Contour plots of the turbulent kinetic energy, TKE, for the turbulence treatment at 65 cm for each slot discharge and length treatments.

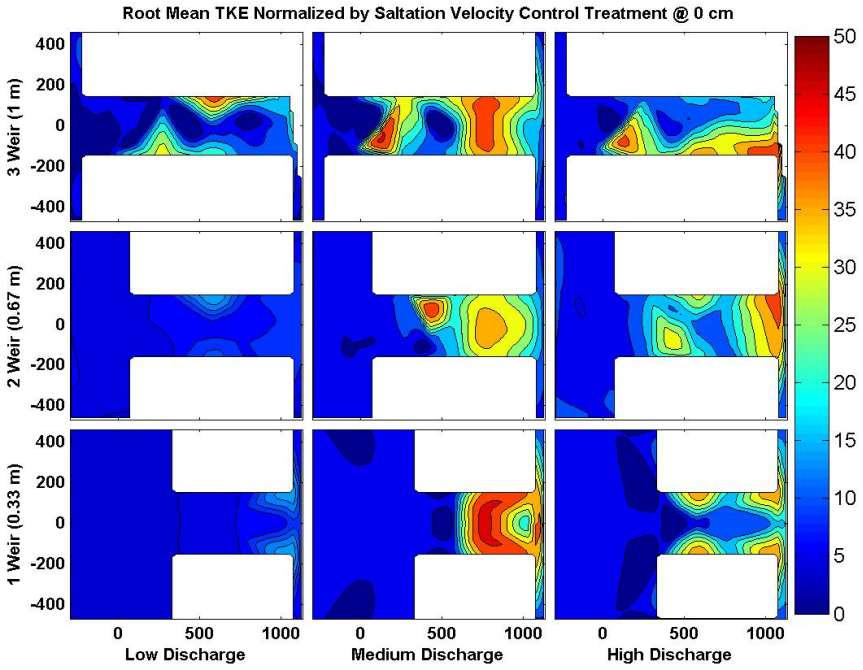

Figure 89: Contour plots of Root Mean of TKE normalized by saltation velocity for the control treatment at 0 cm for each slot discharge and length treatments.

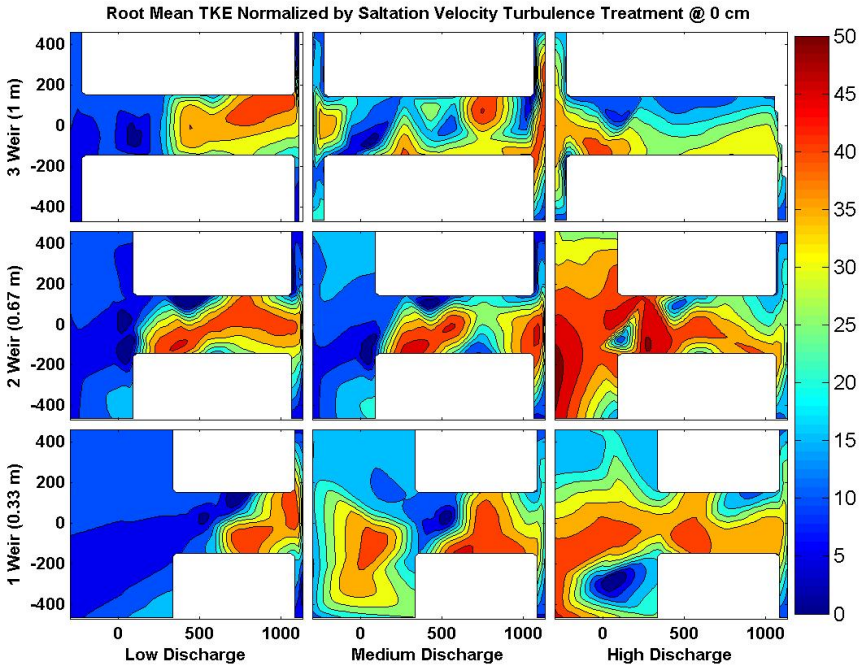

Figure 90: Contour plots of Root Mean of TKE normalized by saltation velocity for the turbulence treatment at 0 cm for each slot discharge and length treatments.

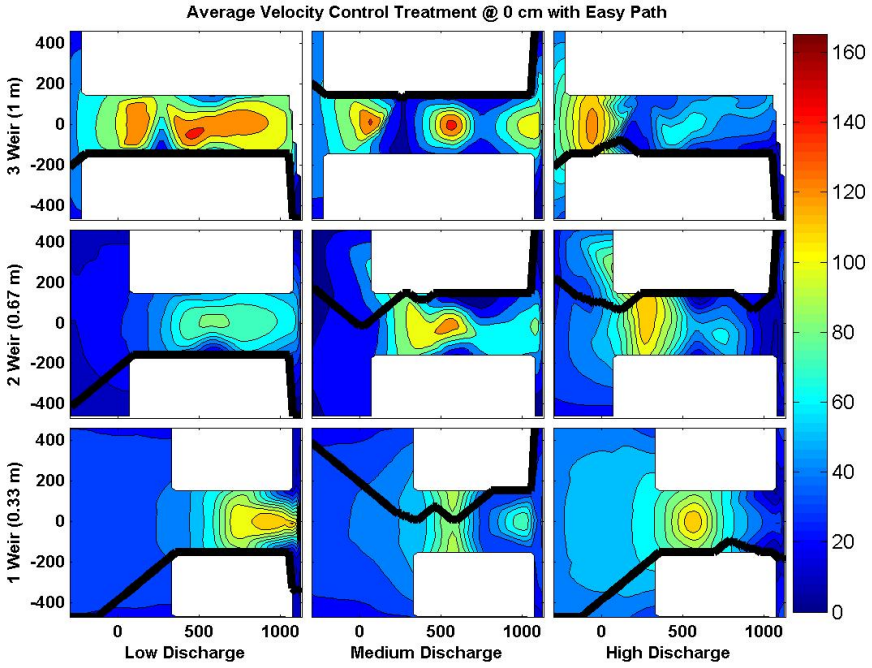

Figure 91: Contour plots of Average Velocity, V, for the control treatment at 0 cm for each slot discharge and length treatments with "easy path" plotted.

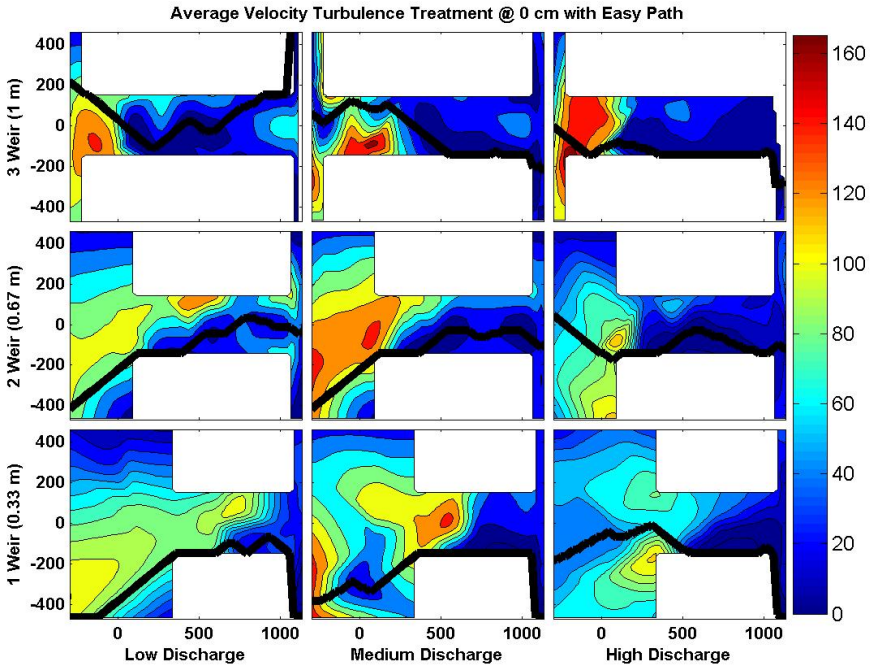

Figure 92: Contour plots of Average Velocity, V, for the turbulence treatment at 0 cm for each slot discharge and length treatments with "easy path" plotted.

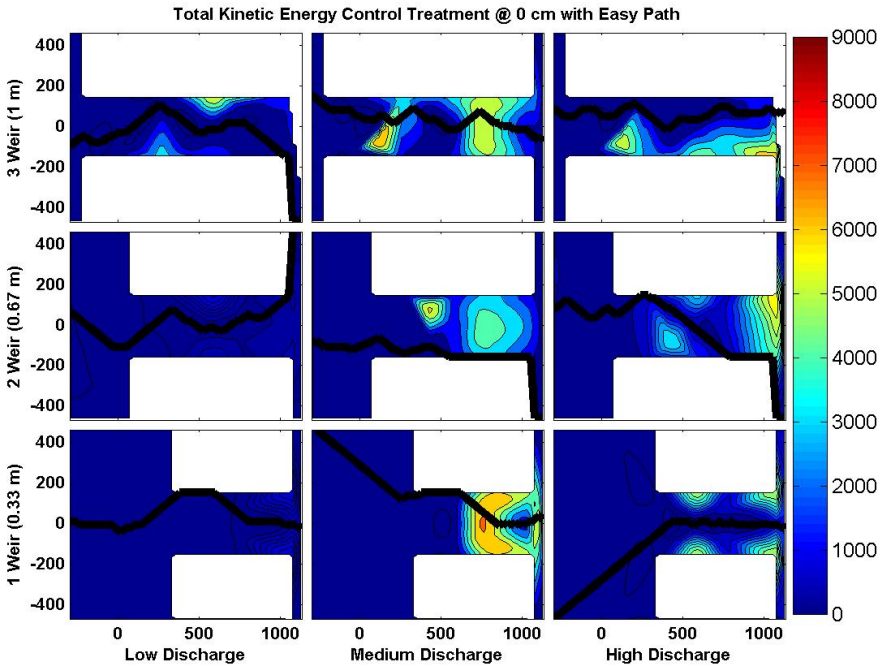

Figure 93: Contour plots of the turbulent kinetic energy, TKE, for the control treatment at 0 cm for each slot discharge and length treatments with "easy path" plotted.

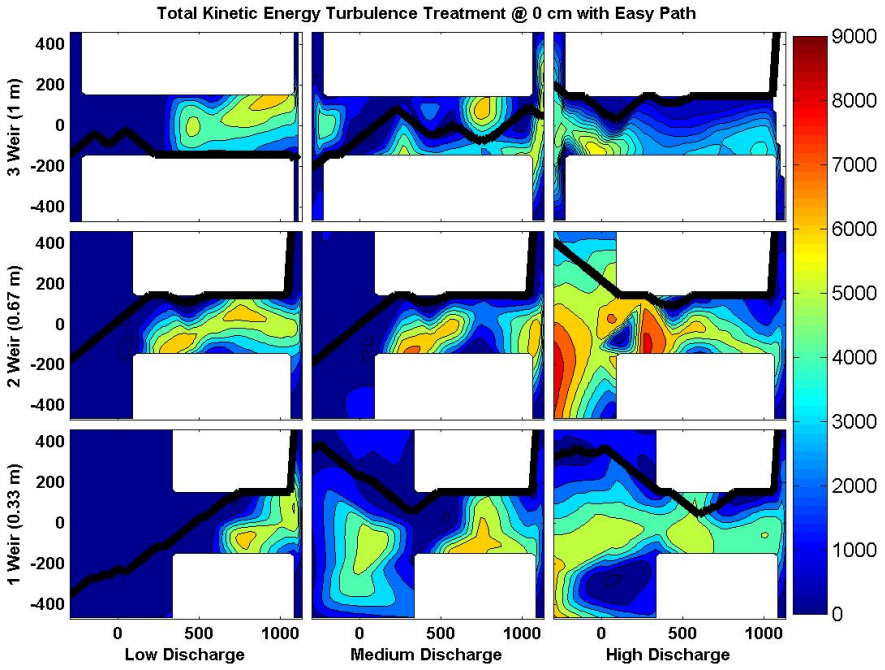

Figure 94: Contour plots of the turbulent kinetic energy, TKE, for the turbulence treatment at 0 cm for each slot discharge and length treatments with "easy path" plotted.

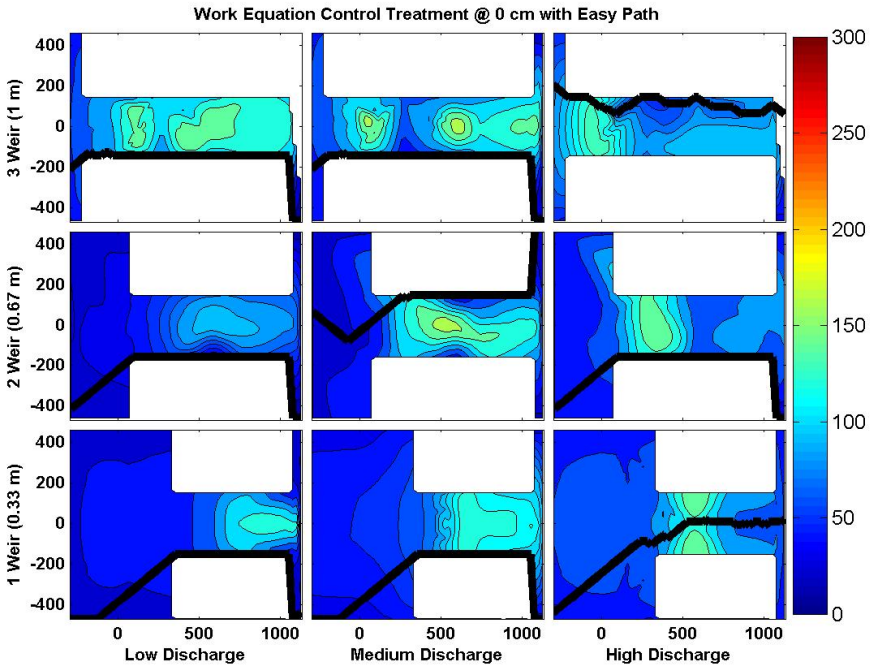

Figure 95: Contour plots of work for the control treatment at 0 cm for each slot discharge and length treatments with "easy path" plotted.

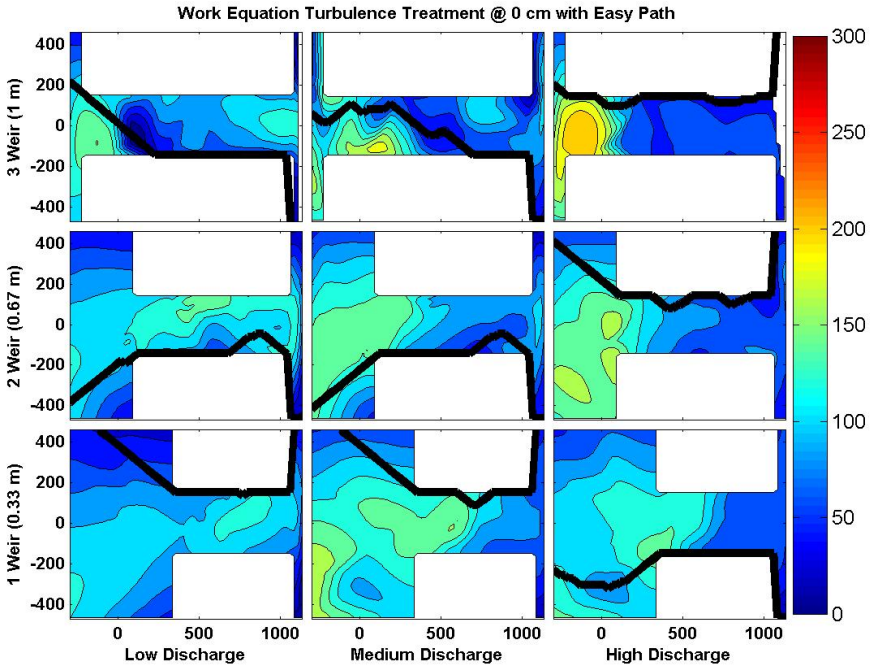

Figure 96: Contour plots of work for the turbulence treatment at 0 cm for each slot discharge and length treatments with "easy path" plotted.

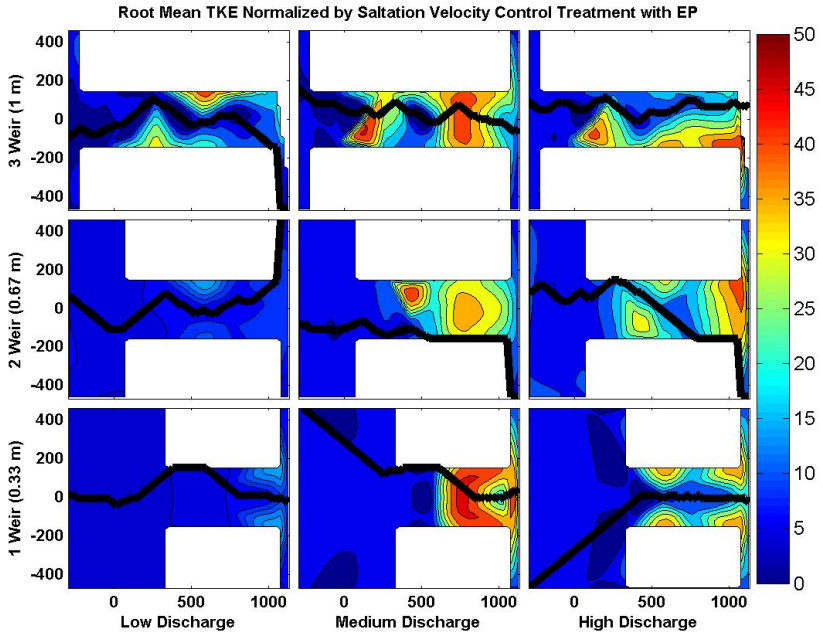

Figure 97: Contour plots of Root Mean of TKE normalized by saltation velocity for the control treatment at 0 cm for each slot discharge and length treatments with "easy path" plotted.

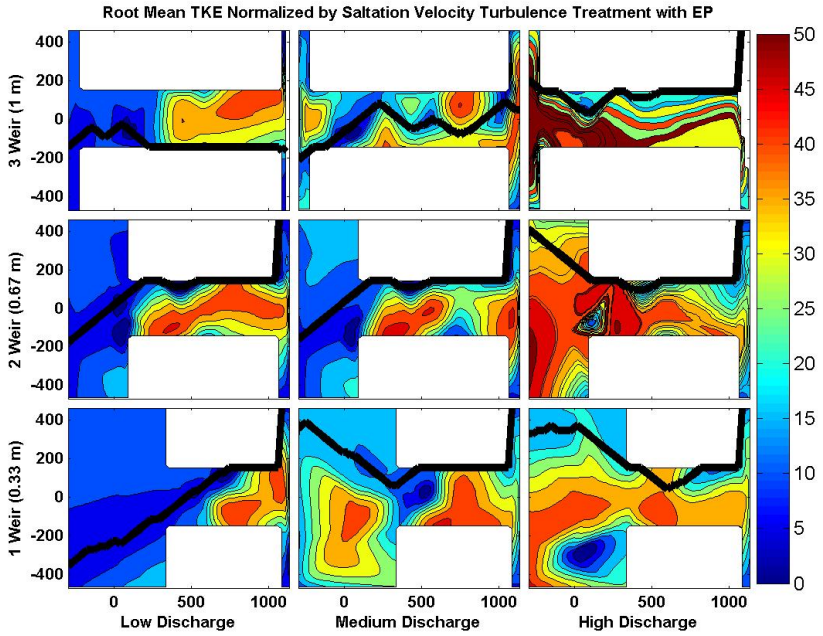

Figure 98: Contour plots of Root Mean of TKE normalized by saltation velocity for the turbulence treatment at 0 cm for each slot discharge and length treatments with "easy path" plotted.

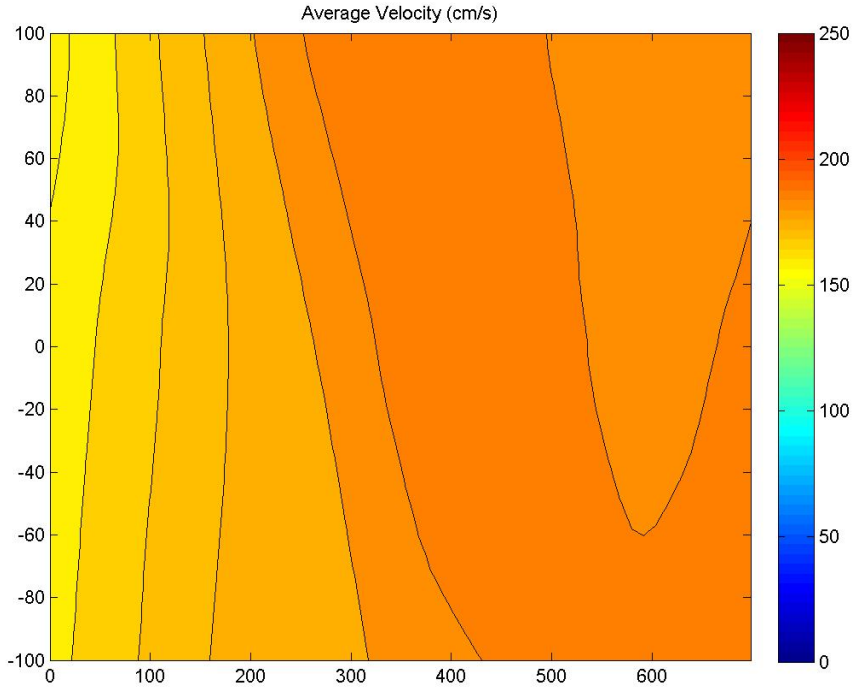

Figure 99: Contour plot of average velocity within slot at Bonneville Dam Serpentine Weir

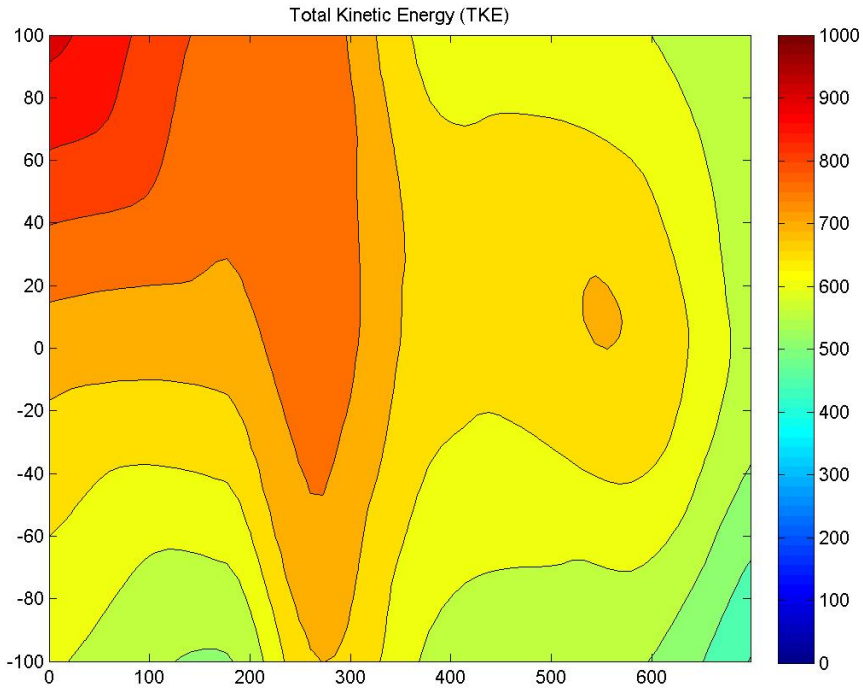

Figure 100: Contour plot of TKE within slot at Bonneville Dam Serpentine Weir

Chapter 2: John Day Lamprey Passage System Design and Installation

Purpose and Need

Pacific lamprey have difficulties ascending the lower fishway at the North Shore Fishway at the John Day Dam, Columbia River, USA (M.L. Keefer et al., 2013). The University of Idaho was asked to develop plans, furnish, and install a Lamprey Passage System (LPS) to collect lamprey just upstream of the entrance. Collected lamprey could then be transported upstream.

Design

The LPS was designed within Solidworks, a solid modeling 3-D CAD software. The LPS system was designed per the guidelines previously developed by the National Oceanic and Atmospheric Administration (NOAA) National Marine Fisheries Service(NMFS, 2008; Zobott et al., 2015). Final design plans were created based on conceptual design and consultation with USACE and NMFS biologists. I worked closely with a structural engineer to complete final stamped drawings per US Army Corps of Engineers (USACOE) specifications. The LPS system consists of climbing flumes, a resting box, an upwelling box, a trap box, and a pump system (Figure 101). The rest box (Figure 102) provides a rest area for the lamprey after a long climb. The upwelling box (Figure 103) spills water down the flume to provide sufficient flows for climbing in lamprey (M. L. Keefer et al., 2011; P. S. Kemp, Tsuzaki, & Moser, 2009; Moser, Keefer, Pennington, Ogden, & Simonson, 2011). The trap box is used to capture the lamprey to relocate them upstream of the dam.

Construction

We contracted with a machine shop to fabricate the parts of the LPS. I created an installation plan for the LPS that was approved by the USACOE. The University of Idaho team installed the LPS over a one-week period at the dam (Figure 105, Figure 106: Lifting Pumps into Place, Figure 107, and Figure 108). During installation I took field notes and redlined plans to be modified as construction occurred. Once construction was complete I worked with the structural engineer to complete as-built drawings that were approved by the USACOE.

Post Construction

The University of Idaho team counted and tagged at the lamprey trap daily and monitored LPS condition. The LPS performed well throughout its first two seasons of use. For example, 1228 lamprey were collected from the LPS in 2014, 4.7% of the total counted at John Day Dam that year. The USACOE took over operation of the John Day LPS in the summer of 2015. The University of Idaho team developed and submitted an Operations and Maintenance Manual to the USACOE for long-term operation of the LPS system.

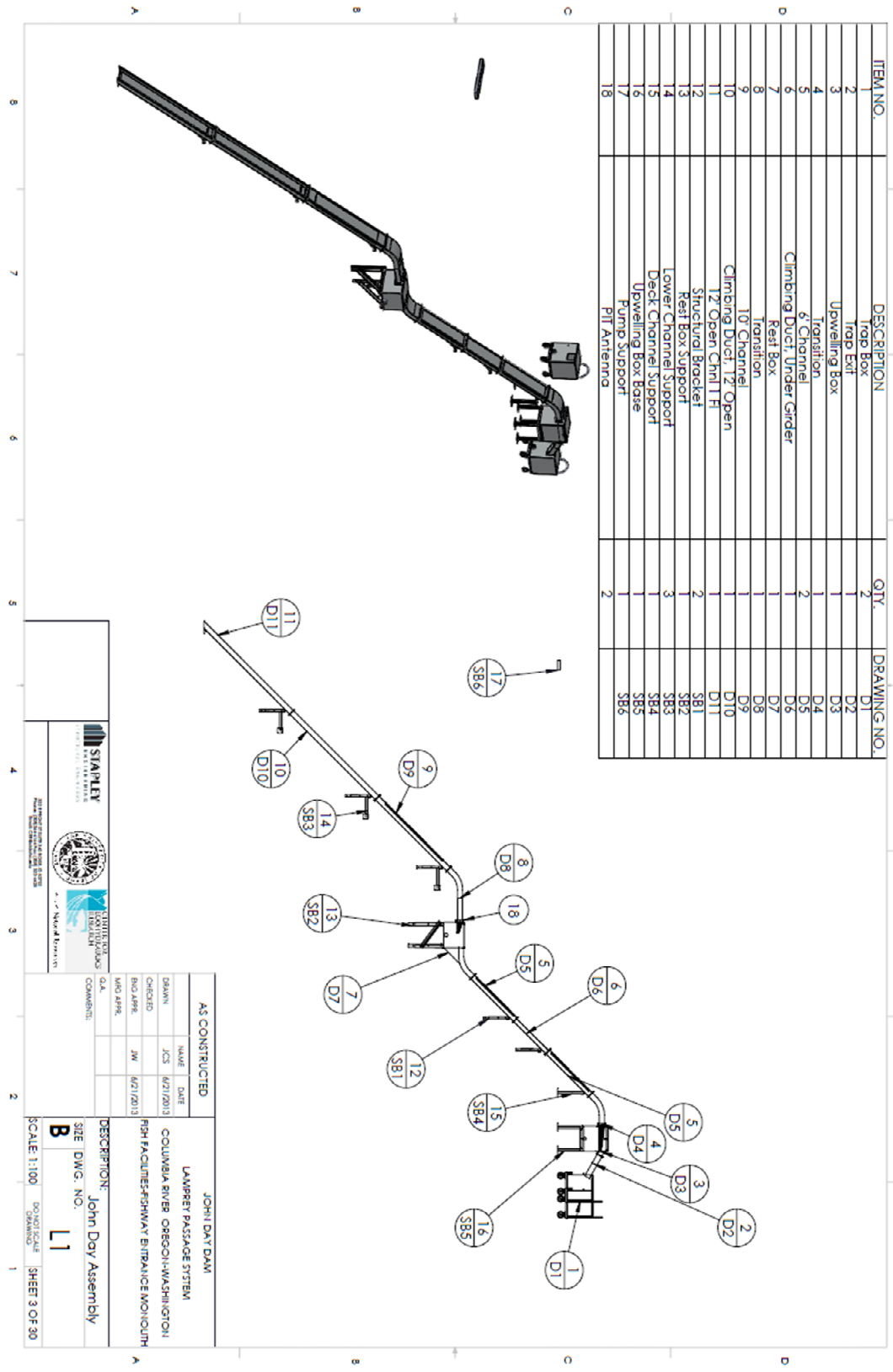

Figure 101: Profile view of Lamprey Passage Structure

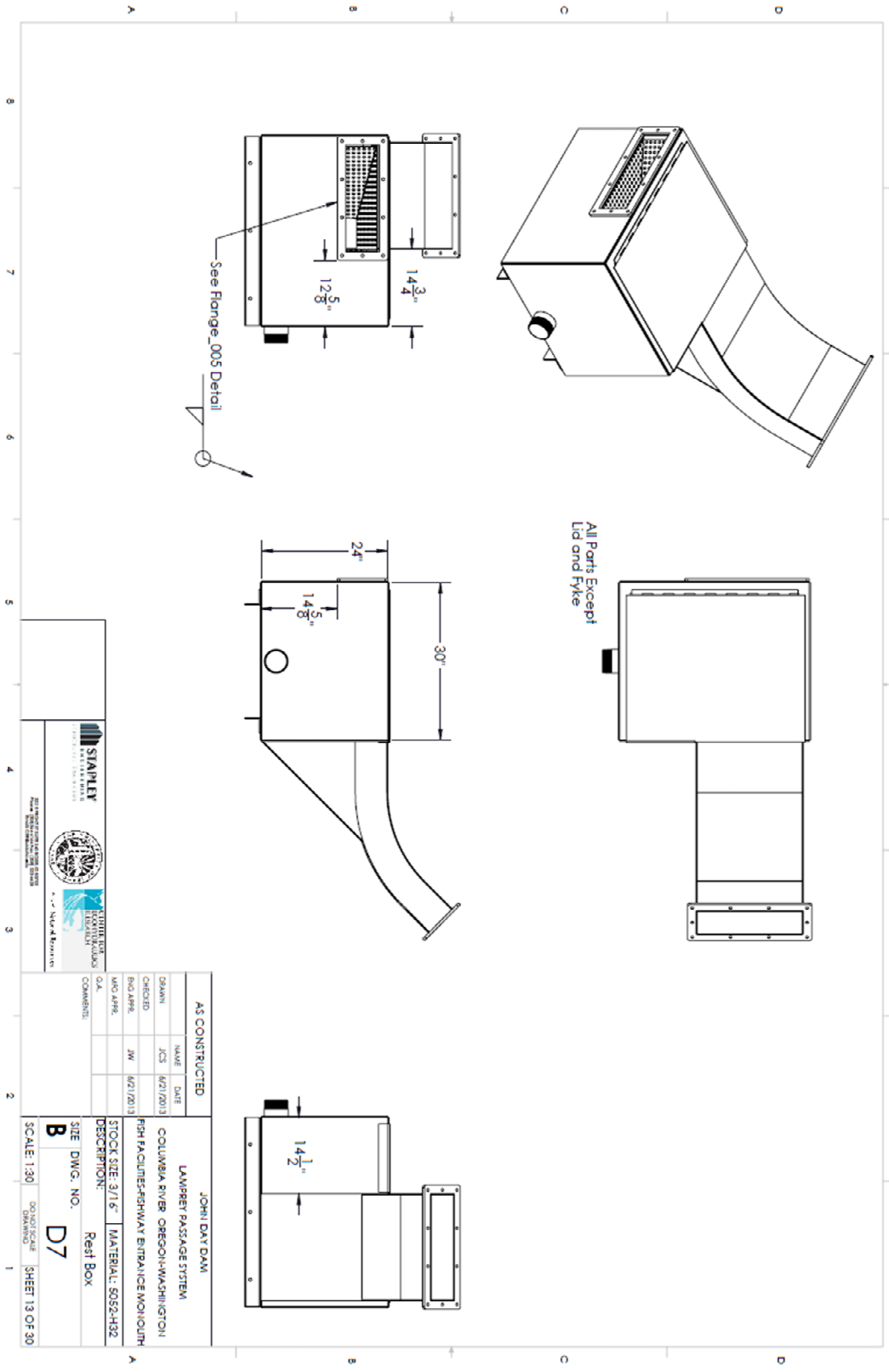

Figure 102: Rest Box of Lamprey Passage Structure

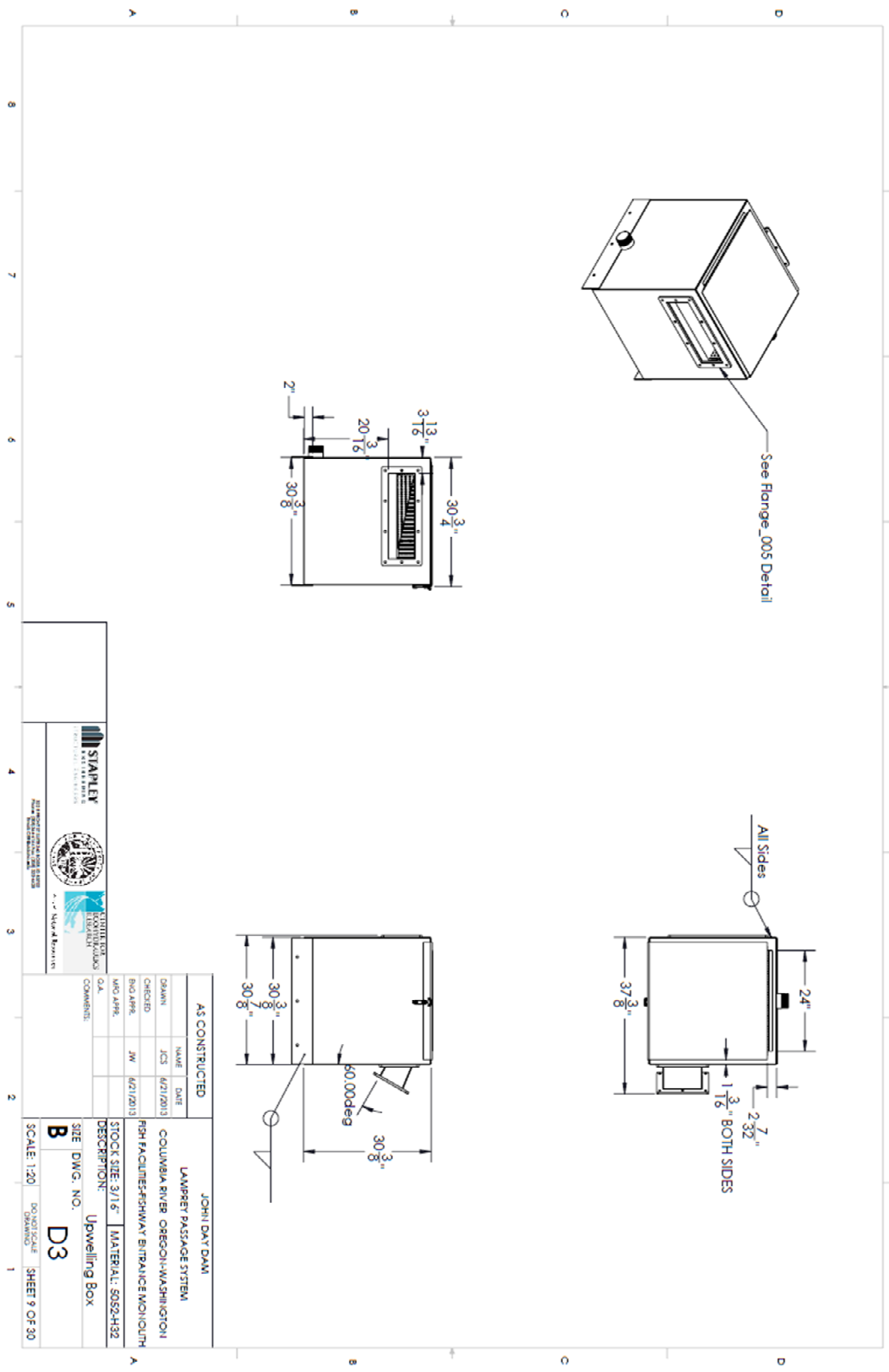

Figure 103: Upwelling Box of Lamprey Passage Structure

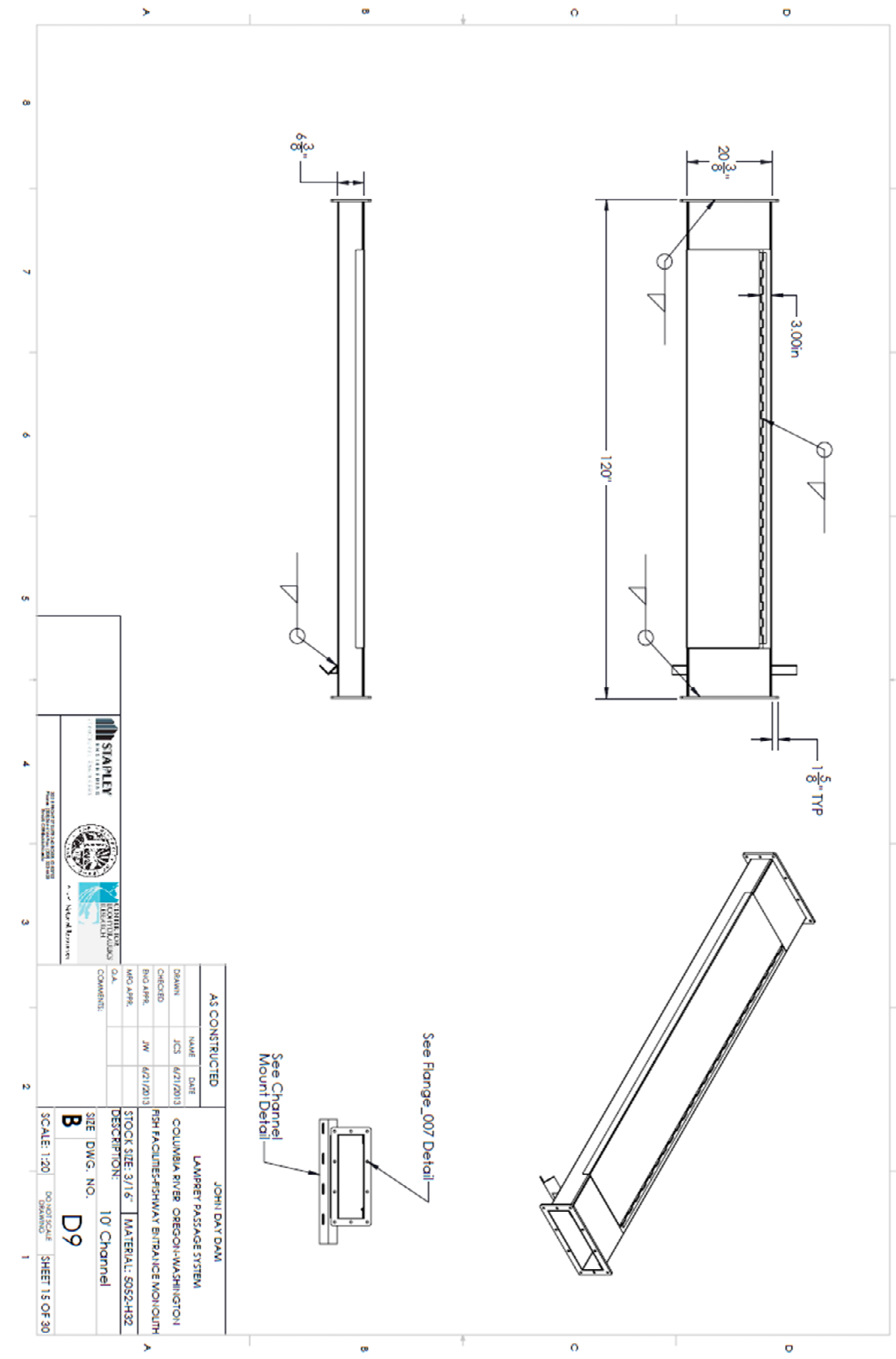

Figure 104: Climbing Duct of Lamprey Passage Structure

Figure 105: Lifting Rest Box into Place

Figure 106: Lifting Pumps into Place

Figure 107: Upwelling and Trap Box in Place

Figure 108: Completed LPS Structure